



Agenzia nazionale per le nuove tecnologie, l'energia
e lo sviluppo economico sostenibile



Ministero dello Sviluppo Economico

RICERCA DI SISTEMA ELETTRICO

Activities in Support to the Assessment of Steam Generator Bayonet Tubes, for GEN-IV Applications

*D. Rozzia, D. Martelli, N. Forgione, M. Moretti, A. Naviglio, D. Vitale di Maio, A. Del
Nevo, M. Tarantino*



Report RdS/2012/050

ACTIVITIES IN SUPPORT TO THE ASSESSMENT OF STEAM GENERATOR BAYONET TUBES, FOR GEN-IV APPLICATIONS

D. Rozzia, D. Martelli, N. Forgione – CIRTEN Università di Pisa, M. Moretti, A. Naviglio, D. Vitale Di Maio – CIRTEN Università di Roma 1, A. Del Nevo, M. Tarantino - ENEA

Settembre 2012

Report Ricerca di Sistema Elettrico

Accordo di Programma Ministero dello Sviluppo Economico - ENEA

Area: Governo, gestione e sviluppo del sistema elettrico nazionale

Progetto: Nuovo nucleare da fissione: collaborazioni internazionali e sviluppo competenze in materia nucleare

Responsabile del Progetto: Mariano Tarantino, ENEA



Titolo

**Activities in Support to the Assessment of Steam Generator Bayonet Tubes,
for GEN-IV Applications**

Descrittori

Tipologia del documento: Rapporto Tecnico

Collocazione contrattuale: Accordo di programma ENEA-MSE: tema di ricerca "Nuovo nucleare da fissione"

Argomenti trattati: Generation IV Reactors
Termoidraulica dei reattori nucleari
Tecnologia del piombo
Trasmissione del calore

Sommario

The overall activity is aimed to verify the feasibility of the superheated steam double wall once through bayonet type steam generation. The work and the relative experimental campaigns will be focused on the single tube evaluation. It spans over three years. The main phases of the experimental campaigns are:

- Individuate a candidate material as gap filler for the bayonet tube.
- Verify the single tube performance in representative operating conditions.

This report is the result of a collaboration between UNIPI-UNIROMA1 and ENEA. It is subdivided in seven sections. The first one points out the objectives and the framework of the activity. Section two describes the ALFRED SG and points out the results of the screening of candidate insulating materials to be placed in the bayonet tube, between the descendent feedwater and the superheated steam riser. In section three, the detailed assessment of the single tube performance by means of RELAP-5 is reported. Systematic comparison with the ANSALDO calculations are included. Section four focuses on the thermal hydraulic conceptual design of the heating power system of the Heavy liquid metal – pressurized water cooled tube facility (HERO). The section points out the geometry of a facility capable to test one 1:1 bayonet tube of ALFRED. RELAP-5 and FLUENT calculations are presented in this section. The preliminary PID of HERO is analyzed in section five. The status of advance of the Tubes for Powders facility (TxP) is discussed in the sixth section. Summary and conclusions are presented in the last section..

Note




Autori:

D. Rozzia, D. Martelli, N. Forgone (UNIPI)
M. Moretti, A. Naviglio, D. Vitale Di Maio (UNIROMA1)
A. Del Nevo, M. Tarantino (ENEA)

Copia n.

In carico a:

1			NOME			
			FIRMA			
0	EMISSIONE	18/09/2012	NOME	D. Rozzia	P. Gaggini	M. Tarantino
			FIRMA	<i>D. Rozzia</i>	<i>P. Gaggini</i>	<i>M. Tarantino</i>
REV.	DESCRIZIONE	DATA	REDAZIONE	CONVALIDA	APPROVAZIONE	

 Ricerca Sistema Elettrico	Sigla di identificazione NNFISS - LP3 - 054	Rev. 0	Distrib. L	Pag. 2	di 117
--	---	------------------	----------------------	------------------	------------------

(This page has been intentionally left blank)

Acknowledgments

The authors express their gratitude to Mr. Gino Venturi who allows the design of the TxP Facility. We acknowledge Alessandro Ventura who provides support to the assembling of the TxP Facility and to the preliminary testing of candidate powders.

We acknowledge Marco Gregorini for the fruitful recommendations that allow the development of the Steam Generator Bayonet Tube RELAP-5 improved input deck.

Abstract


One of the most promising Generation IV concepts is the Lead cooled Fast Reactor (LFR). The use of lead as primary coolant appears motivated by several reasons (low moderation, thermal properties, etc...), nevertheless, it still has several limitations that require further investigations. The actual configuration of LFR pointed out in the framework of the ELSY and LEADER projects deals with the compact pool type reactor in which the steam generators (SG) are located inside the reactor tank. In this scenario, the steam generator design plays an important role because one of the most impacting incidents is the Steam Generator Tube Rupture (SGTR) that may propagate to the near-bough tubes. The SG proposed in ELSY is the flat spirals type. In the framework of the EU project LEADER, an innovative configuration of SG has been proposed: the super-heated steam double wall once through bayonet type. This conceptual design was studied since 60' for Sodium Reactor application. An example of facility that operates with this concept is CIRCE (ENEA Brasimone), nevertheless the application is limited to the heat exchange function.

The single tube vertical unit consists of three concentric tubes. Starting from the smallest one, the water crosses in down-flow the tube and heats-up. At the end of this tube, the water enters the second concentric tube in up-flow where it starts to boil because of the heat exchange with the liquid lead that flows in counter-current at the tube outer surface. The tube design allows the achievement of super-heated steam. The liquid lead is not in direct contact with the second tube. A third concentric tube, that creates an annulus, separates it from the steam-water sides. The study of this configuration is motivated by safety improvement. Indeed, it allows the double physical separation between lead and water sides by means of an intermediate gap. Thus, the probability of vessel pressurization by water-lead contact results reduced. Furthermore, by means of gap pressurization (with Helium), a leakage check system should be introduced in order to prevent incident scenarios. On the other hands, the monitor-ability of the pressurized gap has to be demonstrated and the thermal efficiency has to be improved.

The overall activity is aimed to study the bayonet tube performance. The work and the relative experimental campaigns will be focused on the single tube evaluation. It spans over three years. The main phases of the experimental campaigns are:

- *Individuate and test a candidate material as gap filler in order to increase the thermal efficiency;*
- *Verify the single tube performance in representative operating conditions by means of computational tools and experimental tests.*

This report has been carried out as a collaboration among UNIPI, UNIROMA1 and ENEA. It is subdivided in seven sections. The first one points out the objectives and the framework of the

 Ricerca Sistema Elettrico	Sigla di identificazione	Rev.	Distrib.	Pag.	di
	NNFISS - LP3 - 054	0	L	4	117

activity. Section two describes the ALFRED SG and points out the results of the screening of candidate insulating materials to be placed in the bayonet tube, between the descendent feedwater and the superheated steam riser. In section three, the detailed assessment of the single tube performance by means of RELAP-5 is reported. Systematic comparison with the ANSALDO calculations are included. Section four focuses on the thermal-hydraulic conceptual design of the heating power system of the Heavy liquid metal – pressurized water cooled tube facility (HERO). RELAP-5 and FLUENT calculations are presented in this section. The preliminary PID of HERO is analyzed in section five. The status of advance of the Tubes for Powders facility (TxP) is discussed in the sixth section. Summary and conclusions are presented in the last section.

CONTENTS

ACKNOWLEDGMENTS	3
ABSTRACT	3
ABBREVIATIONS	7
LIST OF FIGURES	9
LIST OF TABLES	13
1 INTRODUCTION.....	15
1.1 Framework and Objective of the Activity	15
1.2 Structure of the report	16
2 ALFRED STEAM GENERATOR BAYONET TUBE	19
2.1 Description	19
2.2 Identification of Potential Insulators for the Inner Tube	22
3 ASSESSMENT OF THE SG BAYONET TUBE BY MEANS OF RELAP-5.....	27
3.1 Development of the Reference Nodalization.....	28
3.2 Assessment of the Reference Nodalization	31
3.2.1 Assessment of the Hydrodynamic Components.....	32
3.2.2 Assessment of the Heat Structures	35
3.2.3 Assessment of 2 ϕ Dynamics in the Water Steam Side	40
3.3 Sensitivity Analyses.....	45
3.4 Development of the Improved Input Deck	46
3.4.1 Assessment of the Hydrodynamic Components.....	47
3.4.2 Assessment of the Heat Structures	50
3.4.3 Assessment of 2 ϕ Dynamics in the Water Steam Side	55
4 THERMAL HYDRAULIC CONCEPTUAL DESIGN OF HERO	59
4.1 Objectives of the HERO Facility and Potential Heating Power System	59
4.2 Calculations in Support to the TH Design of HERO by RELAP-5.....	62
4.2.1 Initial Input Deck Documentation.....	62
4.2.2 Identification of the Potential Geometries of HERO	67
4.2.3 Assessment of the HERO Reference Configuration	70
4.2.4 Comparison Between Selected Lead Levels and SGBT	75
4.3 Calculations in Support to the TH Design of HERO by FLUENT	80

4.3.1	Preliminary 2D Axial-Symmetric Simulations	80
4.3.2	Preliminary 3D Simulations	84
5	PRELIMINARY PIPING AND INSTRUMENTATION DIAGRAM OF HERO.....	95
5.1	Preliminary PID of the Heating Power System	95
5.2	Preliminary PID of the Pressurized Cooling Water System.....	97
6	STATUS OF THE TxP FACILITY.....	99
6.1	Description of TxP	99
6.2	Status of TxP.....	101
6.3	Activities in Support to the Planning of the TxP Experimental Campaigns	103
6.3.1	Description of the Experiments.....	103
6.3.2	Powders Pre-Characterization	105
6.3.3	Main Achievements from the Experiments.....	107
7	CONCLUSIONS	111
	REFERENCES	115

Abbreviations

A	Accepted
Al-N	Aluminum Nitride
ALFRED	Advanced Lead Fast Reactor European Demonstrator
Ar	Argon
CDT	Central Design Team
CFD	Computational Fluid Dynamics
CHF	Critical Heat Flux
CIRCE	CIRColazione Eutettico
Cu	Copper
CR	Centro di Ricerca
DHR	Decay Heat Removal system
DIMNP	Dipartimento di Ingegneria Meccanica, Nucleare e della Produzione
DP	Diamond Powder
ELFR	European Lead cooled Fast Reactor
ELSY	European Lead cooled SYstem
ENEA	Agenzia nazionale per le nuove tecnologie, l'energia, e lo sviluppo economico sostenibile
ETDR	European Technology Demonstrator Reactor
EU	European Union
FR	Fast Reactor
FP	Fission Product
GEN-IV	GENeration four
GIF	Generation four International Forum
He	Helium
HERO	Heavy liquid mEtal – pRessurized water cOoled tube facility
HR	Heating Rod
HP	High conductivity Powder zone
HTC	Heat Transfer Coefficient
IAEA	International Atomic Energy Agency
ID	Inner Diameter
LBE	Lead Bismuth Eutectic
LEADER	Lead-cooled European Advanced DEMonstration Reactor
LFR	Lead cooled Fast Reactor
LMC	Liquid Metal Coolant
LMFR	Liquid Metal cooled Fast Reactors
LWR	Light Water Reactor
N/A	Not Addressed
Na	Sodium
NEA	Nuclear Energy Agency
NRC	Nuclear Regulatory Commission
OD	Outer Diameter
OECD	Organization for Econ. Co-operation and Develop.
PID	Piping and Instrumentation Diagram (or P & I)
Pb	Lead
PP	Primary Pump
PT	Powder Tube
R	Rejected
RVACS	Reactor Vessel Auxiliary Cooling System
SEM	Scan Electron Microscope
SG	Steam Generator
SGBT	Steam Generator Bayonet Tube
SGTR	Steam Generator Tube Rupture



TH	Thermal Hydraulics
TxP	Tubes for Powders facility
U	Unknown
UNUPI	UNiversità degli studi di Pisa
V-I	Visual Inspection
WT	Water Tube

List of figures

<i>Fig. 1 – LEADER Project, ALFRED SG scheme.</i>	<i>20</i>
<i>Fig. 2 – LEADER Project, ALFRED pump casing and heat dispersion removal system.....</i>	<i>21</i>
<i>Fig. 3 – Scheme of the SG double wall bayonet tube of ALFRED.</i>	<i>21</i>
<i>Fig. 4 – ALFRED SG double wall bayonet tube, RELAP-5.3.3 model.</i>	<i>28</i>
<i>Fig. 5 – Thermal conductivity of diamond powder as function of porosity, calculated by Case 1 and Case 2 correlations, 200 °C.....</i>	<i>32</i>
<i>Fig. 6 – SGBT vs. RELAP5 v 3.3, reference simulations, void fraction, water and lead temperatures as function of tube length.</i>	<i>34</i>
<i>Fig. 7 – SGBT vs. RELAP5 v 3.3, reference simulations, pressure drops.....</i>	<i>35</i>
<i>Fig. 8 – SGBT vs. RELAP5 v 3.3, reference simulations, velocities.</i>	<i>35</i>
<i>Fig. 9 – SGBT vs. RELAP5 v 3.3, reference simulations, heat flux in the feedwater tube as function of tube length.....</i>	<i>37</i>
<i>Fig. 10 – SGBT vs. RELAP5 v 3.3, reference simulations, convection HTC at the feedwater tube surfaces as function of tube length.....</i>	<i>38</i>
<i>Fig. 11 – SGBT vs. RELAP5 v 3.3, reference simulations, temperatures at the feedwater tube surfaces as function of tube length.....</i>	<i>38</i>
<i>Fig. 12 – SGBT vs. RELAP5 v 3.3, reference simulations, heat flux in the annular riser as function of tube length.....</i>	<i>39</i>
<i>Fig. 13 – SGBT vs. RELAP5 v 3.3, reference simulations, convection HTC in the annular riser as function of tube length.</i>	<i>39</i>
<i>Fig. 14 – SGBT vs. RELAP5 v 3.3, reference simulations, temperatures at annular riser surfaces as function of tube length.</i>	<i>40</i>
<i>Fig. 15 – Flow regimes for vertical ducts for vertical ducts according to RELAP-5.....</i>	<i>42</i>
<i>Fig. 16 – Heat transfer mode map at heat structures boundaries according to RELAP-5.</i>	<i>42</i>
<i>Fig. 17 – SGBT vs. RELAP5 v 3.3, reference simulation Case 1, flow regimes and heat transfer regimes at tube walls in the water-steam side.</i>	<i>43</i>
<i>Fig. 18 – SGBT vs. RELAP5 v 3.3, reference simulation Case 2, flow regimes and heat transfer regimes at tube walls in the water-steam side.</i>	<i>44</i>
<i>Fig. 19 – SGBT vs. RELAP5 v 3.3, improved input deck Case 1 vs. reference Case 1, thermal-hydraulic parameters of the hydrodynamic components as function of tube length.....</i>	<i>48</i>
<i>Fig. 20 – SGBT vs. RELAP5 v 3.3, improved input deck Case 2 vs. reference Case 2, thermal-hydraulic parameters of the hydrodynamic components as function of tube length.....</i>	<i>49</i>
<i>Fig. 21 – SGBT vs. RELAP5 v 3.3, improved input deck Case 1, heat structure parameters of the feedwater tube as function of tube length and comparison with the reference simulation.....</i>	<i>51</i>
<i>Fig. 22 – SGBT vs. RELAP5 v 3.3, improved input deck Case 2, heat structure parameters of the feedwater tube as function of tube length and comparison with the reference simulation.....</i>	<i>52</i>
<i>Fig. 23 – SGBT vs. RELAP5 v 3.3, improved input deck Case 1, heat structure parameters of the annular riser as function of tube length and comparison with the reference simulation.</i>	<i>53</i>


<i>Fig. 24 – SGBT vs. RELAP5 v 3.3, improved input deck Case 2, heat structure parameters of the annular riser as function of tube length and comparison with the reference simulation.</i>	<i>54</i>
<i>Fig. 25 – SGBT vs. RELAP5 v 3.3, improved input deck Case 1, flow regimes and heat transfer regimes at tube walls in the water-steam side.</i>	<i>56</i>
<i>Fig. 26 – SGBT vs. RELAP5 v 3.3, improved input deck Case 2, flow regimes and heat transfer regimes at tube walls in the water-steam side.</i>	<i>57</i>
<i>Fig. 27 – HERO Facility Reference configuration, lead loop scheme with internal heating rods.....</i>	<i>60</i>
<i>Fig. 28 – HERO Facility Reference configuration, heating rods and fissure.</i>	<i>61</i>
<i>Fig. 29 – HERO Facility Alternative configuration.</i>	<i>61</i>
<i>Fig. 30 – HERO Facility Reference configuration RELAP-5 input deck scheme.</i>	<i>63</i>
<i>Fig. 31 – HERO Facility, calculations in support to the determination of the radial geometry.....</i>	<i>69</i>
<i>Fig. 32 – HERO Facility calculations in support to the determination of the computational time, mass flow rate.</i>	<i>71</i>
<i>Fig. 33 – HERO Facility calculations in support to the determination of the computational time, mass flow rate zoom.....</i>	<i>71</i>
<i>Fig. 34 – HERO Facility calculations in support to the determination of the computational time, lead temperature in pipe 140.</i>	<i>72</i>
<i>Fig. 35 – HERO Facility calculations in support to the determination of the computational time, lead temperature in pipe 140.</i>	<i>72</i>
<i>Fig. 36 – HERO Facility, 4AX-2.5AY, mass flow rate as function of lead level at the fissures inlet.</i>	<i>73</i>
<i>Fig. 37 – HERO Facility, 6AX-2.5AY, mass flow rate as function of lead level at the fissures inlet.</i>	<i>74</i>
<i>Fig. 38 – HERO Facility, max-k, 4AX-2.5AY-0014A and 6AX-2.5AY-0010A versus SGBT, steam-water side.</i>	<i>76</i>
<i>Fig. 39 – HERO Facility, max-k, 4AX-2.5AY-0014A versus SGBT, lead side.</i>	<i>77</i>
<i>Fig. 40 – HERO Facility, max-k, 6AX-2.5AY-0010A versus SGBT, lead side.</i>	<i>77</i>
<i>Fig. 41 – HERO Facility, min-k, 4AX-2.5AY-0010A and 6AX-2.5AY-0007A versus SGBT, steam-water side.</i>	<i>78</i>
<i>Fig. 42 – HERO Facility, min-k, 4AX-2.5AY-0010A versus SGBT, lead side.....</i>	<i>79</i>
<i>Fig. 43 – HERO Facility, min-k, 6AX-2.5AY-0007A versus SGBT, lead side.....</i>	<i>79</i>
<i>Fig. 44– HERO Facility, FLUENT simulations, 2D geometrical domain.</i>	<i>80</i>
<i>Fig. 45 – HERO Facility, FLUENT simulations, temperature profile imposed at the wall separating the primary and the secondary circuit (from RELAP5 simulation).</i>	<i>81</i>
<i>Fig. 46 – HERO Facility, FLUENT simulations, detail of the mesh at the entrance of the cooling annular channel.</i>	<i>82</i>
<i>Fig. 47 – HERO Facility, FLUENT simulations, detail of the mesh at the exit of the cooling annular channel.....</i>	<i>82</i>
<i>Fig. 48 – HERO Facility, FLUENT simulation C, mass flow rate at the inlet of the cooling channel.</i>	<i>83</i>
<i>Fig. 49 – HERO Facility, FLUENT simulation C, temperature at the inlet of the cooling channel.</i>	<i>83</i>
<i>Fig. 50 – HERO Facility, FLUENT calculations, heater schematization for the 3D analyses.....</i>	<i>84</i>
<i>Fig. 51 – HERO Facility, FLUENT calculations, simplified geometry schematization.....</i>	<i>85</i>

Fig. 52 – HERO Facility, FLUENT calculations, detail of the 3D geometry at the entrance of the cooling annular channel.	85
Fig. 53 – Lead level regulation.	86
Fig. 54 – HERO Facility, FLUENT calculations, temperature profile imposed at the wall separating the primary and the secondary circuit (RELAP5 simulation II).	86
Fig. 55 – HERO Facility, FLUENT calculations, details of the mesh at the entrance (a)and at the exit (b) of the cooling annular region.	87
Fig. 56 – HERO Facility, FLUENT calculations, details of the mesh: top view.	87
Fig. 57 – HERO Facility, FLUENT calculations, mass flow rate at the inlet of the cooling channel, (1/16).	88
Fig. 58 – HERO Facility, FLUENT calculations, average lead temperature at the inlet of the cooling channel.	89
Fig. 59 – HERO Facility, FLUENT calculations, temperature difference between the inlet and the outlet of the cooling annular channel.	90
Fig. 60 – HERO Facility, FLUENT calculations, contours of temperature on the fissures and on three different z levels at the entrance of the cooling channel (simulation 4AX-2.5AY-005).	90
Fig. 61 – HERO Facility, FLUENT calculations, contours of temperature on three horizontal planes and on vertical planes trough the fissures symmetry planes at the entrance of the cooling channel (simulation 4AX-2.5AY-001).	91
Fig. 62 – HERO Facility, FLUENT calculations, mean velocity magnitude at the exit of the cooling annular channel.	92
Fig. 63 – HERO Facility, FLUENT calculations, contour of velocity at the exit of the cooling annular channel (simulation 4AX-2.5AY-005).	92
Fig. 64 – HERO Facility, FLUENT calculations, velocity magnitude vector at the exit of the cooling annular channel (simulation 4AX-2.5AY-005).	93
Fig. 65 – PID scheme of the heating power system of HERO.	96
Fig. 66 – PID scheme of the pressurized cooling water system of HERO.	98
Fig. 67 – TxP conceptual scheme.	100
Fig. 68 – TxP design: PID.	101
Fig. 69 – TxP pre-assembling.	102
Fig. 70 – Thermal loads applied to test the candidate powders, scheme.	104
Fig. 71 – Scheme of the experimental facility.	104
Fig. 72 – Electrolytic copper powder LT-12 - 20°C.	105
Fig. 73 – Copper powder W-60-M - 20°C.	105
Fig. 74 – Brass powder OT-63 - 20°C.	105
Fig. 75 – AISI-316 powder - 20°C.	106
Fig. 76 – Sintetic diamond powder - 20°C.	106
Fig. 77 – Si-C powder - 20°C.	106
Fig. 78 – Al-N powder - 20°C.	106
Fig. 79 – Electrolytic copper powder LT-12 - 200°C.	107

<i>Fig. 80 – Copper powder W-60-M - 300°C.....</i>	<i>108</i>
<i>Fig. 81 – Brass powder OT-63 - 500°C.</i>	<i>108</i>
<i>Fig. 82 – AISI-316 powder - 500°C.</i>	<i>108</i>
<i>Fig. 83 – Sintetic diamond powder - 500°C.....</i>	<i>109</i>
<i>Fig. 84 – Si-C powder - 500°C.....</i>	<i>109</i>
<i>Fig. 85 – Al-N powder - 500°C</i>	<i>109</i>

List of tables

<i>Tab. 1 - ALFRED SG main data (from the conceptual design).....</i>	<i>22</i>
<i>Tab. 2 – Summary of the investigated insulating materials.</i>	<i>24</i>
<i>Tab. 3 – Preliminary screening, criterion I: conductivity.</i>	<i>25</i>
<i>Tab. 4 – Summary of the results of the assessment of insulating materials.</i>	<i>26</i>
<i>Tab. 5 - ALFRED SG, hydrodynamic modeling of the feedwater tube.</i>	<i>29</i>
<i>Tab. 6 - ALFRED SG hydrodynamic modeling of the annular steam riser.....</i>	<i>29</i>
<i>Tab. 7 - ALFRED SG, hydrodynamic modeling of the lead channel.....</i>	<i>29</i>
<i>Tab. 8 - ALFRED SG, modeling of the heat structure between the feedwater tube and the annular riser.....</i>	<i>30</i>
<i>Tab. 9 - ALFRED SG, modeling of the heat structure between the annular riser and the lead channel (active height only).</i>	<i>31</i>
<i>Tab. 10 - SGBT vs. RELAP5 v 3.3, reference simulations, assessment of hydrodynamic components.....</i>	<i>35</i>
<i>Tab. 11 - SGBT vs. RELAP5 v 3.3, reference simulations, assessment of heat structures.....</i>	<i>37</i>
<i>Tab. 12 – Summary of the sensitivity analyses.....</i>	<i>46</i>
<i>Tab. 13 – HERO Facility, summary of the initial geometry.....</i>	<i>62</i>
<i>Tab. 14 - HERO Facility, bayonet tube side, hydrodynamic modeling of the lead channel.</i>	<i>64</i>
<i>Tab. 15 – HERO Facility, hydrodynamic modeling of the lead channel down flow area.....</i>	<i>64</i>
<i>Tab. 16 – HERO Facility, hydrodynamic modeling of the lead channel down flow area.....</i>	<i>64</i>
<i>Tab. 17 – HERO Facility, hydrodynamic modeling of the lead channel down flow area.....</i>	<i>65</i>
<i>Tab. 18 – HERO Facility, hydrodynamic modeling of the top holes.....</i>	<i>65</i>
<i>Tab. 19 – HERO Facility, hydrodynamic modeling of the top holes.....</i>	<i>65</i>
<i>Tab. 20 – HERO Facility, hydrodynamic modeling of the bottom holes.....</i>	<i>65</i>
<i>Tab. 21 – HERO Facility, modeling of the heat structure between the feedwater tube and the annular riser.....</i>	<i>66</i>
<i>Tab. 22 – HERO Facility, modeling of the heat structure between the annular riser and the lead channel (active height only).....</i>	<i>67</i>
<i>Tab. 23 – HERO Facility, calculations in support to the determination of the radial geometry, summary of the results.</i>	<i>69</i>
<i>Tab. 24 – HERO Facility, definition of the potential radial geometries.</i>	<i>70</i>
<i>Tab. 25 – HERO Facility, assessment of the potential configurations, mass flow rates as function of fissures flow area (and lead level).</i>	<i>74</i>
<i>Tab. 26 – HERO Facility, max-k, comparison between selected configurations and SGBT.....</i>	<i>76</i>
<i>Tab. 27 – HERO Facility, min-k, comparison between selected configurations and SGBT.</i>	<i>78</i>
<i>Tab. 28 – HERO Facility, summary of the simulations.....</i>	<i>81</i>
<i>Tab. 29 – HERO Facility, FLUENT simulations, mass flow rate results.....</i>	<i>84</i>

 Ricerca Sistema Elettrico	Sigla di identificazione	Rev.	Distrib.	Pag.	di
	NNFISS - LP3 - 054	0	L	14	117

<i>Tab. 30 – Test matrix of 3D simulations.</i>	<i>86</i>
<i>Tab. 31 – TxP main data.</i>	<i>100</i>
<i>Tab. 32 – TxP, schedule of the processing activities performed at the mechanical unit of Brasimone.</i>	<i>102</i>
<i>Tab. 33 – Summary of the experiments.</i>	<i>110</i>

1 Introduction

The Generation IV International Forum (GIF), was chartered in July 2001 to promote the collaborative efforts of the world's leading nuclear technology nations to develop next generation nuclear technology. The main purpose of the initiative is to set-up innovative nuclear systems, candidate to reach technical and commercial maturity by 2040 ^{[1][2]}.

Initially, a large number of innovative Generation IV systems was considered. Liquid Metal cooled Fast Reactors (LMFR) are the most promising conceptual solutions. Among the Liquid Metal Coolants (LMC), sodium (Na) has by far the most important cumulated experience both in experimental and industrial nuclear applications. Nevertheless, due to the advantages of these kind of coolants, lead (Pb) or lead-bismuth eutectic (LBE) nuclear systems are proposed in the GIF together with sodium. Choosing LMCs for Fast Reactors (FR) is due to their high heat removal capabilities coupled with low interaction with neutrons.


The Lead cooled Fast Reactors (LFR) ^{[3][4]} operates in the fast-neutron spectrum and use a closed fuel cycle for an efficient conversion of fertile uranium. The use of lead as primary coolant is motivated by several advantages, which can be summarized as follow ^{[5][6]}:

- The promising nuclear properties, i.e. the low moderation rate.
- The non-existence of exothermic reactions between lead and water or air. This provides favorable conditions for the elimination of the intermediate circuit (typical of past Sodium cooled Fast Reactors).
- The high boiling point of lead (1749 °C at 1 bar). It allows to operate the reactor at low primary system pressure reducing the reactor vessel thickness. Furthermore, it eliminates the risk of core voiding due to coolant boiling.
- The high density of lead that favors fuel dispersion phenomena and prevents fuel compaction phenomena in case of core damage. This reduces the likelihood that fuel collects at the reactor vessel bottom in such a way that re-criticalities may occur.
- The high thermal capacity. It allows a significant grace time in case of loss-of-heat-sink accidents.
- The capability to retain FPs as iodine and cesium forming chemical compounds at temperatures up to 600 °C. This reduces the source term to the confinement/containment during accidents in which volatile fission products are released from the fuel matrix.
- The shielding capability against the γ -radiations.

Nevertheless, the molten lead has limitations. Lead is a an opaque heavy metal and its chemical properties imply corrosion and erosion problems with the structural materials. To partially mitigate them it is mandatory to work at relatively low temperatures compared to the other Generation IV reactors. Moreover, lead solidification may occur due to the high melting temperature (327 °C).

1.1 Framework and Objective of the Activity

The Lead-cooled European Advanced DEMonstration Reactor (LEADER) ^[7] project belongs to the 7th Framework Programme. It starts from the results achieved in the previous ELSY ^[8] (European Lead cooled System) project with the aim to improve its reactor configuration.

 Ricerca Sistema Elettrico	Sigla di identificazione	Rev.	Distrib.	Pag.	di
	NNFISS - LP3 - 054	0	L	16	117

The main objective of LEADER ^[9] deals with the design of a 300 MWth low cost and fully representative scaled down European LFR Technology Demonstrator Reactor (ETDR) named ALFRED (Advanced Lead Fast Reactor European Demonstrator). An additional objective of the project focuses on the development of a new industrial size consistent reactor configuration based on ELSY: the 600 MWe European Lead-cooled Fast Reactor (ELFR).

In this framework, a new configuration of Steam Generator (SG) has been proposed: the superheated steam double wall once through bayonet tube type. This conceptual design was studied since 60' for Sodium Reactor application. An example of facility that operates with this concept is CIRCE (at ENEA Brasimone) even if it is limited to the heat exchange function.

The present activity aims to investigate the TH performance of the single bayonet tube. Its main objective is to test a single 1:1 bayonet tube (eventual improved in design) into an experimental facility representative of the TH in reactor behavior: the Heavy liquid mEtal – pRessurized water cOoled tube Facility (HERO Facility).

The activity starts in 2011 ^[10], the following sub-objectives were reached:

- Design of the TxP (Tubes for Powders) Facility devoted to powders conductivity measurement into an annular geometry representative of the bayonet tube. Its aim is to qualify powders for their application in the annular gap as heat transfer enhancer.
- Selection of candidate powders for the experimental campaigns based on bibliographic research.
- Preliminary assessment of the TH performance of the bayonet tube by means of RELAP-5.
- Feasibility assessment on turbulence promoters for annular geometry subjected to two phase flow.


During 2012, the following sub-objectives have been reached and documented in this report:

- Assessment of the SG single tube conceptual design with focus on the main design aspects that impact on its performance by means of TH system codes (RELAP-5).
- Definition of the main geometrical data of the heating power system of the Heavy liquid mEtal – pRessurized water cOoled tube Facility (HERO Facility) by means of TH system codes and CFD calculations.
- Setup of a preliminary PID of the heating power system and of the pressurized water loop of HERO.
- Experimental activities in support to the planning of the experimental campaigns in the TxP Facility and status of construction of TxP.

1.2 Structure of the report

This report is the result of a collaboration between UNIPI-UNIROMA1 and ENEA. It is subdivided in seven sections.

This first one points out the objectives and the framework of the activity. Section two describes the SG of ALFRED and points out the results of the screening of candidate insulating materials to be placed in the bayonet tube, between the descendent feedwater and the superheated steam riser.

 Ricerca Sistema Elettrico	Sigla di identificazione	Rev.	Distrib.	Pag.	di
	NNFISS - LP3 - 054	0	L	17	117

In section three, the detailed assessment of the single tube performance by means of RELAP-5 is reported. Systematic comparison with the ANSALDO calculations are included. Sensitivity analysis are presented to highlight the influence of design, modeling issues and boundary conditions.

Section four focuses on the thermal hydraulic conceptual design of the heating power system of the Heavy liquid metal – pressurized water cooled tube facility (HERO). The section points out the potential geometries of a facility capable to test one 1:1 bayonet tube of ALFRED. RELAP-5 and FLUENT calculations are presented in this section. The calculations include the comparison between the performance of HERO and the bayonet tube as modeled in section three.

The preliminary PID of HERO is given in section five. Two preliminary schemes have been fixed: the heating power system (the lead circuit) and the pressurized water closed loop.

The status of advancement of the Tubes for Powders Facility (TxP) is discussed in the sixth section. The section includes the results of experimental tests (in furnace thermal loads) conducted at Brasimone.

Summary and conclusions are given in the last section.



2 ALFRED Steam Generator Bayonet Tube

2.1 Description

ALFRED reactor ^[7] includes eight once through double wall bayonet tube bundle type SGs ^{[3] [9]}. Preliminary calculations indicate that each SG has 510 tubes. A scheme of the ALFRED SG is shown in *Fig. 1*. *Tab. 1* summarizes the SG and the bayonet tube main data.

The single unit is capable to remove 37.5 MW. It consists of the SG coupled with its axial pump located in the reactor hot side and integrated in the SGs (axial pump is the reference solution, jet pump is the alternative, *Fig. 2*). The pump suction is directly located above the reactor core, the lead flows into the pump and leaves its casing in appropriate fissures that connect the pump to the SG tube bundle. The lead crosses in down flow the bundle and leaves the SG at its bottom end. The SG active length is 6 m, the top head of the reactor pool is filled by Argon (1 m in height). The heat exchange between the water-steam bayonet tube and the lead is in counter-current.

The single bayonet tube consists of three concentric tubes, *Fig. 3*. It is made of T91. In each bayonet tube, the water flows downward in the inner tube (labeled as feedwater tube) and enters the annular space between the first and the second tube (labeled as annular riser) in up-flow where it starts to boil because of the heat exchange with the liquid lead that flows in counter-current ^[9].

The design requires the achievement of high temperature super-heated steam (450 °C, 180 bar). The molten lead is not in contact with the second tube. The third concentric tube (labeled as lead channel tube) separates it from the water-steam side providing a double barrier and the capability to monitor leakages from the tubes. This last safety function is achieved by means of pressurization of the annular gap with helium.

The study of this configuration is motivated by safety improvement. Indeed, it allows the double physical separation between lead and water sides. Furthermore, the leakage check system should prevent incident scenarios as lead-water-steam interaction due to steam generator tube rupture (SGTR).

On the other hands, the thermal efficiency of this configuration needs to be investigated and improved. In particular, two opened points should be carefully investigated ^[3]:

- The achievement of high temperature superheated steam requires the selection of an appropriate material to be placed within the gap between the annular riser and the lead channel tube (to increase the thermal conductivity of the gap).
- The heat exchange between the feedwater that crosses in down-flow the first tube and the superheated steam that rises up in the annular space should be minimized.

High conductivity powders and turbulence promoters were investigated in Refs. [10], [11] [12] [13] and [15]; insulating materials are presented in the next sub-section and in Ref. [14].

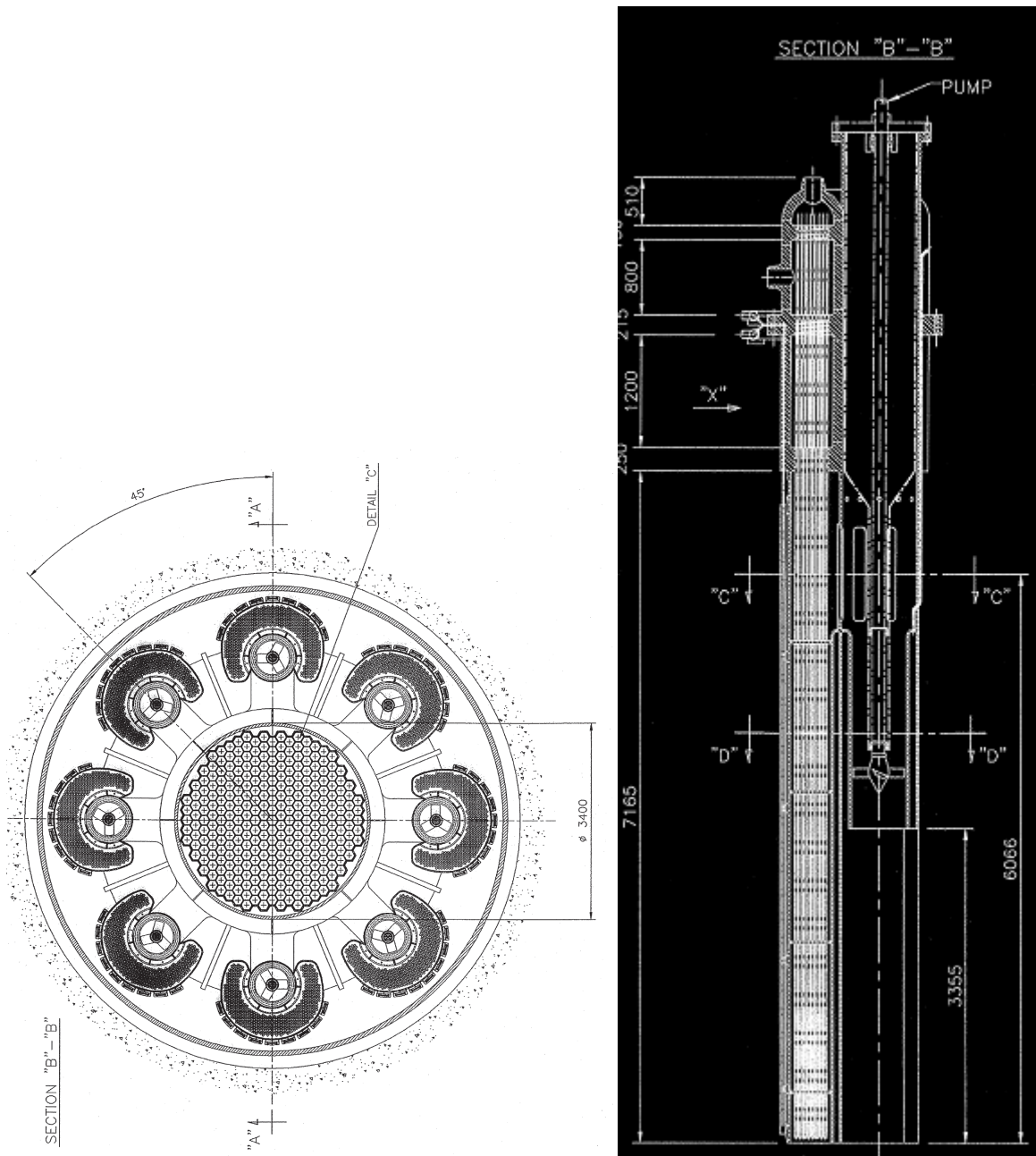


Fig. 1 – LEADER Project, ALFRED SG scheme.

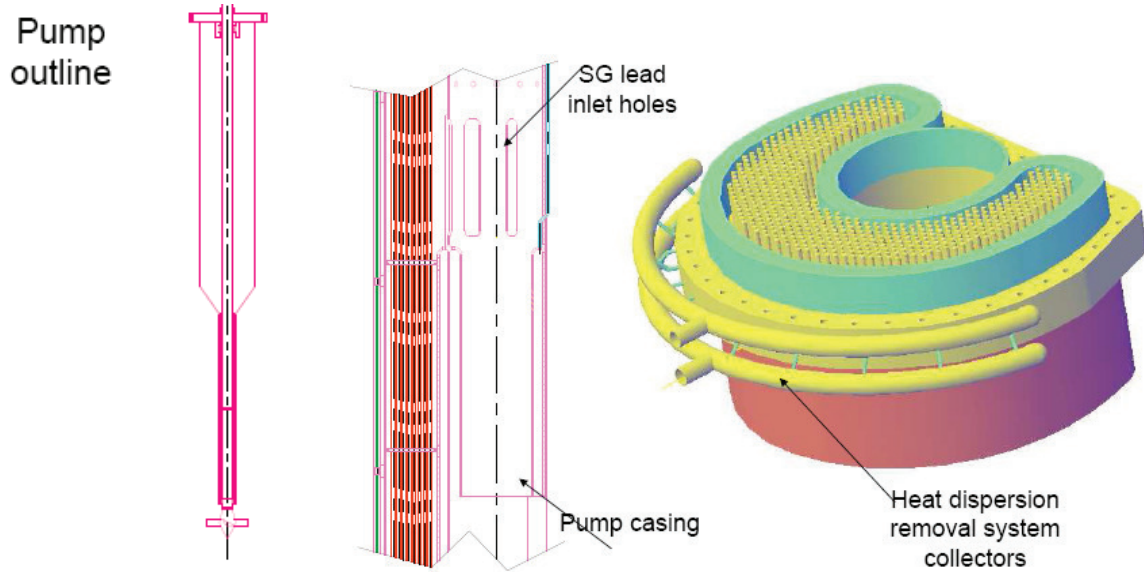


Fig. 2 – LEADER Project, ALFRED pump casing and heat dispersion removal system.

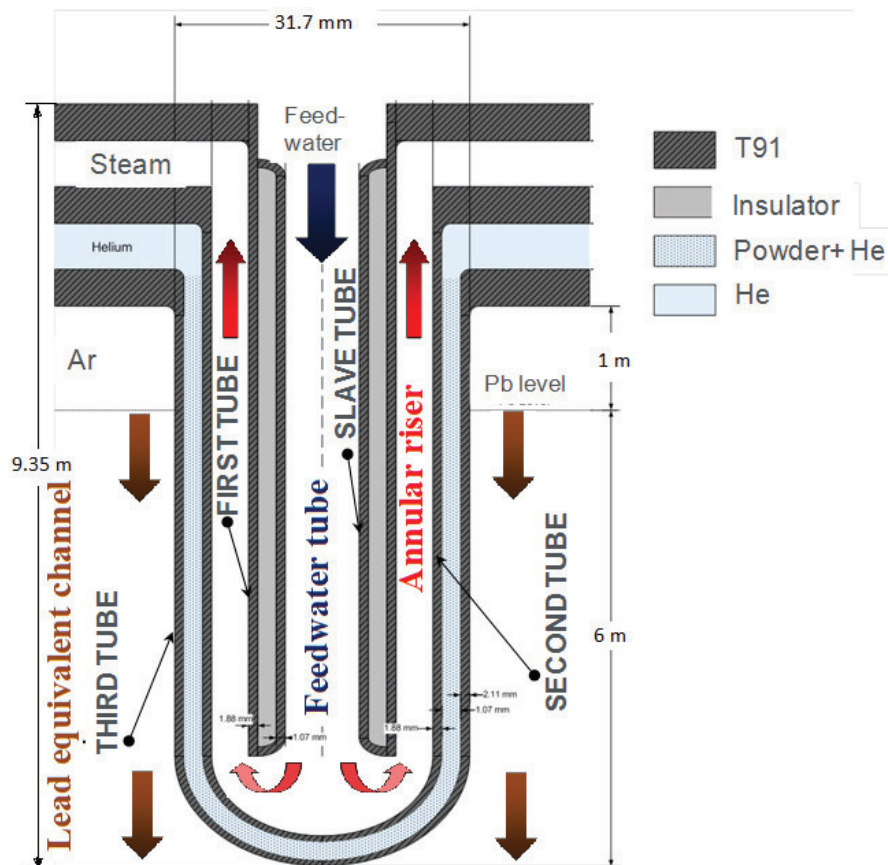


Fig. 3 – Scheme of the SG double wall bayonet tube of ALFRED.

Steam Generator general properties			
Description	Quantity	Description	Quantity
Removed Power [MW]	37.5	Number of tubes	510
Feed-water flow rate [kg/s]	24.1	Water pressure [bar]	180
Bundle geometry	triangular	Pitch / tube diameter	1.42
Feed-water temperature [°C]	335	Steam outlet temperature [°C]	450
Lead inlet temperature [°C]	480	Lead outlet temperature [°C]	400
Bayonet tube geometry			
Description	Quantity	Description	Quantity
Slave tube outer diameter [mm]	9.52	Slave tube thickness [mm]	1.07
Inner tube outer diameter [mm]	19.05	Inner tube thickness [mm]	1.88
Second tube outer diameter [mm]	25.40	Second tube thickness [mm]	1.88
Third tube outer diameter [mm]	31.37	Third tube thickness [mm]	2.11
Powder annular gap width [mm]	1.07	Length of heat exchange [mm]	6000
Argon plenum height [mm]	1000	He plenum height [mm]	800
Steam plenum height [mm]	800	T91 plates thickness [mm]	250
Feed-water flow rate [g/s]	47.3	Tube material	T91

Tab. 1 - ALFRED SG main data (from the conceptual design).

2.2 Identification of Potential Insulators for the Inner Tube

The reference solution proposed by ANSALDO is the use of RLHY-12 insulating paint embedded into an annular region made of T91 (see Fig. 3).

Two design solutions are considered in this work. The first option deals with the sandwich shell proposed by ANSALDO in which the insulating material is bounded by two tubes: traditional fillers, alternative composite materials or thermal insulating paints are examined. The second option is characterized by a single central inner tube joined with an outer insulating ceramic coating. Ten criteria have been developed in order to assess candidate materials suitable to guarantee thermal insulation between the feedwater tube and the annular riser ^[14].

Criterion 1 Thermal conductivity:

In order to minimize the heat transfer between feedwater and superheated steam, the conductivity has been fixed by ANSALDO equal or lower than 0.05 W/mK. As preliminary approach, this limit is increased up to 0.5 W/mK.

Criterion 2 Operating Temperature range:

The operative conditions expected in ALFRED SG are 335 °C in the feedwater line and 450 °C in the steam line. The integrity of the insulating material does not affect the heat removal safety function. Therefore, the maximum temperature can be conservatively fixed to 600 °C.

Criterion 3 Compatibility with tubes material:

The chemical interaction (essentially corrosion) between thermal insulating material and surrounding tubes is not allowed.

Criterion 4 Compatibility with water and steam:

Potential fast chemical reactions with oxygen, water or steam at high temperature (335-450°C) should be considered. They must be avoided.

Criterion 5 Thermo-physical transformations in the temperature range:

In the expected temperature operating conditions, transformations in thermo-physical properties of the candidate materials must be checked. In particular, it should be verified that temperature variations do not induce thermal conductivity increase, specific volume variations or formation of anisotropic strains within the material. Especially in ceramic coating, the worst consequence is separation and removal of insulating film from the tube wall. This may originate heterogeneity of the heat transfer.

Criterion 6 Thermo-mechanical effects in operating conditions:

An important matter is the preservation of the state of thermal insulating material during operation. Vibrations and tube differential thermal expansions due to thermal cycling can cause tubes sliding that induce localized strains within the thermal insulating material. The tube integrity should not be jeopardized by these effects.

Criterion 7 Resistance to radiation damage:

The effect of the radiation damage on thermo-physical properties (conductivity) of thermal insulating materials is quite unknown. Nevertheless, materials that experience strong nuclear reactions with neutrons should be avoided. It can be assumed that materials with high values of thermal neutron capture microscopic cross section (σ_a) that can originate activation are excluded. A limit of σ_a is fixed to 10 barn (in the thermal energy spectrum). Gamma radiation damage should be considered too.

Criterion 8 Ease of installation:

Materials must be characterized by easy techniques of installation and availability: deposition (for ceramic coating materials) or filling.

Criterion 9 Specific heat and mass density:

High specific heat and mass density lead to a low diffusivity coefficient. This last parameter is important in transient condition, when it is necessary to phase shift imposed thermal waves in time and to dampen them in intensity. Usually, insulating materials are characterized by low specific heat (below 2 kJ/kgK) and low density. No particular criterion is established as stringent requirement, in case of similar materials those with higher c_p are preferred.

Criterion 10 Cost:

Cost is the last parameter considered in the selection.

The investigated materials are summarized in *Tab. 2*. They are grouped in four categories:

- A. Traditional fillers,
- B. Alternative composite materials,
- C. Insulating paints and
- D. Ceramic coatings.

Additional details are available in Ref. [14]. The preliminary screening was conducted based on criteria 1 and 2 in order to reduce the amount investigations. The complete assessment was then performed. The partial results (for criterion 1 only) and the final summary of the investigations are included, respectively, in *Tab. 3* and *Tab. 4*. Only six materials survived the screening, they are considered potentially applicable to the ALFRED SG. Five materials refer to the sandwich shell design. Stone wool and Gemcowool® (two high temperature insulation wool produced by Refractory Specialties Incorporated) are traditional fillers. Pyrogel® (a silica aerogel insulation

blanket produced by Aspen Aerogels®) is an alternative composite material. Supertherm (developed by Enercheck Systems Inc. society) and RLHY-12 (produced by Beijing Ronglihengye Technology Company) are thermal insulating paints. The last material refers to tube outer coating. It is a Thermal Barrier Coating based on a recent and still under experimental investigation ceramic compound ($BaLa_2Ti_3O_{10}$), characterized by a thermal conductivity that is close to the acceptability limit.

CATEGORY	SUB-CATEGORY	MATERIALS
<i>Traditional fillers</i>	Mineral or rock wool	Glass wool
		Stone wool
	High temperature insulation wools	Alkaline-earth silicate glass wool
		Alumino-silicate glass wool
		Polycrystalline wool
	--	Fiberglass
	--	Cellular glass
	--	Vermiculite
	--	Perlite
	--	Calcium silicate
	Flexible elastomeric foams	Nitrile butadiene rubber
		Ethylene propylene diene monomer
	--	Polyethylene
Rigid foams	Polyurethane	
	Polyisocyanurate	
	Phenolic	
--	Polystyrene	
<i>Alternative composite materials</i>	Silica aerogel	Spaceloft®
		Pyrogel®
<i>Insulating paints</i>	--	NanoAyegh
	--	Atriathermika
	--	Thermo-Shield®
	--	Supertherm
	--	RLHY-12
<i>Ceramic coatings</i>	--	$BaLa_2Ti_3O_{10}$

Tab. 2 – Summary of the investigated insulating materials.

Material	Category	Conductivity [W/mK]	Criterion 1 limit [W/mK]	Margin k_{limit}/k	Judgment
Glass wool	A	0.04 (35°C) 0.2 (650°C)	0.5	>2.50	Accepted
Stone wool	A	0.04 (35°C) 0.22 (650°C)	0.5	>2.27	Accepted
Gemcowool®	A	0.05 (200°C) 0.23 (980°C)	0.5	>2.17	Accepted
Fiberglass	A	0.03 (35°C) 0.075 (430°C)	0.5	>6.67	Accepted
Cellular glass	A	0.04 (35°C) 0.08 (205°C)	0.5	>6.25	Accepted
Vermiculite	A	0.065 (25°C) 0.14 (1090°C)	0.5	>3.57	Accepted
Perlite	A	0.065 (35°C) 0.135 (500°C)	0.5	>3.70	Accepted
Calcium silicate	A	0.055 (25°C) 0.123 (540°C)	0.5	>4.06	Accepted
NBR	A	0.24 (25°C)	0.5	<2.08	Accepted
EPDM	A	0.21 (25°C)	0.5	<2.38	Accepted
Polyethylene	A	0.042 (10°C)	0.5	<11.90	Accepted
PUR	A	0.025 (25°C)	0.5	<20.00	Accepted
PIR	A	0.027 (25°C) 0.37 (95°C)	0.5	>1.35	Accepted
Phenolic	A	0.021 (25°C)	0.5	<23.81	Accepted
Polystyrene	A	0.03 (25°C)	0.5	<16.67	Accepted
Spaceloft®	B	0.014 (50°C) 0.018 (150°C)	0.5	>27.78	Accepted
Pyrogel®	B	0.02 (0°C) 0.09 (600°C)	0.5	>5.56	Accepted
NanoAyegh	C	-	0.5	-	Unknown
Atriathermika	C	0.02 (25°C)	0.5	<25.00	Accepted
ThermoShield®	C	0.055 (25°C)	0.5	<9.09	Accepted
Supertherm	C	0.019 (25°C)	0.5	<26.32	Accepted
RLHY-12	C	0.03 (25°C)	0.5	<16.67	Accepted
BaLa ₂ Ti ₃ O ₁₀	D	0.6 (300°C) 0.5 (900°C)	0.5	>0.84	Accepted

Tab. 3 – Preliminary screening, criterion 1: conductivity.

Material	Criterion									
	1	2	3	4	5	6	7	8	9	10
Glass wool	A	R	N/A	N/A	N/A	N/A	N/A	N/A	N/A	N/A
Stone wool	A	A	A	A	A	A	U	A	A	A
Gemcowool®	A	A	A	A	A	A	U	A	A	A
Fiberglass	A	R	N/A	N/A	N/A	N/A	N/A	N/A	N/A	N/A
Cellular glass	A	R	N/A	N/A	N/A	N/A	N/A	N/A	N/A	N/A
Vermiculite	A	A	A	A	U	R	U	N/A	N/A	N/A
Perlite	A	A	A	A	R	A	U	N/A	N/A	N/A
Calcium silicate	A	A	A	R	A	A	U	N/A	N/A	N/A
NBR	A	R	N/A	N/A	N/A	N/A	N/A	N/A	N/A	N/A
EPDM	A	R	N/A	N/A	N/A	N/A	N/A	N/A	N/A	N/A
Polyethylene	A	R	N/A	N/A	N/A	N/A	N/A	N/A	N/A	N/A
PUR	A	R	N/A	N/A	N/A	N/A	N/A	N/A	N/A	N/A
PIR	A	R	N/A	N/A	N/A	N/A	N/A	N/A	N/A	N/A
Phenolic	A	R	N/A	N/A	N/A	N/A	N/A	N/A	N/A	N/A
Polystyrene	A	R	N/A	N/A	N/A	N/A	N/A	N/A	N/A	N/A
Spaceloft®	A	R	N/A	N/A	N/A	N/A	N/A	N/A	N/A	N/A
Pyrogel®	A	A	A	A	A	A	U	A	A	A
NanoAyegh	U	R	N/A	N/A	N/A	N/A	N/A	N/A	N/A	N/A
Atriathermika	A	R	N/A	N/A	N/A	N/A	N/A	N/A	N/A	N/A
ThermoShield®	A	R	N/A	N/A	N/A	N/A	N/A	N/A	N/A	N/A
Supertherm	A	A	A	A	U	A	U	A	A	A
RLHY-12	A	A	A	A	A	A	U	A	A	A
BaLa ₂ Ti ₃ O ₁₀	A	A	U	U	A	A	U	A	A	A

A = Accepted
 R = Rejected
 U = Unknown
 N/A = Not Addressed

Tab. 4 – Summary of the results of the assessment of insulating materials.

3 Assessment of the SG Bayonet Tube by Means of RELAP-5

The single bayonet tube has been modeled by means of RELAP version 5.3.3. RELAP5 is a light water reactor transient analysis code developed by the U.S. Nuclear Regulatory Commission (NRC) for use in rulemaking, licensing audit calculations, evaluation of operator guidelines and as a basis for a nuclear plant analyzer. It is a highly generic code that, in addition to calculating the behavior of a reactor coolant system during a transient, can be used for simulation of a wide variety of hydraulic and thermal transients in both nuclear and non-nuclear systems involving mixtures of steam, water, non-condensable and solute ^{[16] [17]}. In particular the version 5.3.3 has the capability to include the lead and LBE as coolant material.

Due to the bundle pitch to diameter ratio (1.45), the model is considered representative of the SG. In fact, as reported in the literature ^[18], for $P/D > 1.35$ the single unit can be considered un-coupled with the boundary units. A schematic overview of the nodalization adopted is reported in *Fig. 4*. The model includes: the feedwater tube, the annular steam riser and the equivalent lead channel. The analysis has been developed on the basis of the following assumptions:

- The heat exchange between the annular steam riser and the Argon zone has been neglected, that means adiabatic behavior of the non-active region located outside the tube.
- The conductivity of the insulating paint has been fixed, in agreement with ANSALDO Nucleare recommendations ^[19], to 0.05 W/mK.
- The filling powder is assumed as 0.3 porosity synthetic diamond based on the experimental tests and the pretest calculations reported in Refs. [10] and [12]. Its conductivity has been selected on the basis of Ref. [10]. Therefore, two different equations are adopted to calculate this quantity, it is assumed that they provide a realistic boundary of the effective conductivity (see also section 3.2). They are labeled as Case 1 and Case 2.
- The heat transfer between the lead side and the annular riser is modeled according to the Mikityuk correlation that has been developed for fuel rod bundle ^[20].

The detailed input deck is included in Ref. [21].

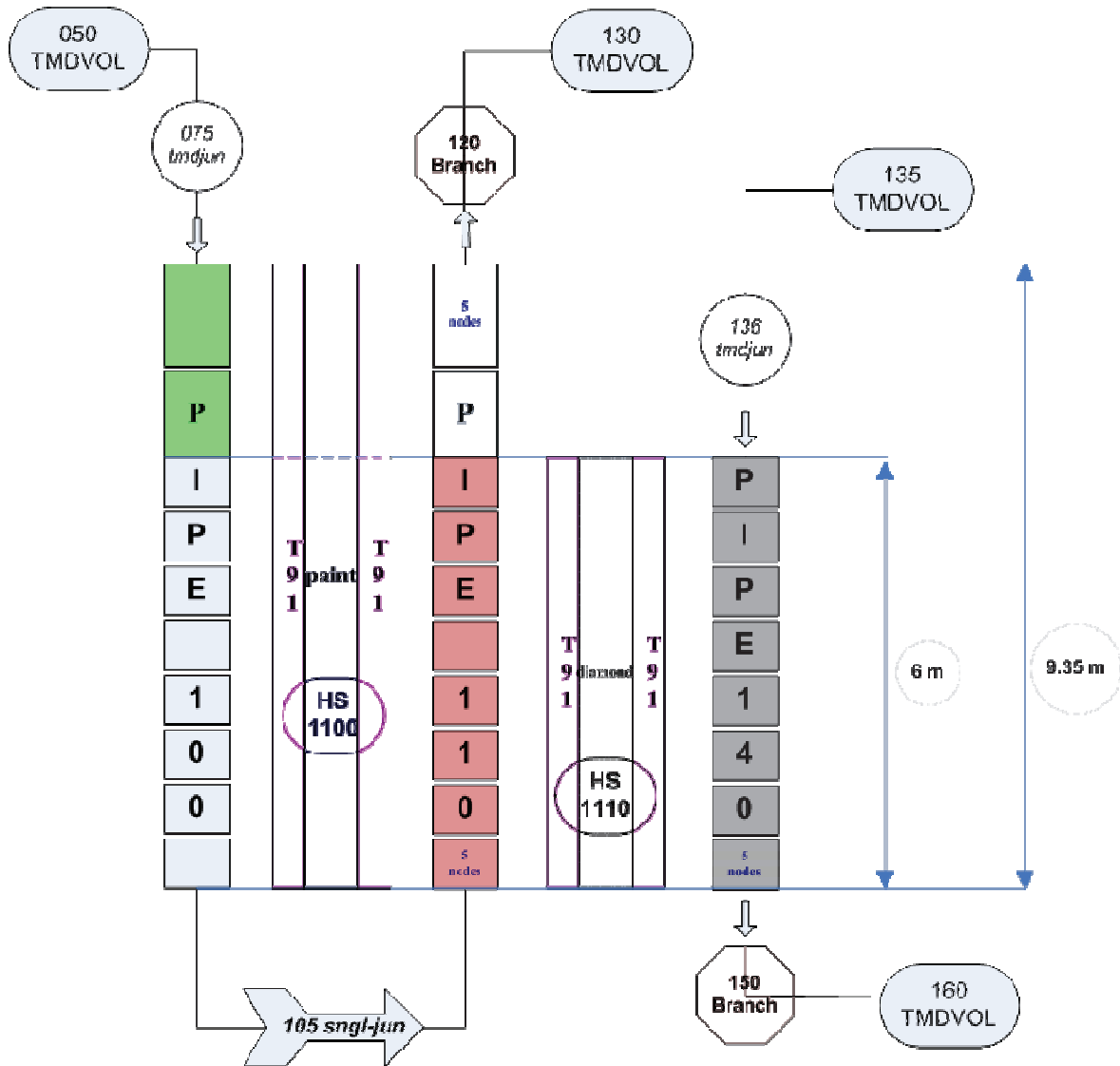


Fig. 4 – ALFRED SG double wall bayonet tube, RELAP-5.3.3 model.

3.1 Development of the Reference Nodalization

The description of feedwater tube (pipe 100), annular steam riser (pipe 110) and equivalent lead channel (pipe 140) hydrodynamic components is reported from *Tab. 5* to *Tab. 7*. The tables include the correlations adopted to calculate the quantities derived from the thermal hydraulic and geometrical data attached in *Tab. 1*. The hydraulic diameter of the equivalent lead channel is calculated assuming triangular array infinite bundle (that means hydraulic diameter equal to heated diameter).

The description of the heat structure between the feedwater tube and the annular riser (HS-1100) is given in *Tab. 8*. The main features of the heat structure between the annular riser and the equivalent lead channel (HS-1110) is summarized in *Tab. 9*.

COMPONENT LABEL		TYPE	DESCRIPTION
Pipe 100		Hydrodynamic component	Feedwater tube
Id.	Parameter	Quantity	Notes
a	Axial node height	0.33500 m	--
b	N° axial nodes	10	--
c	Axial node height	0.15000	--
d	N° axial nodes	40	--
e	Inner radius	0.00369 m	--
f	Flow area	$4.27762 \cdot 10^{-5} \text{ m}^2$	$f = \pi e^2$
g	Operating pressure	180 bar	--
h	Inlet temperature	335 °C	--
i	Mass flow	0.047255 kg/s	
j	Hydraulic diameter	0.00738 m	$j = 2 \cdot e$

Tab. 5 - ALFRED SG, hydrodynamic modeling of the feedwater tube.

COMPONENT LABEL		TYPE	DESCRIPTION
Pipe 110		Hydrodynamic component	Steam riser
Id.	Parameter	Quantity	Notes
a	Axial node height	0.15000 m	--
b	N° axial nodes	40	--
c	Axial node height	0.33500 m	--
d	N° axial nodes	10	--
e	Annulus inner radius	0.00952 m	--
f	Annulus outer radius	0.01082 m	--
g	Flow area	$8.27708 \cdot 10^{-5} \text{ m}^2$	$g = (f^2 - e^2) \cdot \pi$
h	Operating pressure	180 bar	--
i	Inlet temperature	335 °C	--
j	Mass flow	0.047255 kg/s	--
k	Hydraulic diameter	0.00259 m	$k = 4 \cdot g / [2 \pi \cdot (f + e)]$

Tab. 6 - ALFRED SG hydrodynamic modeling of the annular steam riser.

COMPONENT LABEL		TYPE	DESCRIPTION
Pipe 140		Hydrodynamic component	Lead channel
Id.	Parameter	Quantity	Notes
a	Axial node height	0.15000 m	--
b	N° axial nodes	40	--
c	Tube bundle pitch (triangular)	0.04500 m	--
d	Inner radius	0.01586 m	--
e	Equivalent flow area	$9.629680 \cdot 10^{-4} \text{ m}^2$	$e = \{ [(c^2 \cdot 2) \cdot (\cos(\pi / 6))] - [(\pi \cdot d^2) / 2] \} \cdot 2$
f	Operating pressure	1.6 bar	--
g	Inlet temperature	335 °C	--
h	Mass flow	6.367647 kg/s	--
i	Hydraulic diameter (heated)	0.03864 m	$i = 4 \cdot e / 2 \pi \cdot d$

Tab. 7 - ALFRED SG, hydrodynamic modeling of the lead channel.

COMPONENT LABEL		TYPE	DESCRIPTION
1100		Heat structure	Heat transfer between 100-110
Id.	Parameter	Quantity	Notes
a	Axial node height	0.33500 m	--
b	N° axial nodes	10	--
c	Axial node height	0.15000 m	--
d	N° axial nodes	40	--
e	Inner radius	0.00369 m	--
f	Radial interval width	$2.14000 \cdot 10^{-4}$ m	T91
g	N° radial intervals	5	T91
h	Radial interval width	$3.20556 \cdot 10^{-4}$ m	Insulator
i	N° radial intervals	9	Insulator
j	Radial interval width	$3.76000 \cdot 10^{-4}$ m	T91
k	N° radial intervals	5	T91
l	Initial temperature	335 °C	--
m	<i>Inner flow area</i>	$4.27762 \cdot 10^{-5}$ m ²	$m = \pi c^2$
n	Left boundary heated diameter	0.00738 m	$n = 4 \cdot m / 2 \pi \cdot e$
o	<i>Annulus inner radius</i>	0.00952 m	--
p	<i>Annulus outer radius</i>	0.01082 m	--
q	<i>Equivalent flow area</i>	$8.27708 \cdot 10^{-5}$ m ²	$q = (p^2 - o^2) \cdot \pi$
r	Right boundary heated diameter	0.00553 m	$r = 4 \cdot q / 2 \pi \cdot o$

Tab. 8 - ALFRED SG, modeling of the heat structure between the feedwater tube and the annular riser.

COMPONENT LABEL		TYPE	DESCRIPTION
1110		Heat structure	Heat transfer between 110-140
Id.	Parameter	Quantity	Notes
a	Axial node height	0.15000 m	--
b	N° axial nodes	40	--
c	Inner radius	0.01082 m	--
d	Radial interval width	1.88000*10 ⁻⁴ m	T91
e	N° radial intervals	10	T91
f	Radial interval width	1.07000*10 ⁻⁴ m	C powder
g	N° radial intervals	10	C powder
h	Radial interval width	2.09500*10 ⁻⁴ m	T91
i	N° radial intervals	10	T91
j	Initial temperature	335 °C	--
k	<i>Annulus inner radius</i>	0.00952 m	--
l	<i>Annulus outer radius</i>	0.01082 m	--
m	<i>Flow area</i>	8.27708*10 ⁻⁵ m ²	$m = (l^2 - k^2) * \pi$
n	Left boundary heated diameter	0.00487 m	$n = 4 * m / 2 * \pi * l$
o	Riser natural circulation height	9.35000 m	--
p	Left boundary fouling factor	1.105	--
q	Tube bundle pitch (triangular)	0.04500 m	--
r	<i>Right boundary outer radius</i>	0.01586 m	--
s	<i>Equivalent flow area</i>	96.29680*10 ⁻⁵ m ²	$s = \{[(q^2 * 2) * (\cos(\pi / 6))]\} - [(\pi * r^2) / 2]\} * 2$
t	Right boundary heated diameter	0.03864 m	$t = 4 * s / 2 * \pi * r$
u	Lead natural circulation height	6.00000 m	--
v	Pitch to diameter ratio	1.4182	$v = q / 2 * r$
w	Right boundary fouling factor	1.105	--

Tab. 9 - ALFRED SG, modeling of the heat structure between the annular riser and the lead channel (active height only).

3.2 Assessment of the Reference Nodalization

Two distinct cases are analyzed in the reference simulations. They are labeled as case 1 and case 2. Both the calculations assume the annular gap filled by diamond powder at 0.3 porosity. The thermal conductivity of diamond is calculated based on the following correlations ^[10]:

Case 1

$$k_m = k_s^{(1 - \varphi)} * k_f^\varphi \quad \text{Eq. 1}$$

Case 2

$$k_m / k_f = [\lambda]^{(0.208 - 0.757 * \log \varphi - 0.057 * \log \lambda)} \quad \text{Eq. 2}$$

where

φ is the porosity [/],

k is the thermal conductivity [W/(m*K)],
 s, f, m refers to solid, fluid and overall volume respectively,
 $\lambda = (k_s / k_f)$

The conductivity of diamond powder as function of porosity is depicted in *Fig. 5*. It should be pointed out that each correlation calculates the conductivity based on a simple function that depends upon three parameters:

1. The conductivity of the solid material (99.5% dense),
2. The conductivity of the fluid dispersed in the powder and
3. The porosity.

The weakness points of the correlations can be summarized as follow:

1. They are ideal correlations, and apply in specific range of porosity,
2. Each correlation investigated assumes spherical particles and does not account for the particle shape influence and
3. The influence of the particles diameter is not considered.

However, they are considered to embed (or at least provide a lower band) the real conductivity. Experimental campaigns are ongoing at ENEA CR Brasimone in the TxP Facility to assess the conductivity of different powders ^[12]. The analysis is subdivided in three main parts. The first one deals with the assessment of the hydrodynamic components. The second one focuses on the thermal structures, and the last one highlights the thermal-hydraulic behavior of the bayonet tube. Systematic comparison between the reference simulations and the results obtained by ANSALDO Nucleare is performed (when data are available).

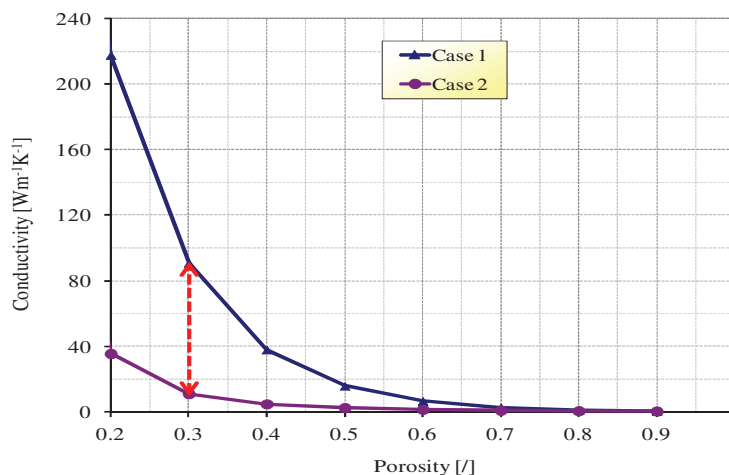



Fig. 5 – Thermal conductivity of diamond powder as function of porosity, calculated by Case 1 and Case 2 correlations, 200 °C.

3.2.1 Assessment of the Hydrodynamic Components

The results of the simulations are summarized in *Tab. 10*. The table contains the inlet and outlet temperature of each hydrodynamic component, the void fraction at tube outlet, the pressure drop in the bayonet unit and the lead velocity in the equivalent channel. The quantities refer to Case 1, Case 2 and ANSALDO Nucleare calculations ^[19].

 Ricerca Sistema Elettrico	Sigla di identificazione	Rev.	Distrib.	Pag.	di
	NNFISS - LP3 - 054	0	L	33	117

The details of the main thermal-hydraulic parameters are depicted in *Fig. 6 a)* and *b)*. They deal with Case 1 and Case 2 respectively. Each figure reports:

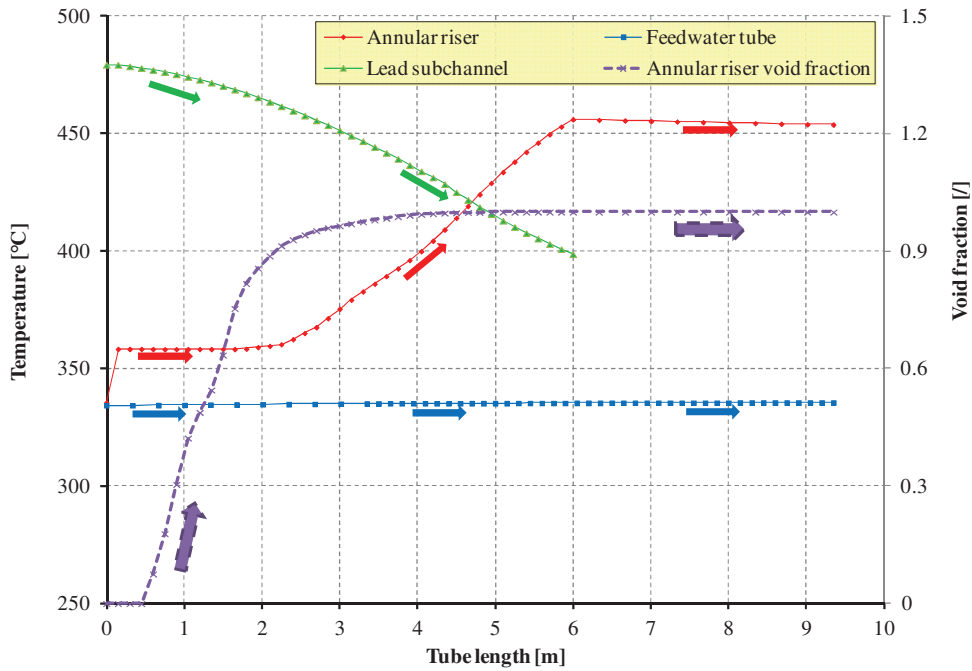
- The feedwater tube temperature as function of the tube length,
- The steam temperature in the annular riser as function of its length,
- The primary coolant temperature (only the lead submerged length) and
- The void fraction as function of annular riser axial elevation.

In agreement with ANSALDO, both the reference simulations predict a temperature increase in the feedwater tube in the range of 1.0 °C – 1.2 °C. The maximum steam temperature is predicted in the range 438-456 °C depending on the diamond conductivity (Case 2 and Case1 respectively). The ANSALDO simulation agrees with Case 1. In all the simulations the lead temperature drop is in the order of 80 °C. Void fraction close to 1 is reached within the first 3 meters of the annular riser (Case 1, Case 2 and ANSALDO) although different void fraction trends are highlighted in the three simulation before 3 m. In particular, ANSALDO calculations ^[19] highlight a void fraction plateau between 1.5 and 2 meters. This could be related to modeling issues (annulus component is used in ANSALDO model instead of pipe) and/or to the effect of an eventual spacer grid. Furthermore, the reference void fraction reaches the unit in a smoother way.

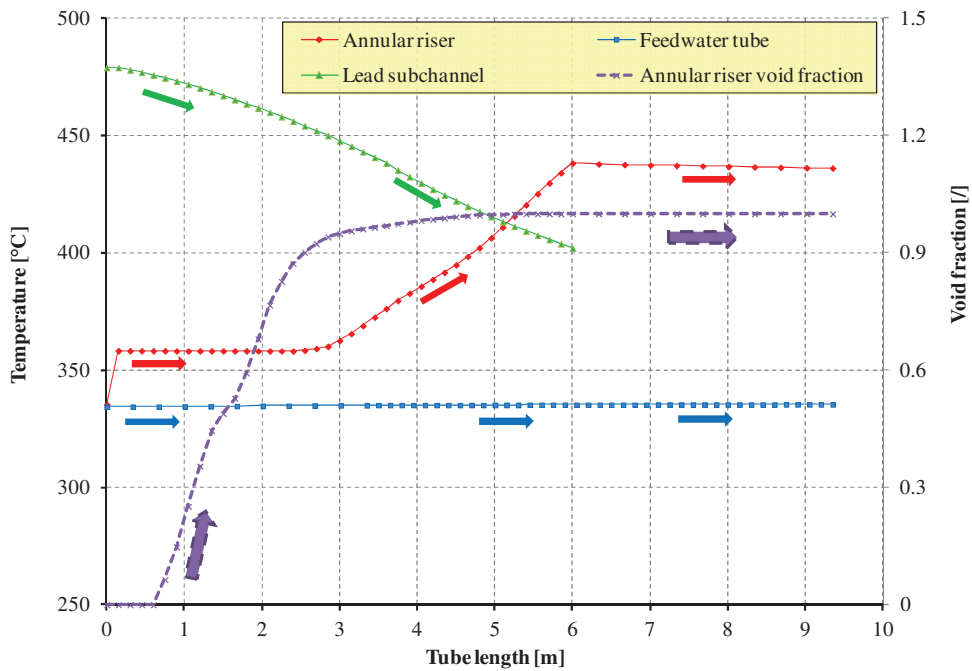
Pressure drops and velocities are represented in *Fig. 7* and *Fig. 8* (the indexes *a)* and *b)* refer to Case 1 and Case 2 respectively). The figures report:

- The feedwater pressure drop as function of the tube length, *Fig. 7*;
- The water-steam pressure drop in the annular riser as function of its length, *Fig. 7*;
- The lead velocity (only in the immersed tube length), *Fig. 8*;
- The feedwater velocity as function of the tube length, *Fig. 8*;
- The water phase velocity in the annular riser as function of axial elevation, *Fig. 8* and
- The steam phase velocity in the annular riser as function of its length, *Fig. 8*.

The total pressure drop in the bayonet tube is predicted in the range of 2.6 bar – 2.8 bar. These values are close to the ANSALDO results even if they are lower. In the reference simulations, the lead and the feedwater velocities are characterized by approximately constant values along the tube length. These are equal to about 0.65 m/s in the lead channel and about 1.70 m/s in the feedwater side. The water and steam phase velocities increase within the lead submerged height (first 6 meters) because of boiling. Then, in the upper superheated steam zone, the super-heated steam velocity is predicted approximately constant in the range of 8 m/s – 8.5 m/s.

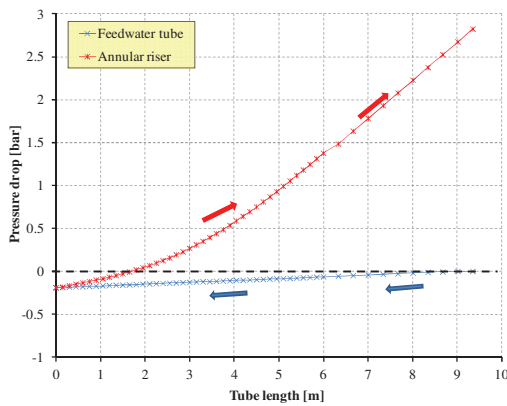


a) Case 1

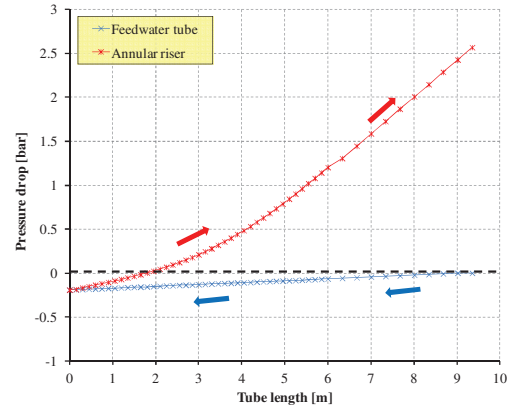


b) Case 2

Fig. 6 – SGBT vs. RELAP5 v 3.3, reference simulations, void fraction, water and lead temperatures as function of tube length.

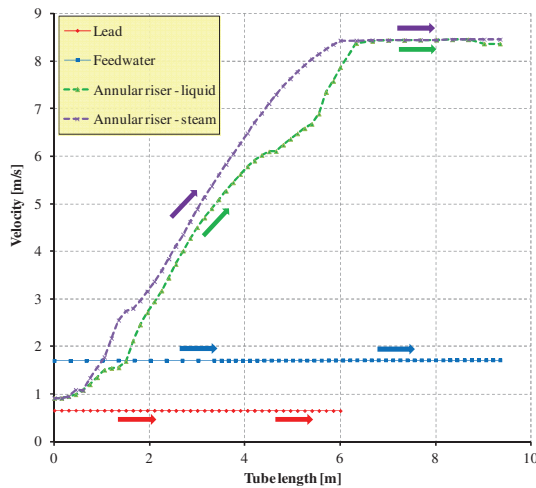


a) Case 1

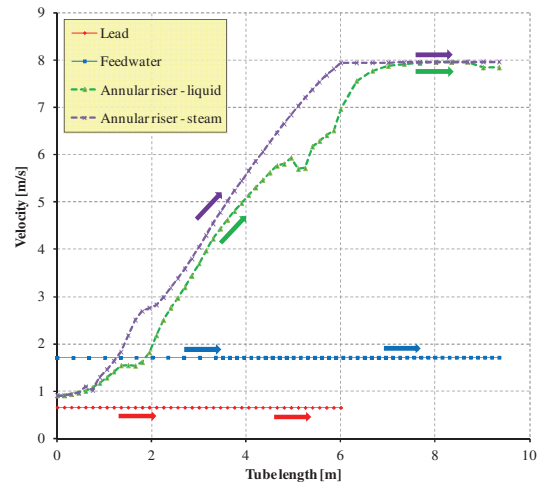


b) Case 2

Fig. 7 – SGBT vs. RELAP5 v 3.3, reference simulations, pressure drops.



a) Case 1



b) Case 2


Fig. 8 – SGBT vs. RELAP5 v 3.3, reference simulations, velocities.

Parameter	Unit	Calc. Ref. CASE 1	Calc. Ref. CASE2	Calc. ANSALDO
Lead inlet temperature	°C	479.4	479.0	480.0
Lead outlet temperature	°C	400.4	402.1	401.5
Feedwater inlet temperature	°C	334.4	334.4	335.0
Feedwater tube temperature drop	°C	1.2	1.0	<5.0
Immersed tube steam temperature	°C	456.1	438.3	451.5
Superheated steam outlet temperature	°C	453.9	436.1	450.1
Void fraction	--	1.0	1.0	1.0
Pressure drop	bar	2.8	2.6	3.3
Lead velocity	m/s	0.652	0.652	--
Lead velocity peak factor	--	1.004	1.004	--

Tab. 10 - SGBT vs. RELAP5 v 3.3, reference simulations, assessment of hydrodynamic components.

3.2.2 Assessment of the Heat Structures

The assessment of the heat structures is summarized in Tab. 11. The table contains the average heat fluxes and surface temperatures in the feedwater tube and the annular riser surface boundaries. The

 Ricerca Sistema Elettrico	Sigla di identificazione	Rev.	Distrib.	Pag.	di
	NNFISS - LP3 - 054	0	L	36	117

axial peak factor is also reported. Moreover, the table includes the total power exchanged by the annular riser outer surface with the lead side. The quantities reported in the table refer to Case 1, Case 2 and ANSALDO Nucleare calculations (when available) ^[19].

The thermal parameters of the feedwater tube are depicted from *Fig. 9* to *Fig. 11*. Those of the annular riser are given from *Fig. 12* to *Fig. 14*. The indexes *a*) and *b*) refer to Case 1 and Case 2 respectively. The figures include the following quantities:

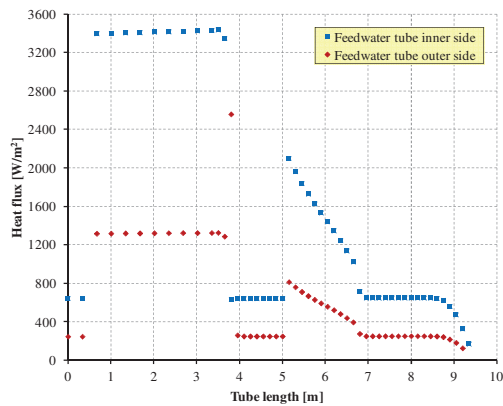
- The heat flux that crosses the inner surface as function of the tube length,
- The heat flux that crosses the outer surface as function of the length,
- The heat transfer coefficient (HTC) at the inner surface as function of the tube length,
- The HTC at the outer surface as function of the length,
- The temperature at the inner surface as function of the tube length and
- The temperature at the outer surface as function of the length.

In the reference simulations, the feedwater tube heat flux at the inner side shows three discontinuities, *Fig. 9*. The first one is at the steam outlet, the second one is about 4 meters far from the outlet, close to the end of the active region and, the last one, is located in the active region between 5-7 m. The outer side heat flux trend is similar to the inner side, it is scaled by the outer to inner surface ratio. The inner side HTC and surface temperature are approximately constant, this is due to the contact with sub-cooled water. The outer side HTC and surface temperature have a discontinuous behavior that reveals the occurrence of several heat transfer modes, *Fig. 10* and *Fig. 11*. In order to explain these trends, further investigations are given in the next sub-section.

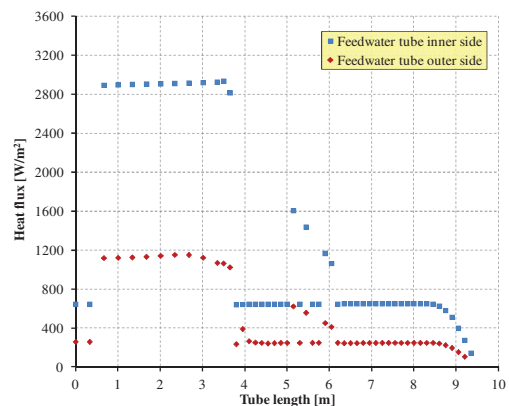
Both the reference simulations highlight a continuous increase of the heat flux at the outer and inner sides of the annular riser within the first 2.0 - 2.5 meters, *Fig. 12*. In fact, at the tube bottom, the water reaches saturated condition and begins to boil. This is reflected in the corresponding high HTC (*Fig. 13*). When superheated steam is reached, the HTC (and thus the heat flux at the inner side), decreases. At the outer side, the HTC is approximately constant, according to the Mikityuk correlation. The maximum temperature is close to 470 °C and it is reached at the end of the active length, *Fig. 14*. In agreement with ANSALDO calculations, the total power removed by the bayonet tube is in the range of 71.3 kW – 74.5 kW.

Parameter	Unit	Calc. Ref. CASE 1	Calc. Ref. CASE2	Calc. ANSALDO
Average heat flux feedwater tube ID	W/m ²	1769	1470	--
Heat flux peak factor feedwater tube ID	--	1.940	1.997	--
Average heat flux feedwater tube OD	W/m ²	722	569	--
Heat flux peak factor feedwater tube OD	--	3.540	2.028	--
Average heat flux annular riser ID	W/m ²	182675	174951	--
Axial heat flux peak factor annular riser ID	--	1.700	1.512	--
Average heat flux annular riser OD	W/m ²	124585	119316	--
Heat flux peak factor annular riser OD	--	1.700	1.512	--
Average temperature feedwater tube ID	°C	335.3	335.2	--
Axial temperature peak factor feedwater tube ID	--	1.001	1.001	--
Average temperature feedwater tube OD	°C	397.3	386.8	--
Axial temperature peak factor feedwater tube OD	--	1.147	1.132	--
Average temperature annular riser ID	°C	408.8	395.0	--
Axial temperature peak factor annular riser ID	--	1.146	1.155	--
Average temperature annular riser OD	°C	431.8	430.3	--
Axial temperature peak factor annular riser OD	--	1.101	1.099	--
Total power removed annular riser OD	kW	74.514	71.362	73.764

Tab. 11 - SGBT vs. RELAP5 v 3.3, reference simulations, assessment of heat structures.

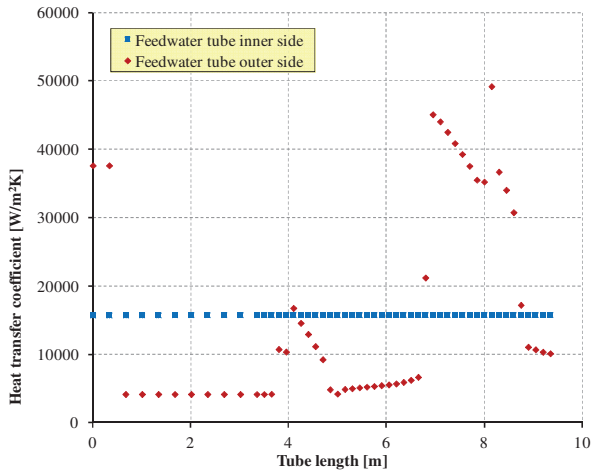


a) Case 1

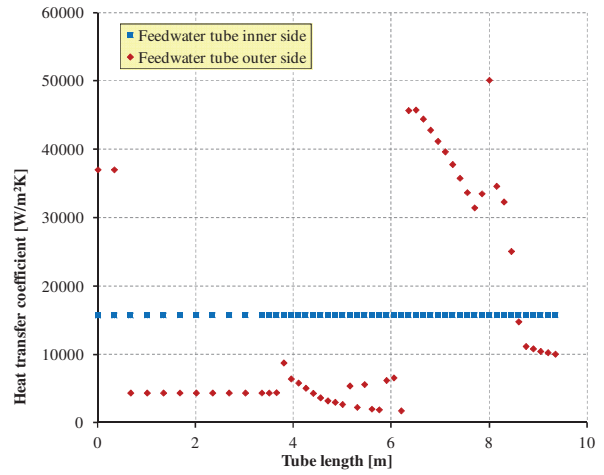


b) Case 2

Fig. 9 – SGBT vs. RELAP5 v 3.3, reference simulations, heat flux in the feedwater tube as function of tube length.

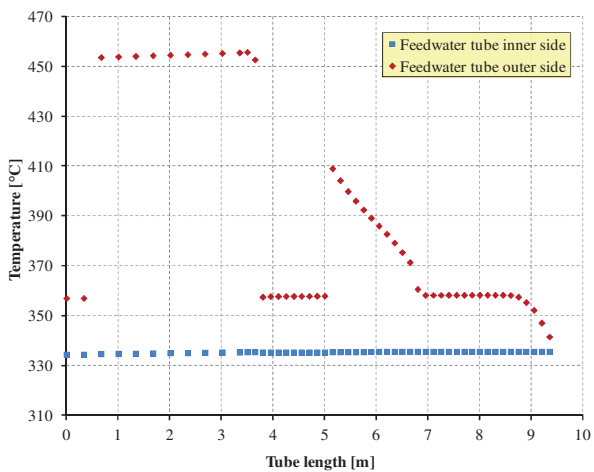


a) Case 1

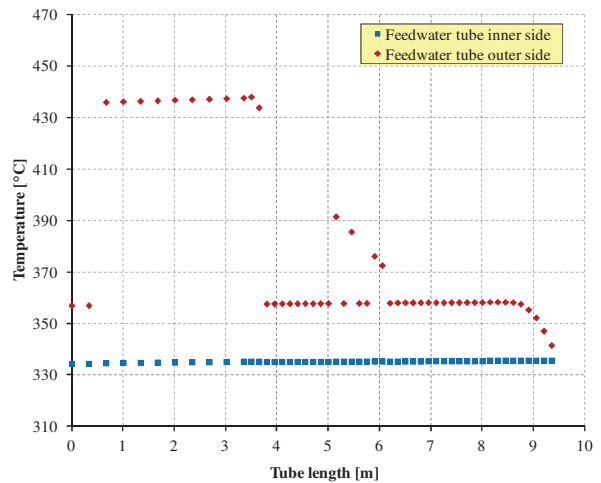


b) Case 2

Fig. 10 – SGBT vs. RELAP5 v 3.3, reference simulations, convection HTC at the feedwater tube surfaces as function of tube length.

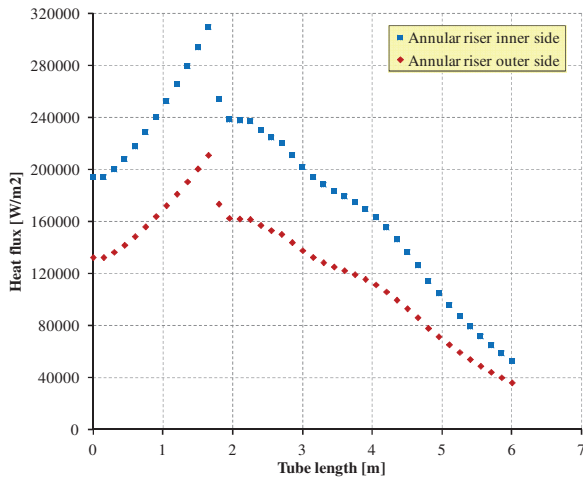


a) Case 1

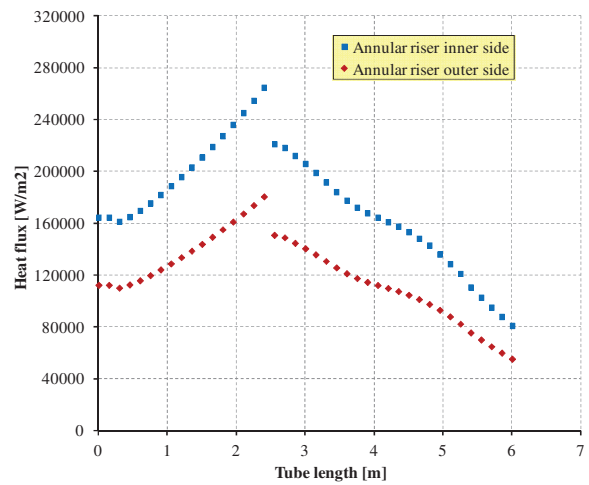


b) Case 2

Fig. 11 – SGBT vs. RELAP5 v 3.3, reference simulations, temperatures at the feedwater tube surfaces as function of tube length.

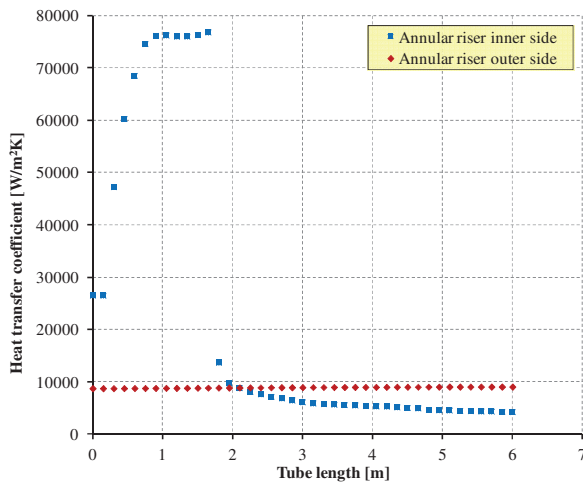


a) Case 1

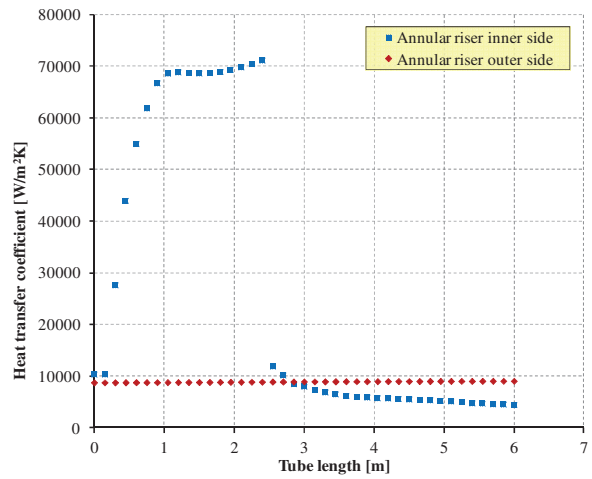


b) Case 2

Fig. 12 – SGBT vs. RELAP5 v 3.3, reference simulations, heat flux in the annular riser as function of tube length.

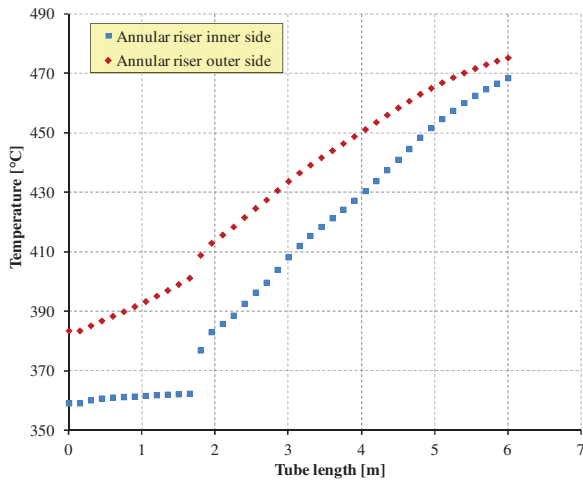


a) Case 1

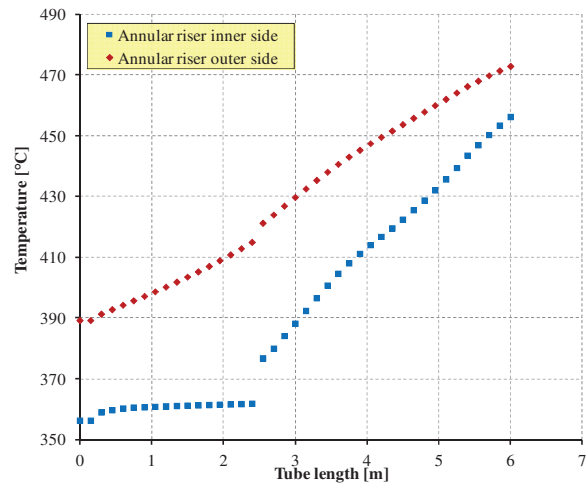


b) Case 2

Fig. 13 – SGBT vs. RELAP5 v 3.3, reference simulations, convection HTC in the annular riser as function of tube length.



a) Case 1



b) Case 2

Fig. 14 – SGBT vs. RELAP5 v 3.3, reference simulations, temperatures at annular riser surfaces as function of tube length.

3.2.3 Assessment of 2 ϕ Dynamics in the Water Steam Side

The present section is aimed to point out the main thermal-hydraulic phenomena that occur in the water-steam side of the bayonet tube [22] [23] [24]. RELAP5 code selects the flow regime in the two-phase bulk through a series of parameters, such as the void fraction (to switch the flow regime) and the ΔT_{gw} “wall surface temp. – steam temp.” (to reach and overpass CHF conditions), Fig. 15 [25]. In this way, it is possible to predict the interfacial heat transfer mode inside each volume. The heat transfer mode between the tube surfaces and the steam-water mixture is selected according to the boiling curve used in RELAP5 to govern the selection of heat transfer correlations (Fig. 16, in which T_{spp} is the saturation temperature based on the partial pressure of steam in the bulk, T_w is the wall surface temperature and T_{spt} is the saturation temperature based on the total pressure [25]).

Three pictures are given in Fig. 17, they are representative of Case 1.

- The heat transfer modes at the feedwater tube outer wall are reported in the first picture. The figure includes the temperature difference ΔT_{gw} “steam - wall surface” and the HTC at the tube wall. The following modes are predicted:
 - Single-phase liquid convection at low void fractions.
 - Two large zones in which condensation takes place at low and high void fractions (>0.9). They are separated by a zone in which relatively high temperature liquid film is predicted at tube surface ($\Delta T_{gw} < 0$ in this zone) that induces the code to assume single-phase liquid convection at supercritical pressure mode.
 - Wall drying and single-phase vapor convection takes place in the higher part of the active length.
 - Condensation starts again at the tube outlet, 2.5m far from the active length. The liquid fraction is very low and the code predicts $v_f=1.0000$ and $v_g= 1.15379E-06$.
 - This sequence of heat transfer regimes (in particular the condensation) explains the heat flux and surface temperature trends in the feedwater tube.
- In the intermediate picture, the flow regimes and the corresponding void fraction in the annular riser are reported:

- Bubbly flow, slug flow and annular mist flow are predicted to occur within 2 meters in the void fraction range 0.0-0.9.
- Mist flow dominates the remaining part of the active length with the exception of the last nodes in which post CHF mist flow takes place (that corresponds to feedwater tube wall post dry-out).
- Above the active length pre CHF mist flow is predicted, this could be connected with the condensation that occurs at tube outlet and the adiabatic conditions at the outer wall of the third tube (instead of heat exchange with Ar, He and steam).
- In the third picture the heat transfer modes at the annular riser inner wall are reported. The figure includes the temperature difference ΔT_{gw} “wall surface – steam” and the HTC at the tube wall. The following regimes are predicted:
 - Sub-cooled nucleate boiling at low void fractions.
 - Saturated nucleate boiling and saturated transition boiling up to void fraction of about 0.85.
 - When ΔT_{gw} becomes negative (-30°C) the wall temperature largely exceed the steam temperature, it is the film boiling mode.
 - Wall drying and single-phase vapor convection takes place in the higher part of the active length.

Case 2 is depicted in *Fig. 18*. The considerations reported above apply to this case too. The main differences can be summarized as follows:

- Feedwater tube outer side: oscillations between single-phase liquid convection at supercritical pressure and condensation are observed instead of one zone characterized by single-phase liquid convection at supercritical pressure heat transfer.
- Flow regimes in the bulk: post CHF mist flow regime is never reached.

Should be pointed out that condensation is not expected in the normal operation of the main nuclear power plants that rely on U-tube or straight tube SG. RELAP5 code has been designed for Light Water Reactor (LWR) and it is suitable for these types of SG. Therefore, it is not completely accurate in simulating the bayonet tube configuration. Nevertheless, although the accuracy of the results should be verified, condensation phenomena are predicted to take place in the bayonet tube close to the feedwater tube surface. In particular, condensation above the active length at tube outlet should be avoided.

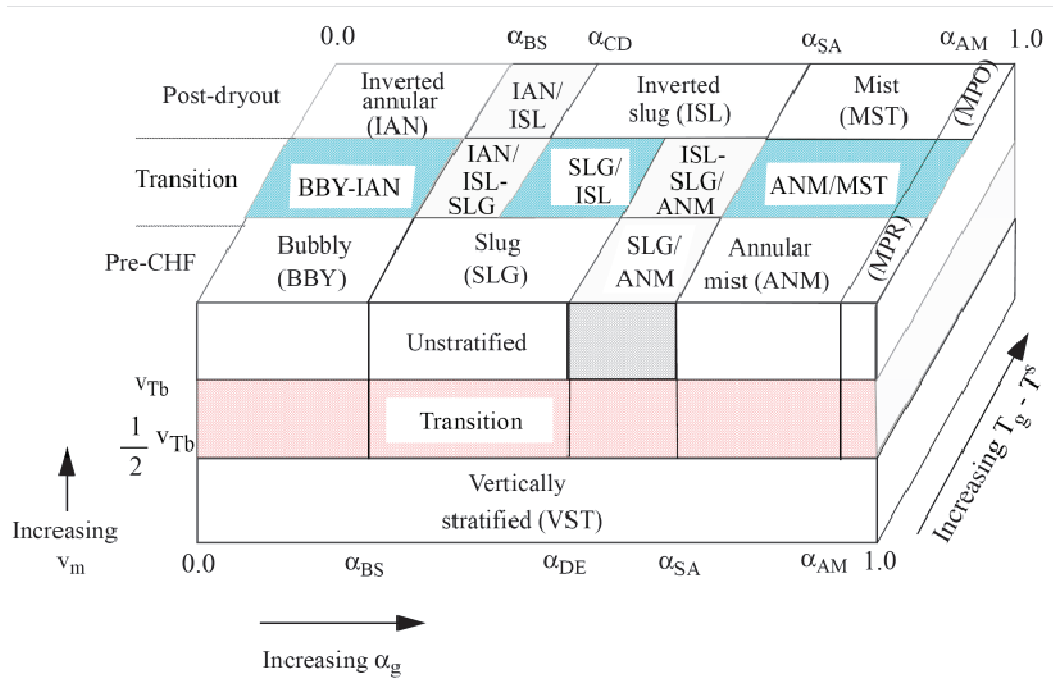


Fig. 15 – Flow regimes for vertical ducts according to RELAP-5.

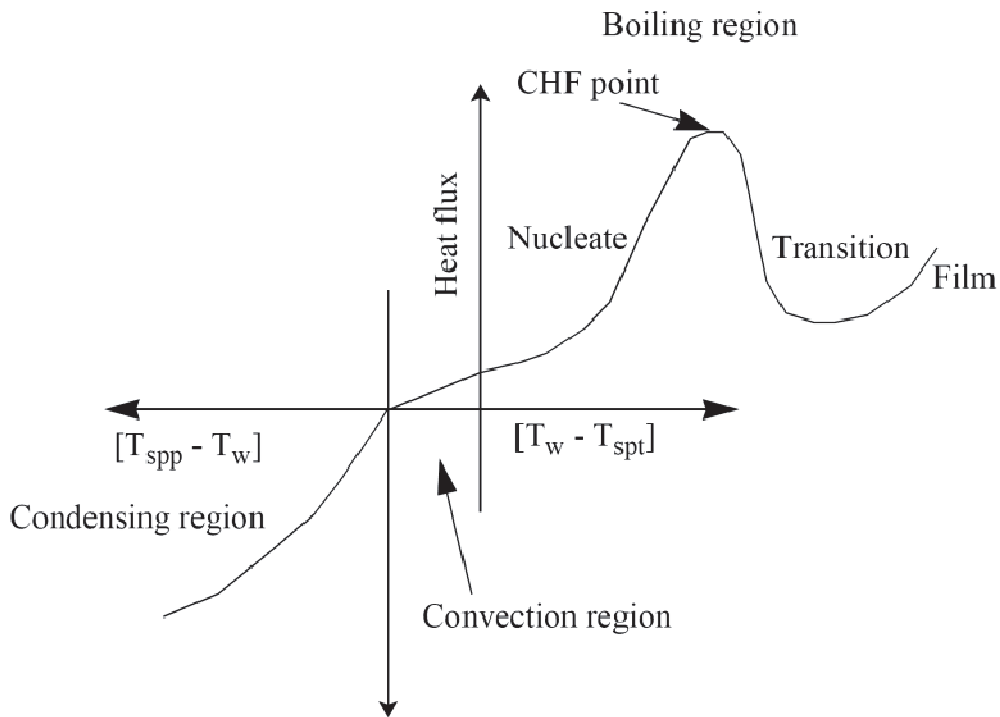


Fig. 16 – Heat transfer mode map at heat structures boundaries according to RELAP-5.

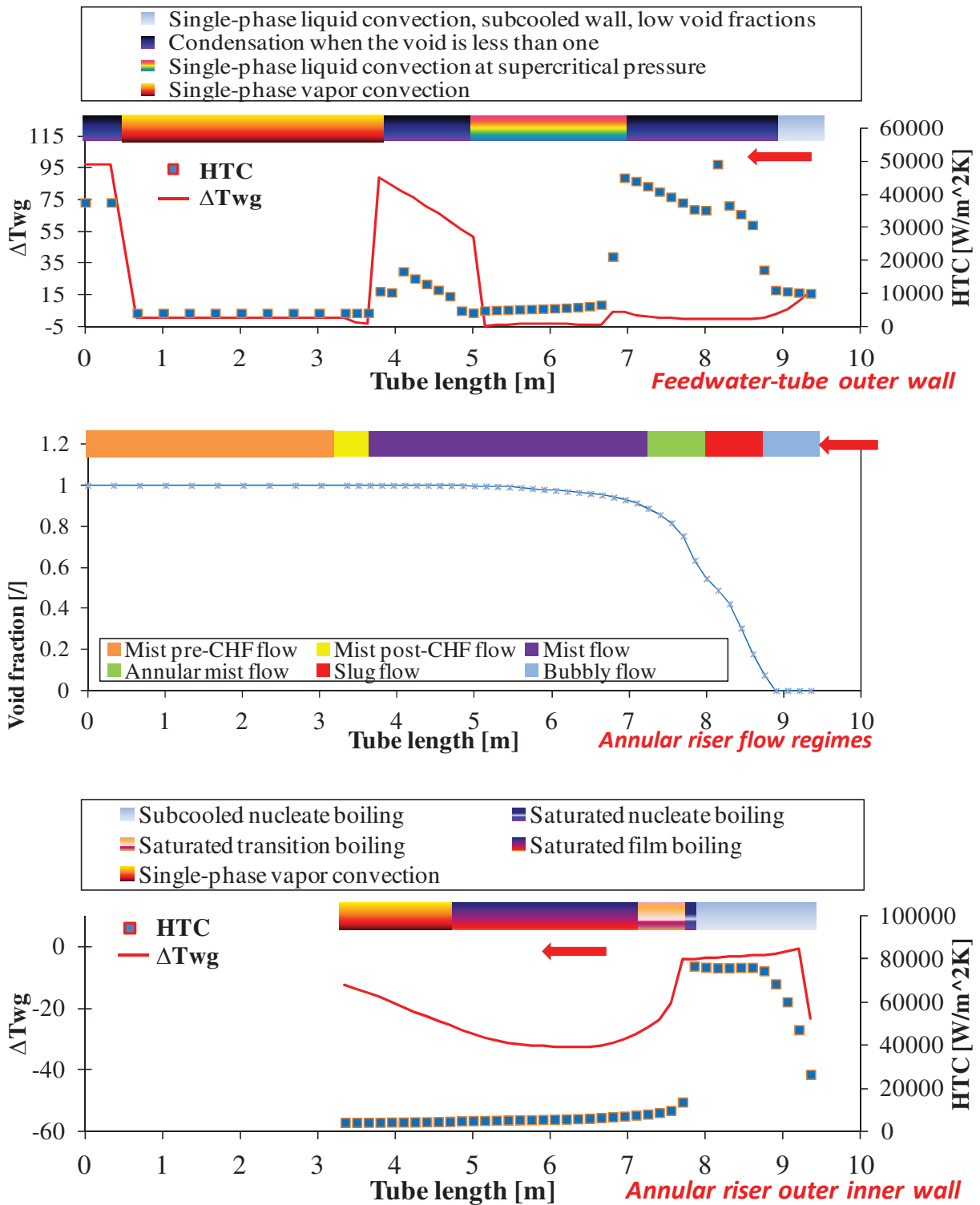


Fig. 17 – SGBT vs. RELAP5 v 3.3, reference simulation Case 1, flow regimes and heat transfer regimes at tube walls in the water-steam side.

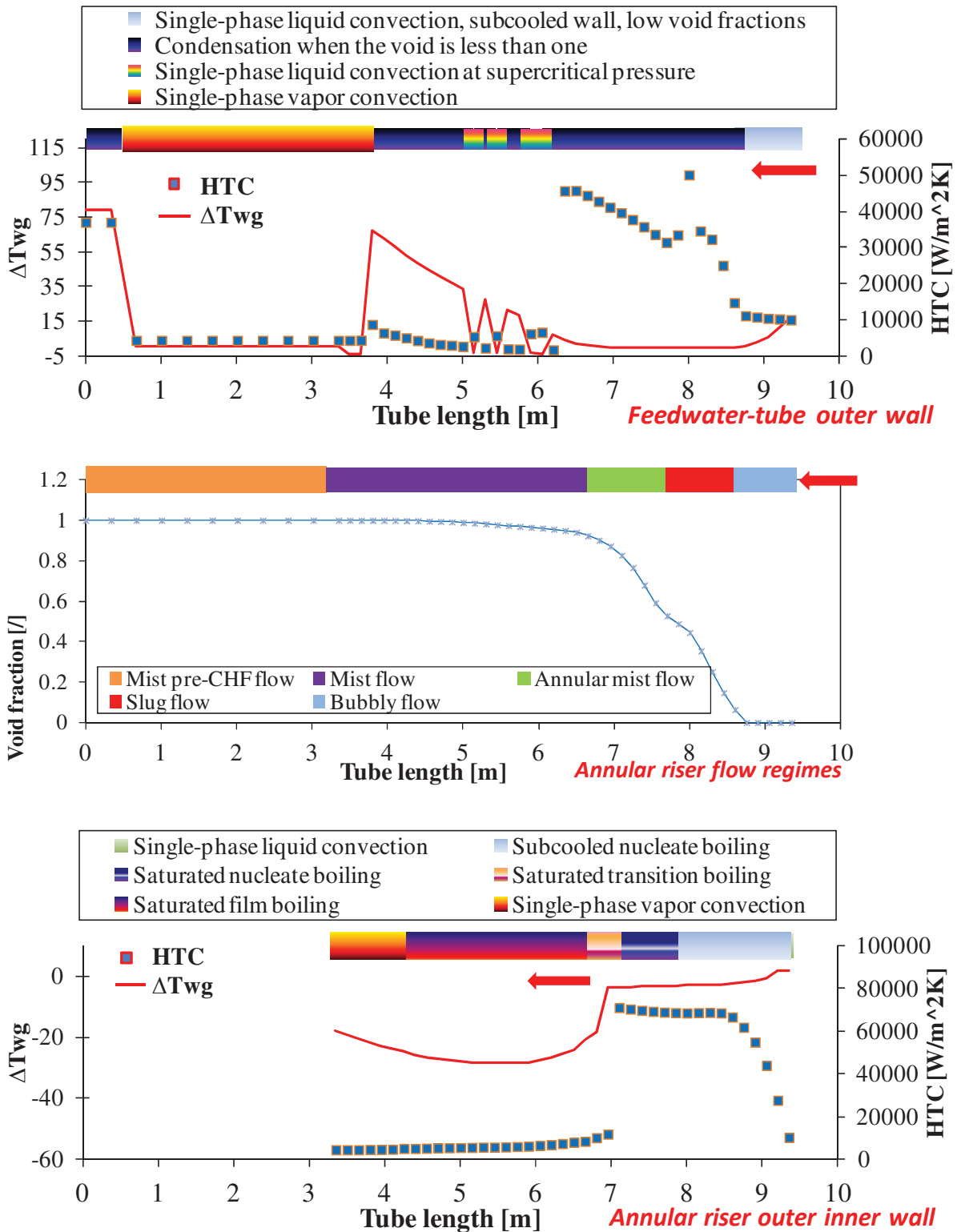


Fig. 18 – SGBT vs. RELAP5 v 3.3, reference simulation Case 2, flow regimes and heat transfer regimes at tube walls in the water-steam side.

3.3 Sensitivity Analyses

The sensitivity analysis is a fundamental tool for the assessment of the code capabilities and the design options. Different objectives shall be fulfilled such as to demonstrate the robustness of the calculation, to characterize the reasons for possible discrepancies between calculated trends, to optimize code results and user option choices, to improve the knowledge of the code by the user and to optimize the detailed design. Several sensitivity analyses are performed, they are reported in *Tab. 12*. The simulations pursue the following main objectives:

- To assess the nodalization effects,
- To assess input deck initialization,
- To assess materials changes,
- To assess alternative design solutions,
- To assess the tube bundle geometry and
- To assess ageing effects during operation of the tube

The detailed documentation of the analyses is given in Ref. [21]. The main achievements are summarized as follows:

- Assessment of the nodalization effects:
 - 40 axial nodes (the reference) result representative of the active length behavior.
 - Annulus component is not completely suitable to model two phase flow phenomena that occur in the annular riser. Indeed, this component has been developed mainly for LWR SG or RPV down-comers. It differs with the pipe component in the treatment of the annular mist flow regime. Anyway, no major deviations (in term of global performance) are observed between the reference simulations and those with annulus component.
- Assessment of materials changes:
 - Si-C powder is a suitable alternative filling material.
 - The Insulating materials presented in section 2.2 allows a good insulations of the annular riser: the water temperature drop in the feedwater tube remains lower than 3 °C with except the ceramic coating discussed below. Vacuum isolation has also be considered, it eliminates condensation heat transfer mode at tube outlet.
- Assessment of alternative design solutions:
 - The application of a finned surface treatment to the annular riser does not reveal appreciable enhancement of the TH performance.
 - The application of ceramic coating at the feedwater tube outer surface instead of sandwich shell worsen the TH performance of the tube. This is due to the relatively high conductivity of ceramic materials (about 10 times that of the insulating paint).
- Assessment of tube bundle geometry:
 - The effect of the tube length on the steam temperature is appreciable.
 - The effect of the tube bundle pitch on the steam temperature is appreciable.
- Assessment of ageing effects during operation of the tube:
 - Lead oxidation has a minor impact on the TH performance of the tube.
- Assessment of the input deck initialization
 - Cold start up was assumed in the reference simulation. This sensitivity was conducted in hot start-up conditions. It has been adopted to develop an improved

input deck since it provides evidence that condensation at tube outlet is a matter of numeric. The analysis is presented in section 3.4.

Category	Parameter	Simulations
<i>Nodalization effects</i>	Nodes number	<ul style="list-style-type: none"> • 10 + 10 nodes • 20 + 10 nodes • 40 + 10 nodes (Reference) • 80 + 10 nodes
	Component 110	<ul style="list-style-type: none"> • Pipe (Reference) • Annulus nodes
<i>Materials changes</i>	Powder	<ul style="list-style-type: none"> • Sintetic diamond (Reference) • Silicon Carbide
	Insulating Material (constant thickness)	<ul style="list-style-type: none"> • 0.05 W/mK (Reference) • Stone wool • Gemcowool • Pyrogel • Supertherm • RLHY-12
	Insulating Material (constant insulating power)	<ul style="list-style-type: none"> • 0.05 W/mK (Reference) • Supertherm • RLHY-12
<i>Alternative design solutions</i>	Ceramic coating	<ul style="list-style-type: none"> • 4.765 mm • 400 μm
	Finned surface	<ul style="list-style-type: none"> • Increased wetted perimeter (+30%)
<i>Tube bundle geometry</i>	Tube active length	<ul style="list-style-type: none"> • 5.5 m • 6.0 m (Reference) • 6.5 m
	Pitch to diameter ratio	<ul style="list-style-type: none"> • 1.35 • 1.42 (Reference) • 1.5 • 1.6
<i>Ageing effects</i>	Oxidation	<ul style="list-style-type: none"> • Decreased conductivity + increased thickness
<i>Initialization</i>	Initial temperatures	<ul style="list-style-type: none"> • Hot start-up

Tab. 12 – Summary of the sensitivity analyses.


3.4 Development of the Improved Input Deck

The initial conditions selected in the reference simulations are the following (“cold start-up”):

- Time 0 s: the temperature is equal to the feedwater temperature (335 °C) in the water and lead sides and in the heat structures. Water is flowing in the feedwater tube, lead is stagnant.
- Up to 500s: The lead side temperature gradually increases up the maximum value of 480 °C. The lead flow rate gradually increases up to the steady value of 6.3676 kg/s (at 500 s).
- After 1100s the system is found to be in equilibrium (based on simulations extended up to 6000 s).

The aim of this analysis is to assess the influence of different initialization on the performance and the condensation occurrence along the feedwater tube. In agreement with the ANSALDO Nucleare recommendations, the following new conditions are fixed (“hot start-up”):

- Time 0 s: the lead side is at 480 °C and the heat structures 1100 and 1110 are initialized at 450 °C. The mass flow rate of lead and water is null.

 Ricerca Sistema Elettrico	Sigla di identificazione	Rev.	Distrib.	Pag.	di
	NNFISS - LP3 - 054	0	L	47	117

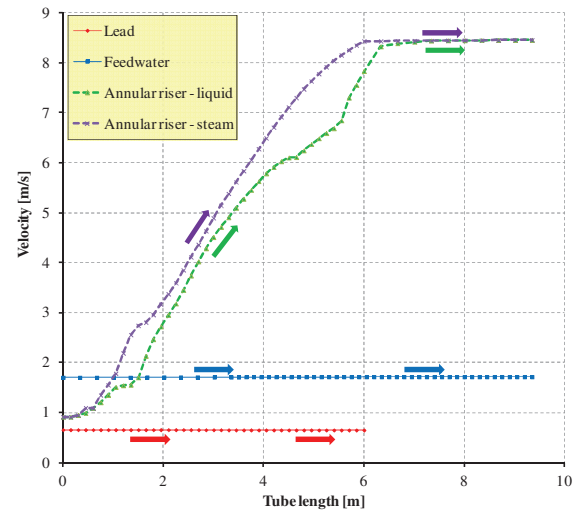
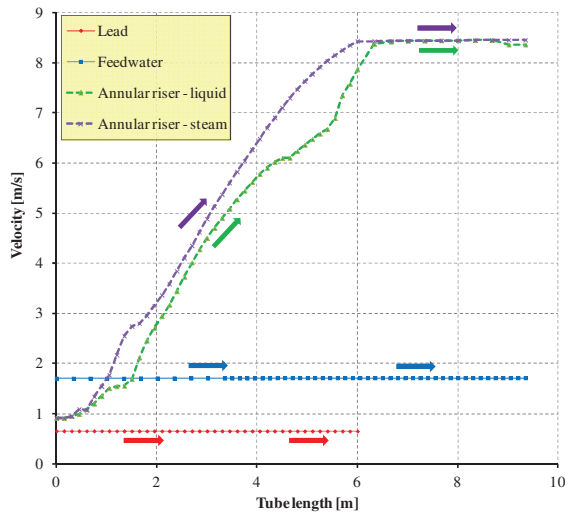
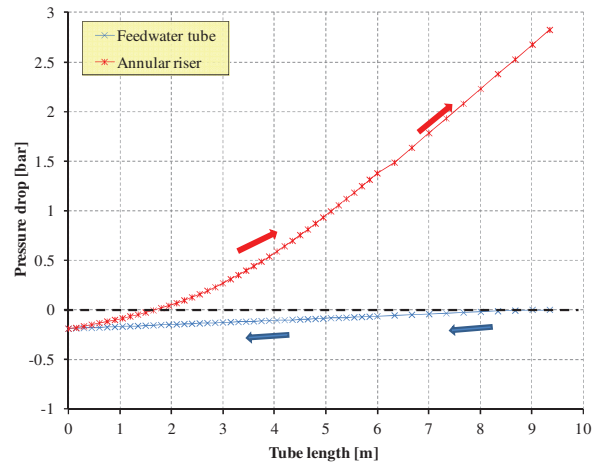
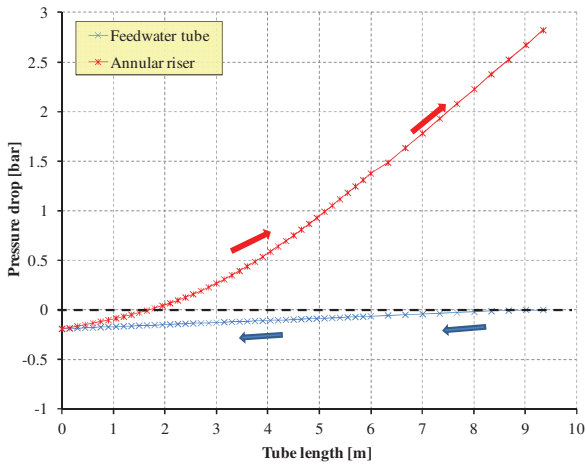
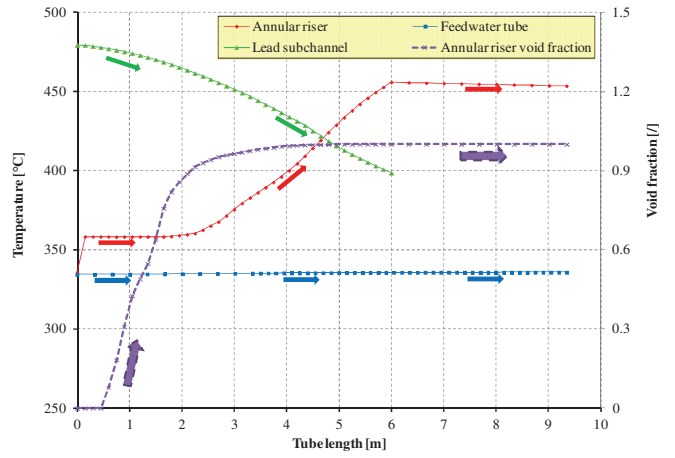
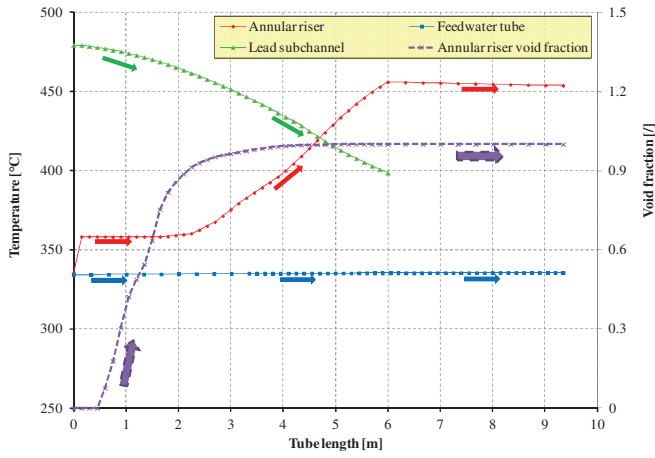
- Up to 50 s: The lead and water flow rate increases to their steady value: 0.0473 kg/s for water and 6.3676 kg/s for lead.
- The calculation has been extended to 6000 s in order to reach steady state conditions with high confidence.

3.4.1 Assessment of the Hydrodynamic Components

The main thermal-hydraulic parameters of the hydrodynamic components are depicted in *Fig. 19* and *Fig. 20*, dealing with Case 1 and 2 respectively. Each couple of figures reports the comparison between the reference and improved input deck results. The physical quantities represented are:

- The feedwater tube temperature as function of the tube length,
- The water-steam temperature in the annular riser as function of its length,
- The primary coolant temperature (only the lead submerged length),
- The void fraction as function of annular riser axial elevation,
- The feedwater pressure drop as function of the tube length,
- The water-steam pressure drop in the annular riser as function of its length,
- The lead velocity (only in the immersed tube length),
- The feedwater velocity as function of the tube length,
- The water phase velocity in the annular riser as function of axial elevation and
- The steam phase velocity in the annular riser as function of its length.

Different boundary and initial conditions do not introduce significant differences in the main thermal-hydraulics parameters. This entails that the improved simulation is consistent with the reference one and the new input deck in meaningful.



Reference

Improved input deck

Fig. 19 – SGBT vs. RELAP5 v 3.3, improved input deck Case 1 vs. reference Case 1, thermal-hydraulic parameters of the hydrodynamic components as function of tube length.

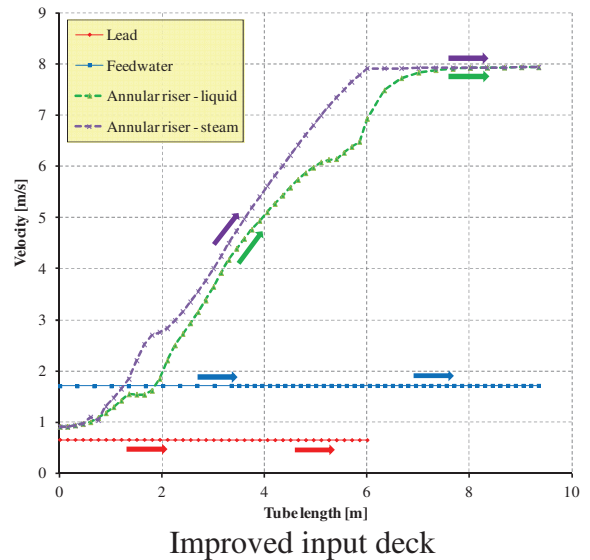
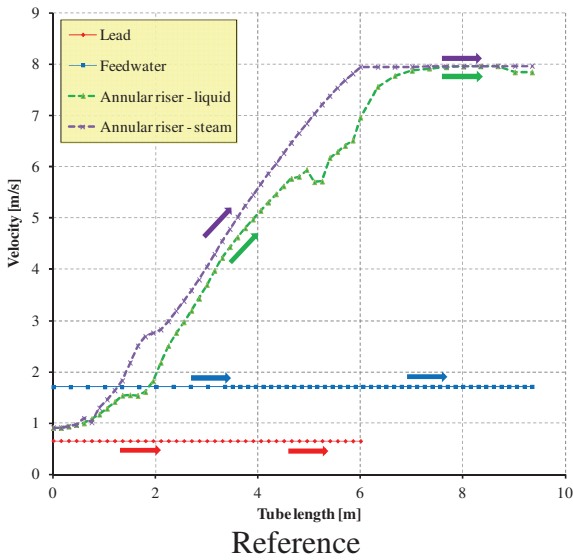
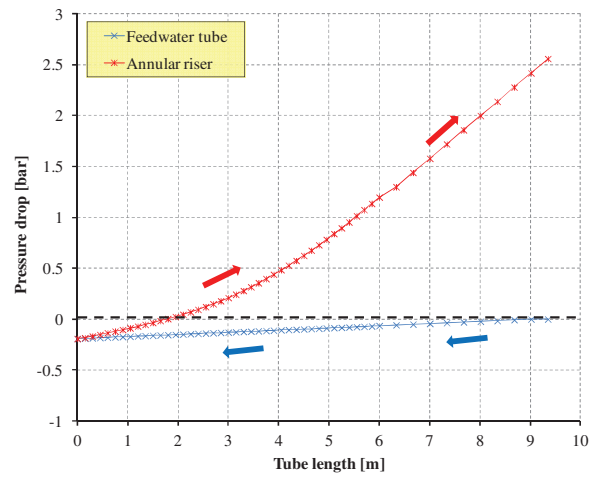
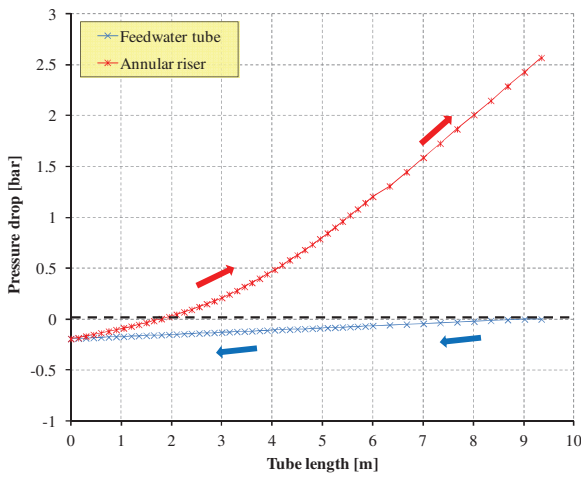
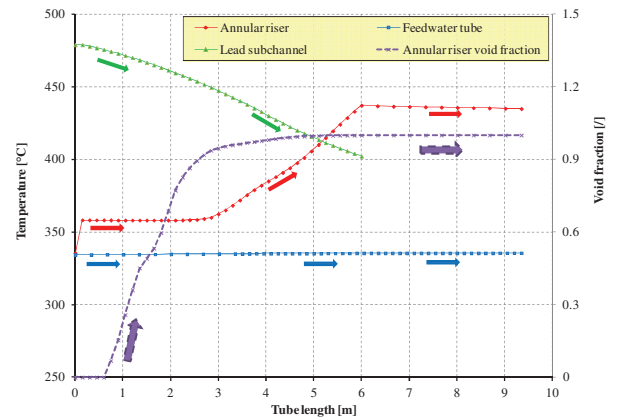
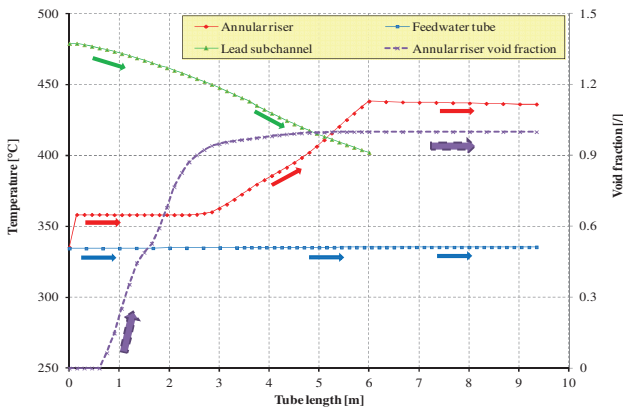



Fig. 20 – SGBT vs. RELAP5 v 3.3, improved input deck Case 2 vs. reference Case 2, thermal-hydraulic parameters of the hydrodynamic components as function of tube length.

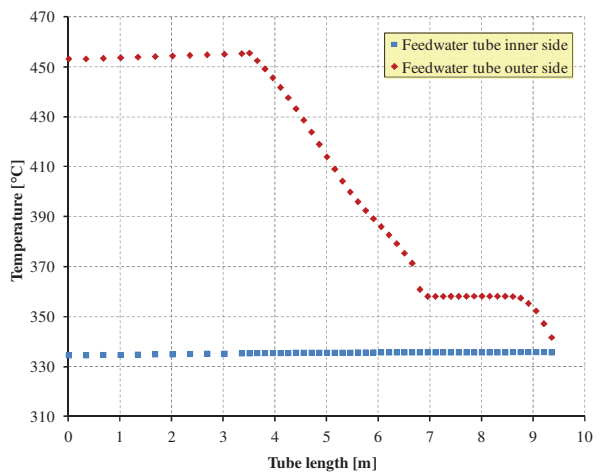
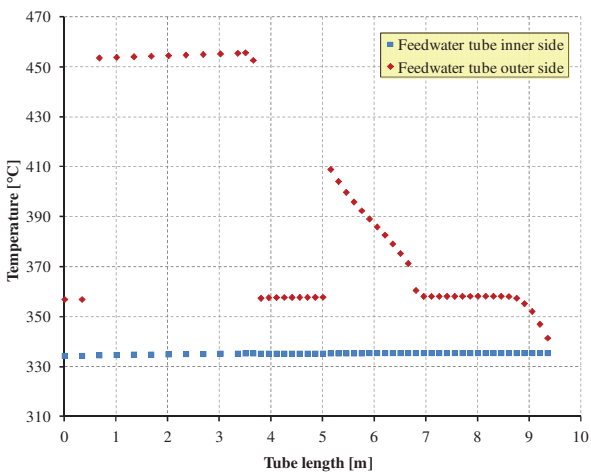
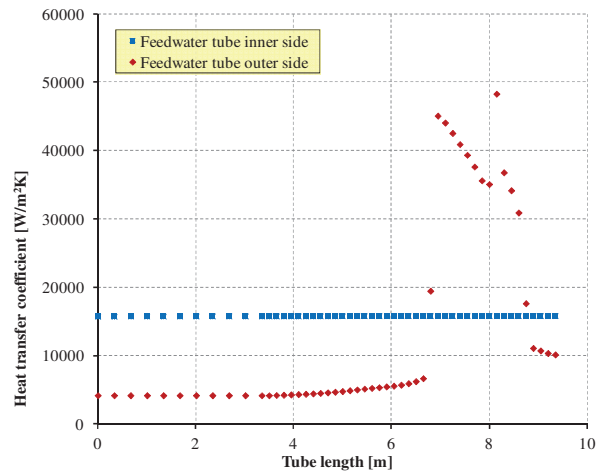
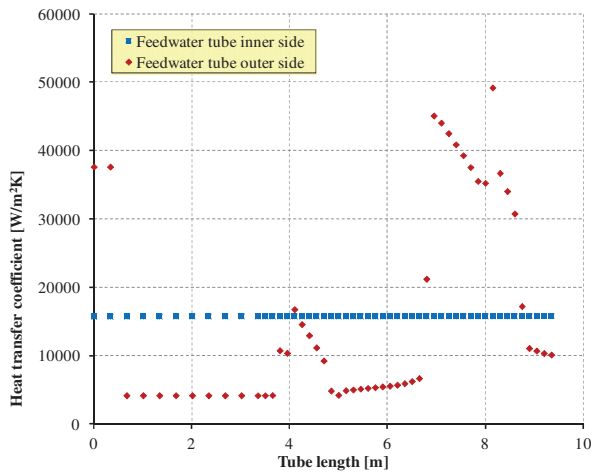
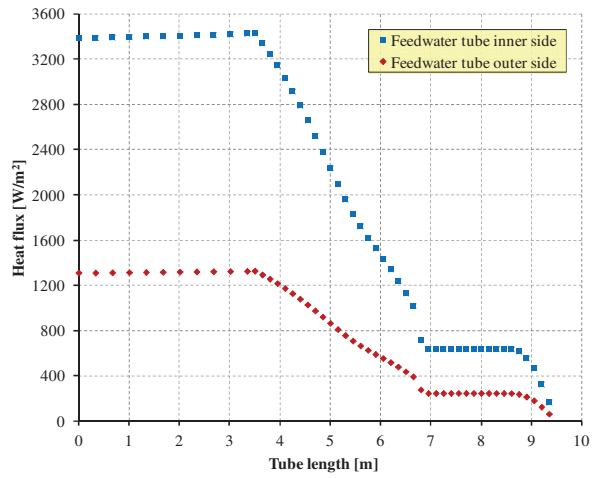
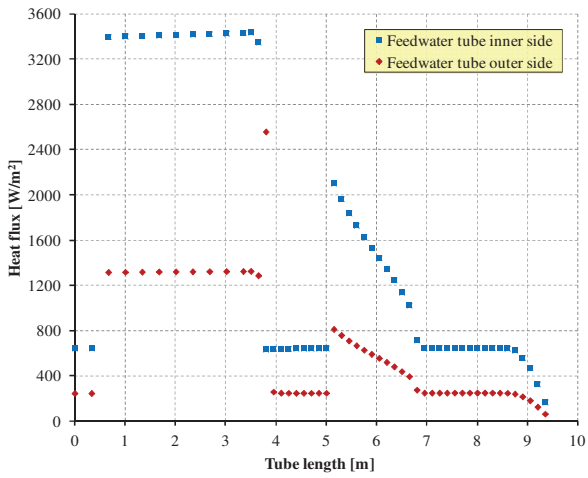
 Ricerca Sistema Elettrico	Sigla di identificazione	Rev.	Distrib.	Pag.	di
	NNFISS - LP3 - 054	0	L	50	117

3.4.2 Assessment of the Heat Structures

The feedwater tube's thermal parameters are depicted in *Fig. 21* and *Fig. 22* (dealing with Case 1 and 2 respectively). Those of the annular riser are given in *Fig. 23* and *Fig. 24* (dealing with Case 1 and 2 respectively). Each couple of figures report the comparison between the reference results (in the left column), and the improved input deck results (right column). The physical quantities represented are:

- The heat flux that crosses the inner surface as function of the tube length,
- The heat flux that crosses the outer surface as function of the length,
- The HTC at the inner surface as function of the tube length,
- The HTC at the outer surface as function of the length,
- The temperature at the inner surface as function of the tube length and
- The temperature at the outer surface as function of the length.

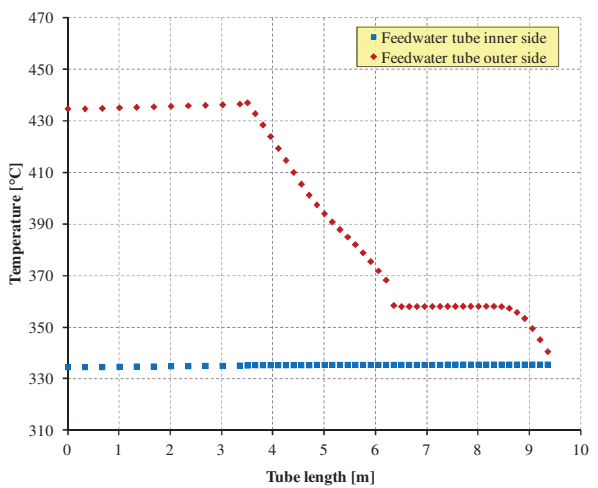
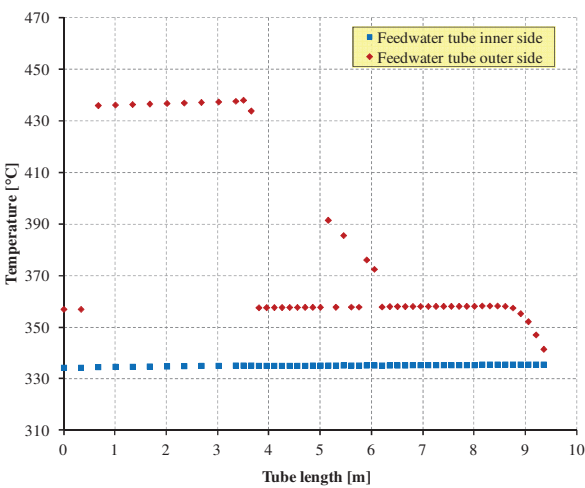
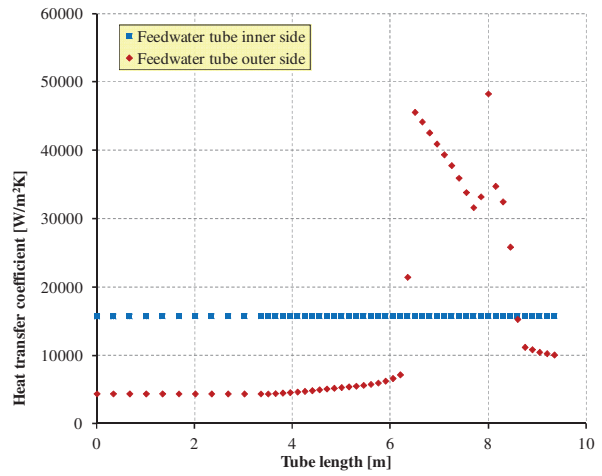
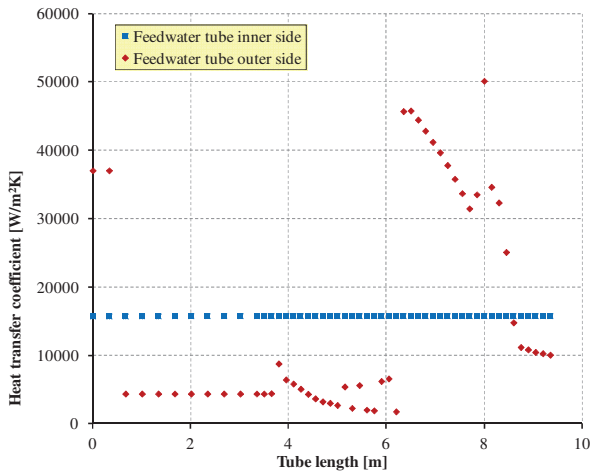
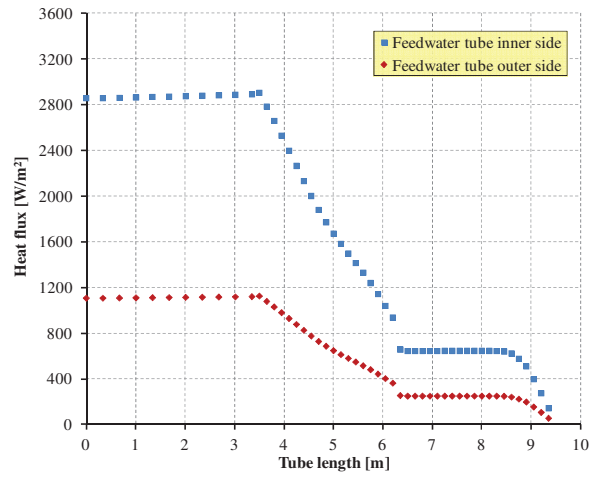
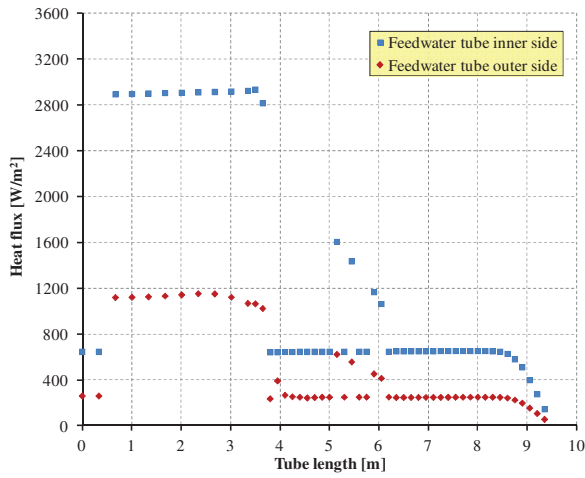
It should be noted that the different initialization involves no significant modification in the thermal parameters of the annular riser heat structure, that remains substantially equal to the reference simulation. This highlights that the overall bayonet tube performance and the total removed power predicted by the code do not depend on the initial conditions. However, differences can be detected in the feedwater tube thermal parameters. This is expected since they are connected to the occurrence of the condensation heat transfer mode. The absence of condensation in the intermediate zone and in the outlet section causes a more regular trend of the HTC along the tube length. This entails that the discontinuous behavior of some physical quantities (temperature and heat flux) at the outer surface predicted in the reference simulations is eliminated.



Reference

Improved input deck

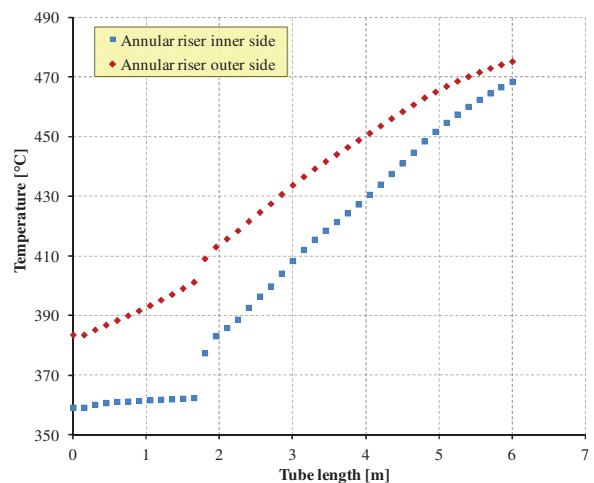
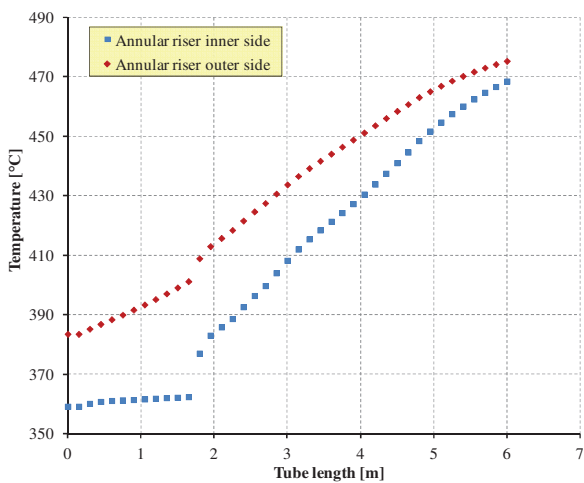
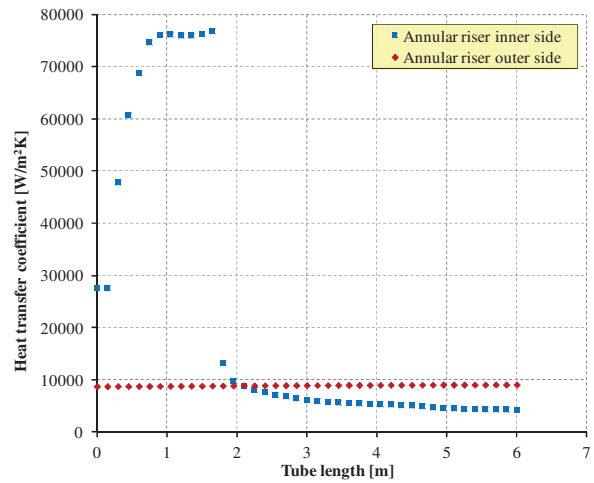
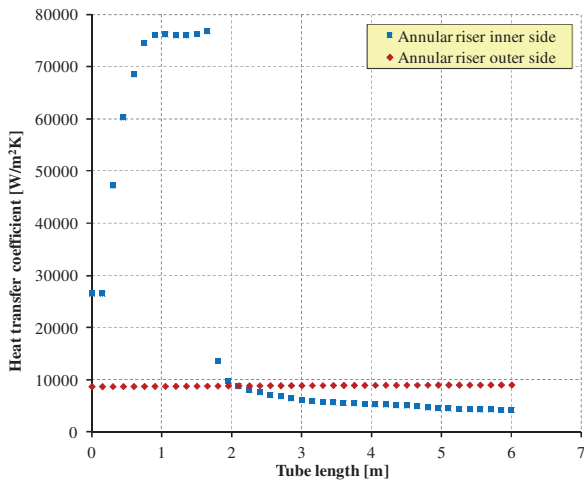
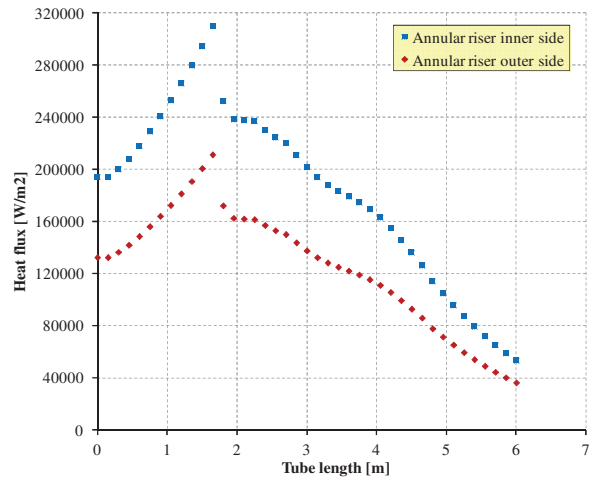
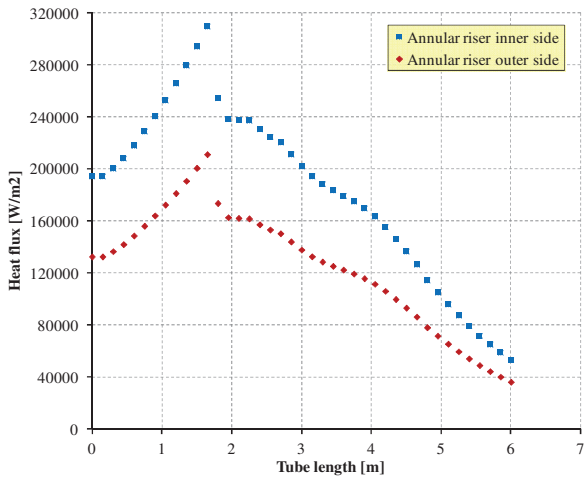
Fig. 21 – SGBT vs. RELAP5 v 3.3, improved input deck Case 1, heat structure parameters of the feedwater tube as function of tube length and comparison with the reference simulation.



Reference

Improved input deck

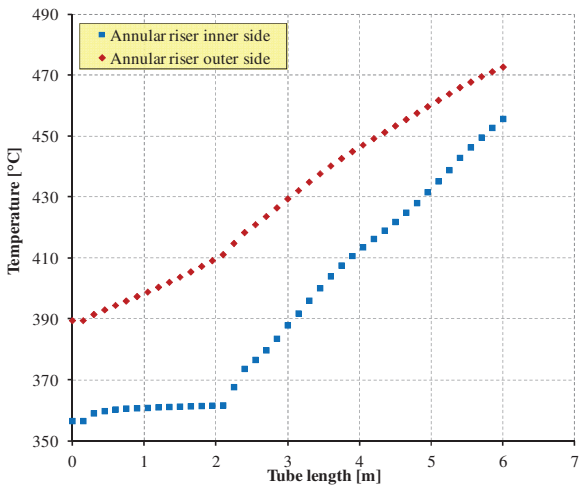
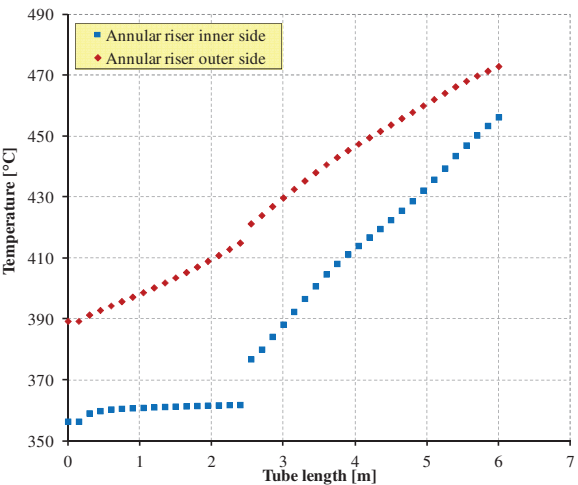
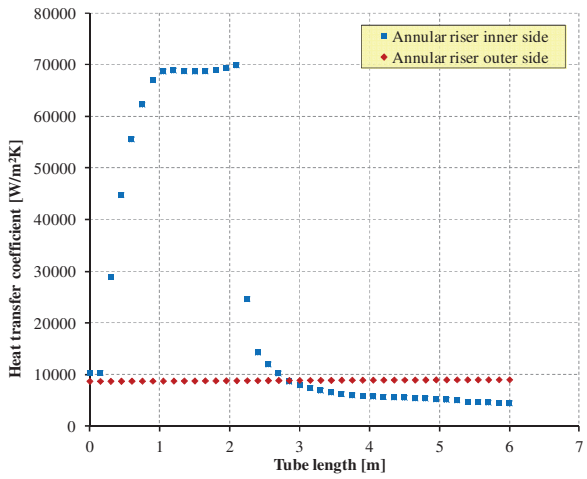
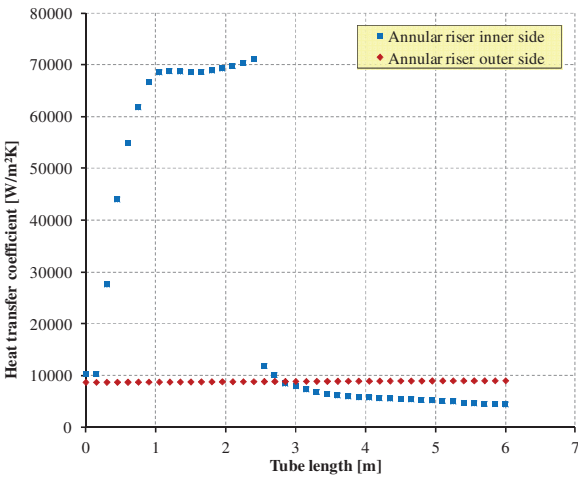
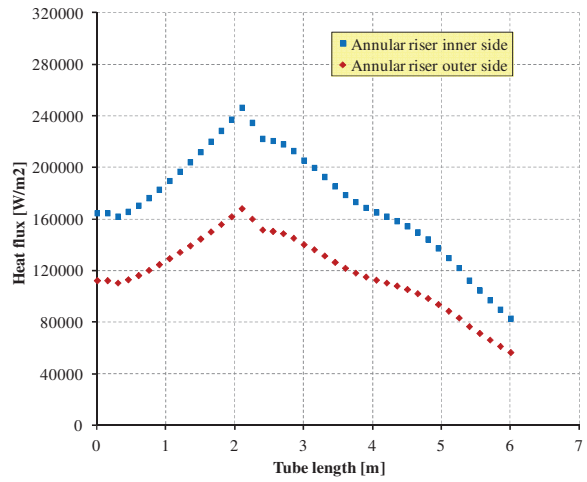
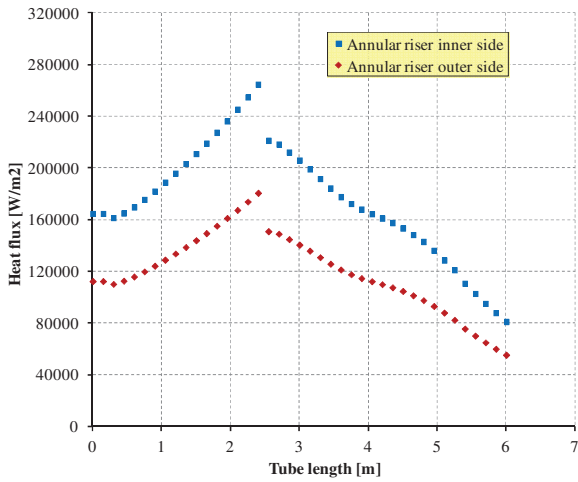
Fig. 22 – SGBT vs. RELAP5 v 3.3, improved input deck Case 2, heat structure parameters of the feedwater tube as function of tube length and comparison with the reference simulation.



Reference

Improved input deck


Fig. 23 – SGBT vs. RELAP5 v 3.3, improved input deck Case 1, heat structure parameters of the annular riser as function of tube length and comparison with the reference simulation.



Reference

Improved input deck

Fig. 24 – SGBT vs. RELAP5 v 3.3, improved input deck Case 2, heat structure parameters of the annular riser as function of tube length and comparison with the reference simulation.

 Ricerca Sistema Elettrico	Sigla di identificazione	Rev.	Distrib.	Pag.	di
	NNFISS - LP3 - 054	0	L	55	117

3.4.3 Assessment of 2 ϕ Dynamics in the Water Steam Side

The present section focuses on the main thermal-hydraulic phenomena that occur in the water-steam side of the bayonet tube. Three pictures are given in *Fig. 25*, they are representative of Case 1.

- The heat transfer modes at the feedwater tube outer wall are reported in the first picture. The figure includes the temperature difference ΔT_{gw} “steam – wall surface” and the HTC at the tube wall. The following modes are predicted:
 - Single-phase liquid convection at low void fractions.
 - Condensation at low void fractions in the boiling zone.
 - Single-phase liquid convection at supercritical pressure mode at high void fractions. It is induced by a high temperature liquid film at tube surface ($\Delta T_{gw} < 0$ in this zone) predicted by the code.
 - Wall drying and single-phase vapor convection in the higher part of the active length up to the outlet section.
 - Condensation is avoided at the tube outlet.
 - This sequence of heat transfer regimes is more regular than the reference case and it prevents oscillations or discontinuities in heat flux, HTC and surface temperature. Moreover, it should be noted that also ΔT_{gw} has a smoother trend and its maximum value is about 15 °C (it is 95 °C in the reference simulation).
- In the intermediate picture, the flow regimes and the corresponding void fraction in the annular riser are reported. No difference are observed compared to the reference results.
- In the third picture the heat transfer regimes at the annular riser inner wall are reported. The figure includes the temperature difference ΔT_{gw} and the HTC at the tube wall. There are no significant modifications in the annular riser compared to the reference simulations.

The considerations reported above apply also to Case 2, that is depicted in *Fig. 26*. The main difference concerns the flow regimes in the bulk: post CHF mist flow regime is never reached. The “hot start-up” initialization allows to avoid the condensation heat transfer mode at the outlet section of the feedwater tube outer wall.

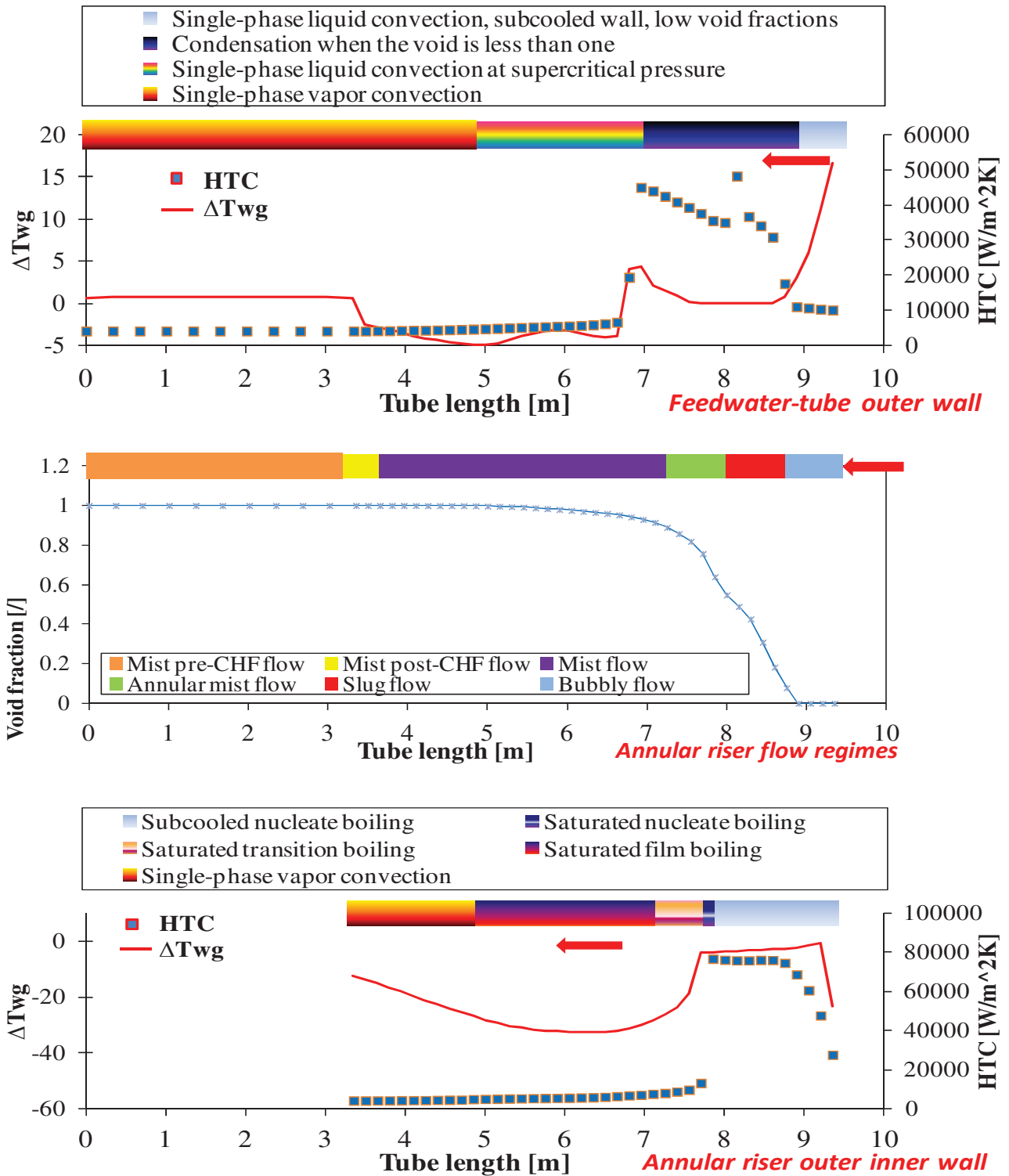


Fig. 25 – SGBT vs. RELAP5 v 3.3, improved input deck Case 1, flow regimes and heat transfer regimes at tube walls in the water-steam side.

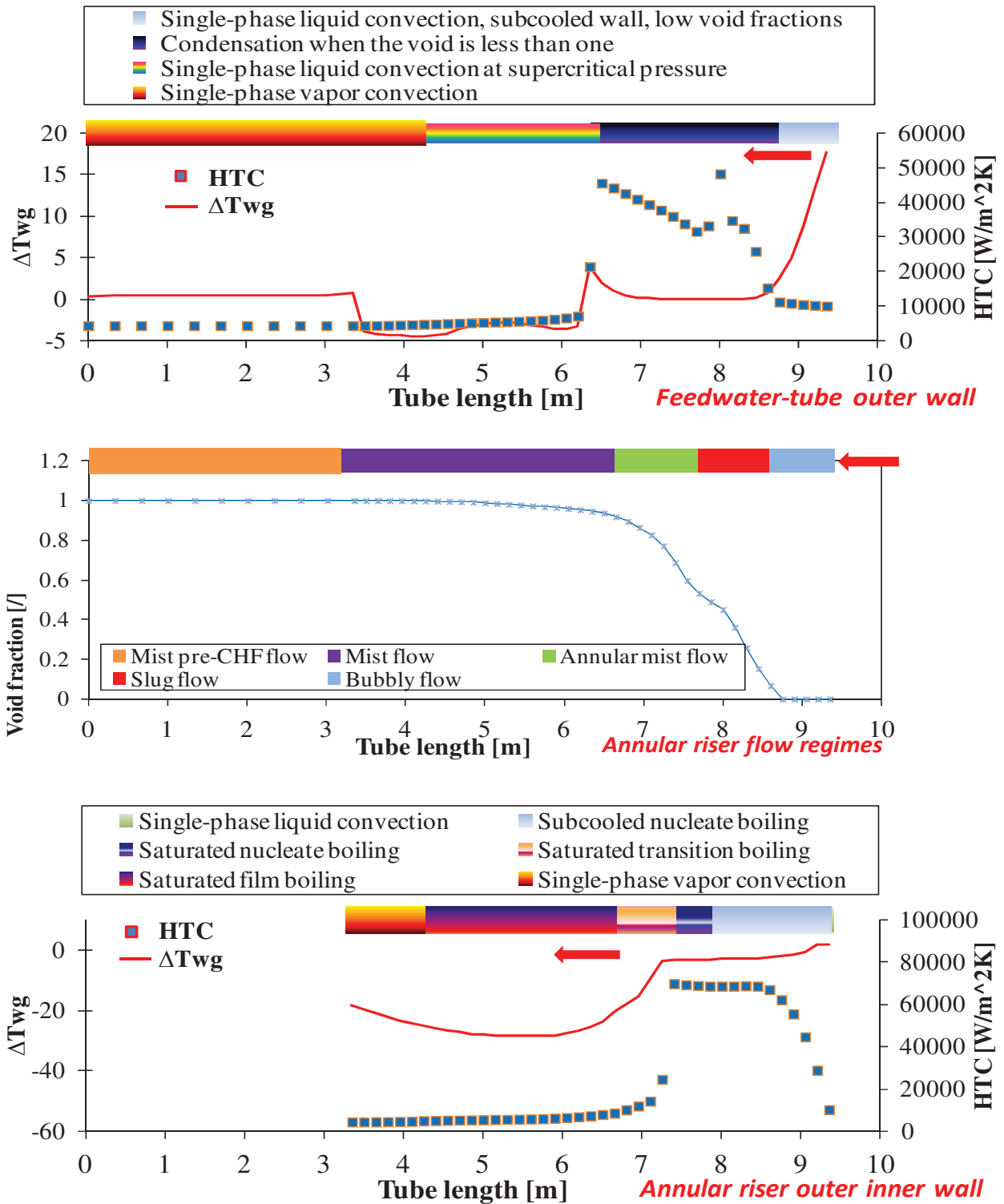


Fig. 26 – SGBT vs. RELAP5 v 3.3, improved input deck Case 2, flow regimes and heat transfer regimes at tube walls in the water-steam side.



4 Thermal Hydraulic Conceptual Design of HERO

The HERO Facility conceptual design has been subdivided in two parts: the heating power system and the pressurized steam water system. The present document focuses on the heating power system (lead loop).

4.1 Objectives of the HERO Facility and Potential Heating Power System

The calculations in support to the TH conceptual design of the Heavy liquid metal – pressurized water cooled tube (HERO) is presented in the following sections. The main aim of the facility is to study a 1:1 bayonet tube under conditions that represent, as much as possible, the operation in the ALFRED SG. The facility is expected to be a suitable tool to support the validation process of TH-Sy codes and CFD codes coupled simulations. The reference solution is based on natural circulation flowing lead, *Fig. 27*. Two different concepts are proposed.

Lead side: the bayonet tube is immersed into a pipe filled with lead.

- The submerged height is 6 meters, according to the SG conditions.
- Argon atmosphere is realized above the active length (1 m in height as in the SG).
- The liquid lead heats-up in the bottom part of the facility. The power is supplied by electrically heated rods located inside the facility and it corresponds to the power removed by the single bayonet unit (about 74 kW, as calculated by means of RELAP 5 in Ref. [21]).
- The liquid lead flows by natural circulation in the outer annular region (*Fig. 27*). Then it enters in down flow the bayonet tube channel from the top (as in the SG). The lead channel and the outer annular region are separated by a sandwich wall composed of AISI-304-insulating medium-AISI-304. In the preliminary concept, the insulating medium consists of paint, the same adopted in the bayonet tube to avoid heat exchange between the descending feedwater and the superheated steam annular riser.
- The sandwich wall should be fixed both at the top and at the bottom, in order to keep it in position. This means that fissures are required to allow the lead to flow. In the preliminary configuration (to be verified by calculations), 16 identical fissures are considered 8 located at the top and 8 at the bottom (their shape should be defined).
- The zone located below the bayonet tube is fixed to 3.1 m in length (preliminary, to be verified by calculations). The power is supplied in the lead side by means of 8 heating rods located between the sandwich wall and the outermost tube (*Fig. 28 a*). In the preliminary concept, their active length is fixed to 1 m (to be checked in term of feasibility).
- The main requirement of the lead loop is to provide a mass flow rate of 6.367 kg/s and 74 kW in the lead channel (as in the SG) in order to be representative of the SG.
- Therefore, the main parameters to be calculated are X and Y, *Fig. 27*. Should be pointed out that Y represents the P/D of the ALFRED SG. It is expected that P/D will not be reproduced (the facility must provide 6.367 kg/s without pumps). Therefore, any deviation from P/D = 1.45 (as in the SG) must be assessed in term of discrepancies from the in reactor behavior.
- In order to be conservative, the lead mass flow rate should have a certain flexibility. This is realized by means of (lead) level regulation at the top fissures, *Fig. 28 b*).

Bayonet tube: the bayonet tube is that designed by ANSALDO ^[19]. The high conductivity powder material inserted between the double wall is sintetic diamond or Si-C ^[12].

Two alternative configurations are still under consideration. The first one deals with the forced circulation (by means of axial pump or gas enhanced circulation technique). This solutions has two main disadvantages: the cost (if axial pump is introduced) and the loss of the capability to use the facility in support to CFD tools validation (gas enhanced circulation). The last alternative is to provide the electrical power at the bayonet tube outer surface by means of heating cables, *Fig. 29*. The axial power shape should be computed by means of RELAP-5. It is considered alternative to the reference solution. Although the simplest concept, this configuration is characterized by high complexity in term of construction. In fact, the cables assembling could impair its feasibility.

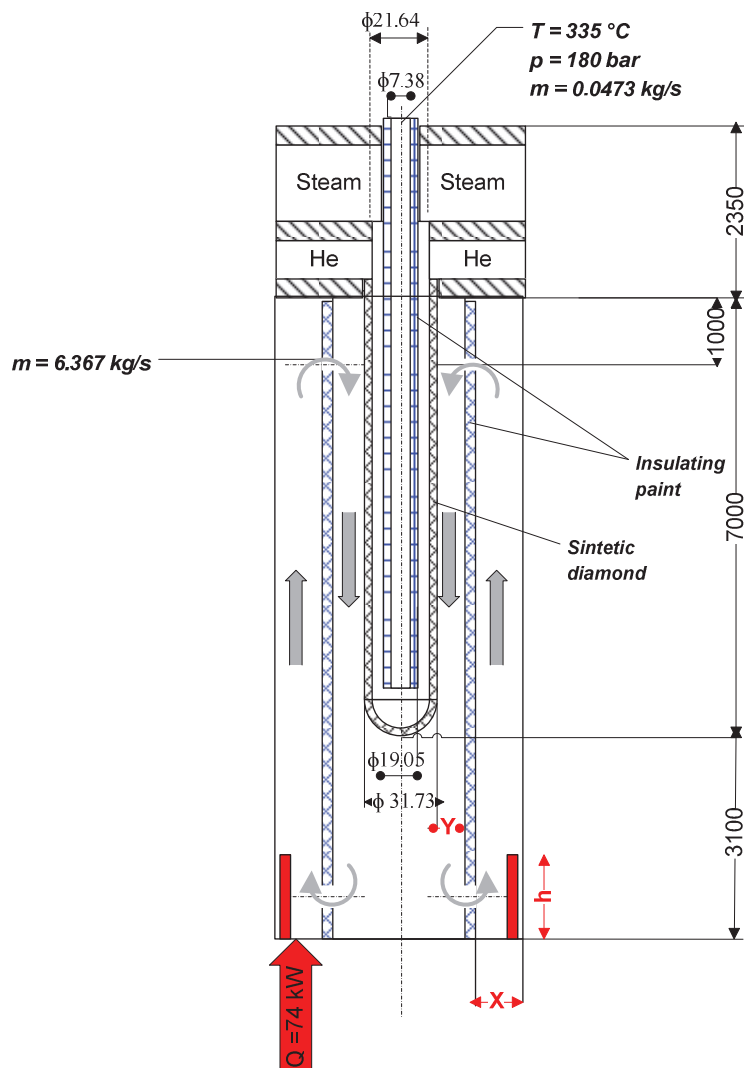


Fig. 27 – HERO Facility Reference configuration, lead loop scheme with internal heating rods.

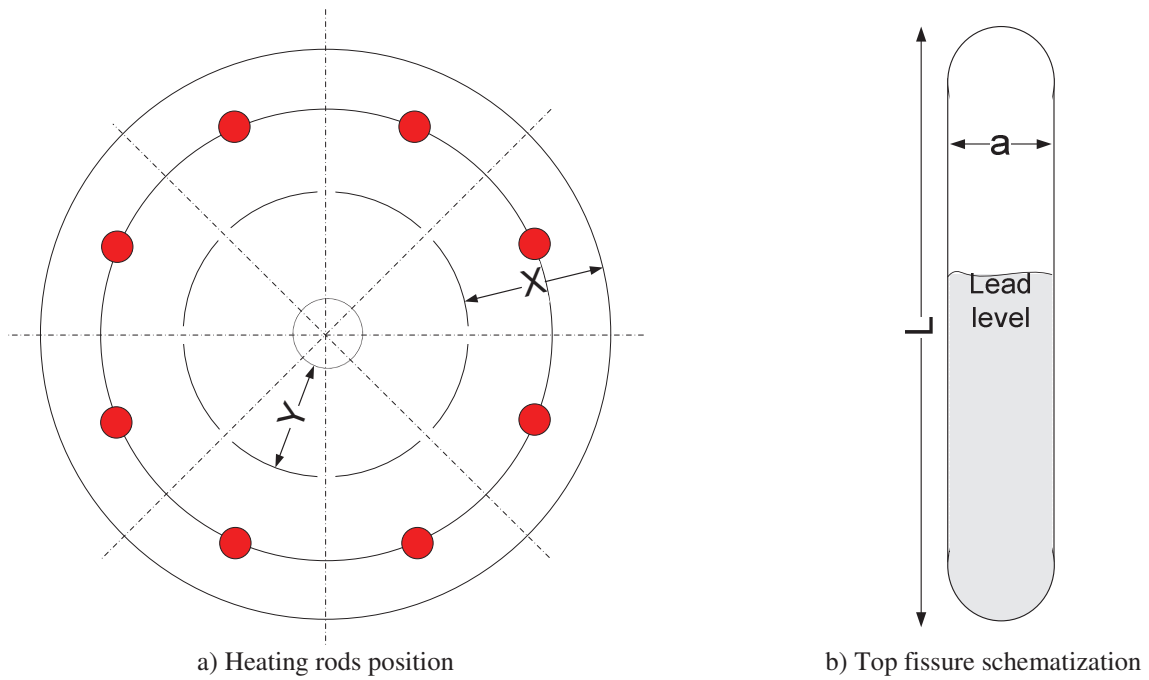


Fig. 28 – HERO Facility Reference configuration, heating rods and fissure.

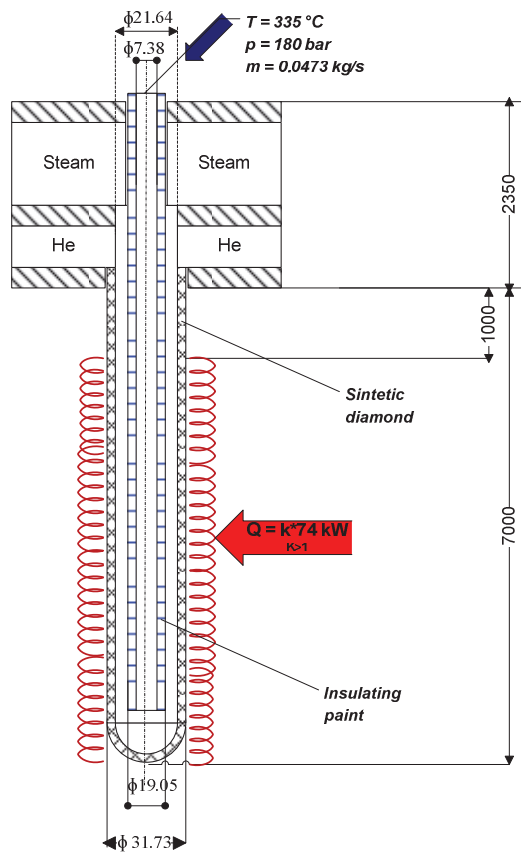


Fig. 29 – HERO Facility Alternative configuration.

4.2 Calculations in Support to the TH Design of HERO by RELAP-5

4.2.1 Initial Input Deck Documentation

The first RELAP-5 ^{[16][17][25]} input deck is developed according to the scheme reported in *Fig. 30*. The bayonet tube is that of Ref. [21] and section 3. The hydraulic model includes: the feedwater descending tube (pipe 100), the annular riser (pipe 110) the lead down flow region (pipe 140 and pipe 160) the lead up flow region (pipe 170 and pipe 180) and the fissures (branches 165-166 and branches 136-137). The bayonet tube heat structures includes the T91-paint-T91 double wall (HS1100), the T91-sintetic diamond-T91 double wall (HS1110). The remaining heat structures are the AISI-304-paint-AISI-304 double wall (HS1140) and the outermost AISI-304 tube wall in which the heat source is modeled in the lower nodes of its outer surface (Power999). In steady state conditions, it represents the scheme reported in *Fig. 27* since the heating source is modeled without heat losses. In addition, the following assumptions have been introduced:

- The heat exchange between the annular steam riser and the Argon zone has been neglected, that means adiabatic behavior of the non-active region located outside the tube.
- The conductivity of the insulating paint has been fixed, in agreement with ANSALDO Nucleare recommendations [19], to 0.05 W/mK.
- The filling powder is assumed as 0.3 porosity sintetic diamond based on the experimental tests and the pretest calculations reported in Refs. [10] and [12]. Its conductivity has been assumed those of Case 1 (see section 3).
- The heat transfer between the lead side and the annular riser is modeled according to the Seban correlation ^[28].
- The outermost tube outer surface is considered adiabatic.

The detailed input deck is reported in Ref. [30]. The main geometrical data of initial configuration are summarized in *Tab. 13*.

Component	Description	Quantity	Component	Description	Quantity	
<i>Inner feedwater tube</i>	OD	9.52 mm	<i>Lead Down flow double wall</i>	OD	51.23 mm	
	T91 thickness	1.07 mm		SS thickness	2.00 mm	
	Paint thickness	2.88 mm		Paint thickness	3.00 mm	
	OD	19.05 mm		OD	61.25 mm	
	T91 thickness	1.07 mm		SS thickness	2.00 mm	
<i>Annular riser</i>	OD	25.40 mm	<i>Outermost tube</i>	OD	88.77 mm	
	T91 thickness	1.88 mm		SS thickness	5 mm	
	diamond thickness	1.07 mm	<i>Fissures</i>	Total flow area	1740 mm ²	
	OD	31.73 mm		--	X	8.76 mm
	T91 thickness	2.11 mm		--	Y	7.76 mm

Tab. 13 – HERO Facility, summary of the initial geometry.

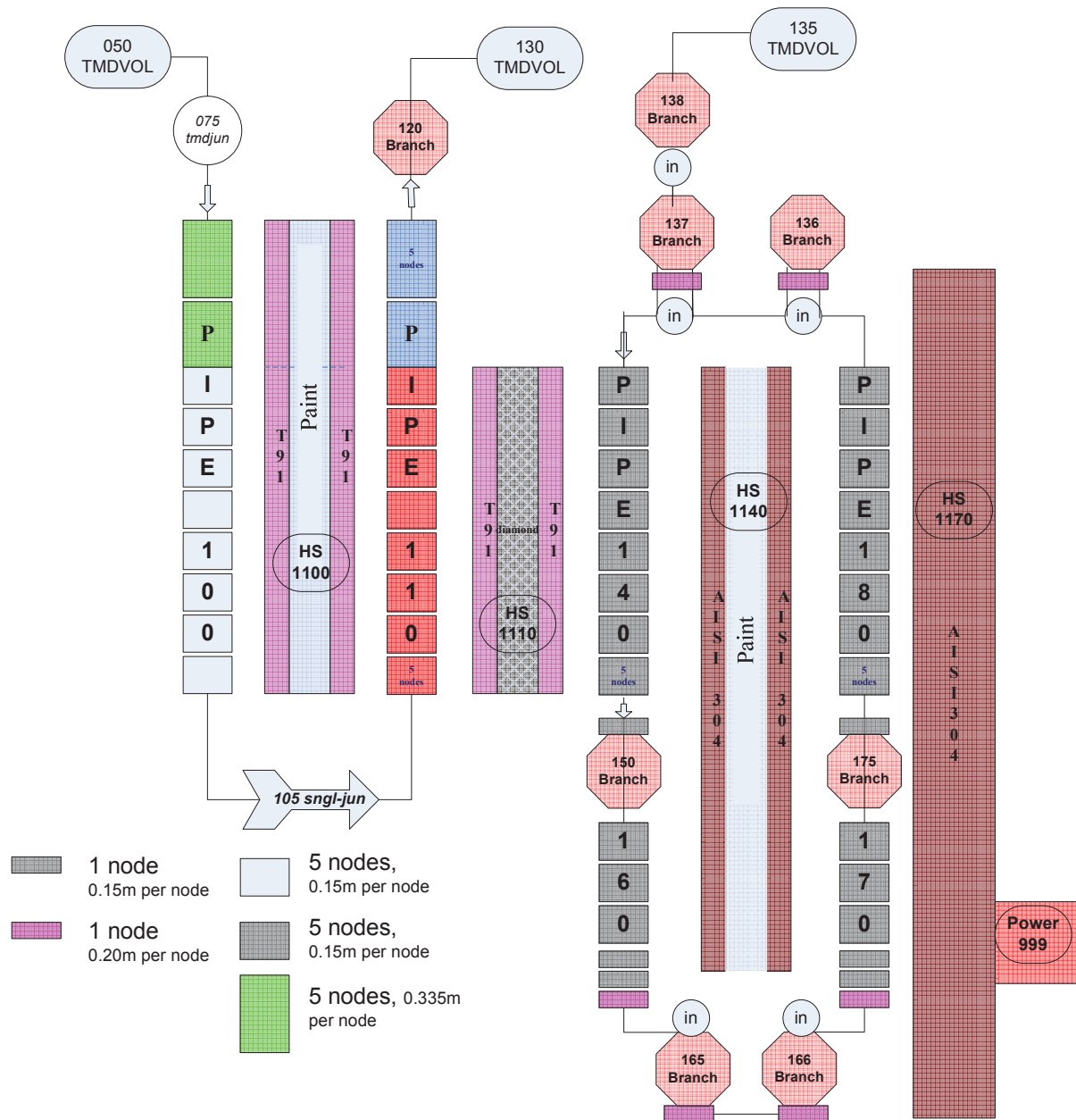


Fig. 30 – HERO Facility Reference configuration RELAP-5 input deck scheme.

4.2.1.1 Modeling of the hydrodynamic components

The feedwater descending tube and the annular steam riser hydrodynamic components (Pipe 100 and Pipe 110) are modeled as documented in Ref. [21] and section 3. The lead channel, Pipe 140, is modeled as in Ref. [21] excepts the hydraulic diameter that considers the tube outer surface *Tab. 14*. This means that the lead flow area corresponds to the SG configuration, $Y = 7.8$ mm (even if its hydraulic diameter is different).

Pipe 160 accounts for the lead lower descending region, it is summarized in *Tab. 15*. The annular lead riser is modeled by Pipe 170 and Pipe 180, *Tab. 16* and *Tab. 17*. Their flow area is assumed double time the flow area of pipe 140 that means $X = 8.8$ mm.

The local pressure loss coefficient between the lead channel and the lead lower descending region is modeled in branch 150. It is assumed 0.20 (based on Ref. [29]).

The 8 fissures at the top and those at the bottom are modeled assuming to keep as constant their flow area. The initial value is selected equal to the bottom holes inlet flow area (0.0017 m^2). They are modeled as branches 136, 137 and 165, 166. The main parameters are given in *Tab. 19* and *Tab. 20*. The corresponding local pressure loss coefficients are modeled as boundaries of a range that has been calculated based on Ref. [29]. Two calculations are thus performed assuming maximum and minimum local pressure losses.

COMPONENT LABEL		TYPE	DESCRIPTION
Pipe 140		Hydrodynamic component	Lead channel SGBT
Id.	Parameter	Quantity	Notes
a	Axial node height	0.1500 m	--
b	N° axial nodes	40	--
d	<i>Inner radius</i>	<i>0.0159 m</i>	--
de	<i>Outer radius</i>	<i>0.0236 m</i>	--
e	Equivalent flow area	$9.6297 \cdot 10^{-4} \text{ m}^2$	That of SGBT channel
i	Hydraulic diameter	0.01552 m	$i = 4 \cdot e / [2 \pi \cdot (d + de)]$

Tab. 14 - HERO Facility, bayonet tube side, hydrodynamic modeling of the lead channel.

COMPONENT LABEL		TYPE	DESCRIPTION
Pipe 160		Hydrodynamic component	Lead channel down
Id.	Parameter	Quantity	Notes
a	Axial node height	0.1500 m	--
b	N° axial nodes	17	--
c	Axial node height	0.2000 m	--
b	N° axial nodes	1	--
d	<i>Inner radius</i>	<i>0.0000 m</i>	--
e	<i>Outer radius</i>	<i>0.0236 m</i>	--
e	Equivalent flow area	0.0017 m^2	$\pi \cdot e^2$
i	Hydraulic diameter	0.0472 m	$2 \cdot e$

Tab. 15 – HERO Facility, hydrodynamic modeling of the lead channel down flow area.

COMPONENT LABEL		TYPE	DESCRIPTION
Pipe 170		Hydrodynamic component	Lead channel up-1
Id.	Parameter	Quantity	Notes
a	Axial node height	0.1500 m	--
b	N° axial nodes	17	--
c	Axial node height	0.2000 m	--
d	N° axial nodes	1	--
e	<i>Inner radius</i>	<i>0.0306 m</i>	--
f	<i>Outer radius</i>	<i>0.0394 m</i>	--
g	Equivalent flow area	$1.9259 \cdot 10^{-3} \text{ m}^2$	$g = \pi \cdot (f^2 - e^2)$, That of SGBT
h	Hydraulic diameter	0.0175 m	$h = 4 \cdot g / [2 \pi \cdot (e + f)]$

Tab. 16 – HERO Facility, hydrodynamic modeling of the lead channel down flow area.

COMPONENT LABEL		TYPE	DESCRIPTION
Pipe 180		Hydrodynamic component	Lead channel up-2
Id.	Parameter	Quantity	Notes
a	Axial node height	0.15000 m	--
b	N° axial nodes	40	--
c	<i>Inner radius</i>	<i>0.0306m</i>	--
d	<i>Outer radius</i>	<i>0.0394 m</i>	--
e	Equivalent flow area	$1.9259 \cdot 10^{-3} \text{ m}^2$	$e = \pi \cdot (d^2 - c^2)$, That of SGBT
f	Hydraulic diameter	0.0175 m	$f = 4 \cdot e / [2 \pi \cdot (c+d)]$

Tab. 17 – HERO Facility, hydrodynamic modeling of the lead channel down flow area.

COMPONENT LABEL		TYPE	DESCRIPTION
Branch 150		Hydrodynamic component	Flow expansion
Id.	Parameter	Quantity	Notes
a	Axial node height	0.1500 m	--
b	N° axial nodes	1	--
c	Flow area	0.0017 m^2	--
d	HD	0.0472 m	--
e	local pressure loss coefficient	0.20	--

Tab. 18 – HERO Facility, hydrodynamic modeling of the top holes.

COMPONENT LABEL		TYPE	DESCRIPTION
branches 136 and 137		Hydrodynamic component	Top fissures
Id.	Parameter	Quantity	Notes
a	Axial node height	0.2000 m	--
b	N° axial nodes	1	--
c	Flow area branch 136	$1.9259 \cdot 10^{-3} \text{ m}^2$	That of PIPE 180
d	HD branch 136	0.0175 m	That of PIPE 180
e	Flow area branch 137	$9.6297 \cdot 10^{-4} \text{ m}^2$	That of PIPE 140
f	HD branch 137	0.0155	That of PIPE 140
g	Branch junction	From 136 inlet to 137 inlet	Flow area: 0.00175 m^2
h	local pressure loss coefficient	0.5-1.0	Branch 136

Tab. 19 – HERO Facility, hydrodynamic modeling of the top holes.

COMPONENT LABEL		TYPE	DESCRIPTION
Branches 165 and 166		Hydrodynamic component	Bottom fissures
Id.	Parameter	Quantity	Notes
a	Axial node height	0.2000 m	--
b	N° axial nodes	1	--
c	Flow area branch 165	0.0017 m^2	That of PIPE 160
d	HD branch 165	0.0472 m	That of PIPE 160
e	Flow area branch 166	$1.9259 \cdot 10^{-3} \text{ m}^2$	That of PIPE 170
f	HD branch 166	0.0175 m	That of PIPE 170
g	Branch junction	From 165 outlet to 166 outlet	Flow area: 0.00175 m^2
h	local pressure loss coefficient	0.3-0.5	Branch 165

Tab. 20 – HERO Facility, hydrodynamic modeling of the bottom holes.

4.2.1.2 Modeling of the heat structures

The heat structures HS-1000 and HS-1100 are modeled as reported in Ref. [21] and section 3.1. HS-1140 is summarized in *Tab. 21*, it accounts for the insulating paint (the same of the bayonet tube) and the AISI-304 double wall. The heating power is supplied in HS-1170 at pipe-170 outer surface (6 out of 18 nodes), *Tab. 22*.

COMPONENT LABEL		TYPE	DESCRIPTION
HS-1140		Heat structure	Heat transfer between 140+150+160 and - 180+175+170
Id.	Parameter	Quantity	Notes
a	Axial node height	0.1500 m	Pipe 140 - Pipe 180
b	N° axial nodes	40	Pipe 140 - Pipe 180
c	Axial node height	0.1500 m	Branch 150 - Branch 175
d	N° axial nodes	1	Branch 150 - Branch 175
e	Axial node height	0.1500 m	Pipe 160 - Pipe 170
f	N° axial nodes	17	Pipe 160 - Pipe 170
g	Axial node height	0.2000 m	Pipe 160 - Pipe 170
h	N° axial nodes	1	Pipe 160 - Pipe 170
i	Inner radius	0.0236 m	--
j	Radial interval width	$3.3333 \cdot 10^{-4}$ m	AISI-304
k	N° radial intervals	6	AISI-304
l	Radial interval width	$3.7500 \cdot 10^{-4}$ m	Insulator
m	N° radial intervals	8	Insulator
n	Radial interval width	$3.3333 \cdot 10^{-4}$ m	T91
o	N° radial intervals	6	T91
p	Initial temperature	335 °C	--
q	Left boundary heated diameter	0.0259 m	
r	Left boundary heated diameter	0.0473 m	Pipe 160
s	Right boundary heated diameter	0.0400 m	

Tab. 21 – HERO Facility, modeling of the heat structure between the feedwater tube and the annular riser.

COMPONENT LABEL		TYPE	DESCRIPTION
HS-1170		Heat structure	Heat transfer between 136+180+ +175+170+165 and Power999
Id.	Parameter	Quantity	Notes
a	Axial node height	0.2000 m	Branch 136
b	N° axial nodes	1	Branch 136
c	Axial node height	0.1500 m	Pipe 180
d	N° axial nodes	40	Pipe 180
e	Axial node height	0.1500 m	Branch 175
f	N° axial nodes	1	Branch 175
g	Axial node height	0.1500 m	Pipe 170 - Power999 (5 nodes)
h	N° axial nodes	17	Pipe 170 - Power999 (5 nodes)
i	Axial node height	0.2000 m	Pipe 170 - Power999 (1 node)
j	N° axial nodes	1	Pipe 170 - Power999 (1 node)
k	Axial node height	0.2000 m	Branch 165
l	N° axial nodes	1	Branch 165
m	Inner radius	0.0394 m	--
n	Radial interval width	$6.2500 \cdot 10^{-4}$ m	AISI-304
o	N° radial intervals	8	AISI-304
p	Initial temperature	335 °C	--
q	Left boundary heated diameter	0.0311 m	

Tab. 22 – HERO Facility, modeling of the heat structure between the annular riser and the lead channel (active height only).


4.2.2 Identification of the Potential Geometries of HERO

Each calculation is repeated four times:

- Two simulations account for the maximum and minimum concentrated pressure losses. They are labeled as “k-max” and “k-min”.
- Two simulations account for different time. The first stops at 900 s in order to shorten the computational time and to obtain preliminary results; the second has been launched “a posteriori” and stops at 1100 s in order to capture eventual discrepancies from steady state conditions (in terms of mass flow rate).
- In this preliminary analysis, the 8 fissures at the top and those at the bottom are modeled assuming to keep as constant the flow area at the bottom holes inlet of the initial geometry (0.0017 m^2). The influence of this parameter is essential to control the mass flow rate and will be investigated in detail.

The main aim of the analysis is to point out the reference geometry. In order to get an appropriate margin of operation, the goal is to obtain a mass flow rate larger than 6.367 kg/s, possibly close to 7.0-7.5 kg/s. The lead flow area is expected to dominate the mass flow rate. Therefore, three types of simulations are performed starting from the initial configuration.

- The first investigates the influence of the outer flow area AX. The initial flow area is assumed two times those of the bayonet tube lead channel (in the SG configuration): 2AX. The analysis exploits 4AX, 6AX and 10AX. The main modifications applied to the input deck are described in Ref. [30].

 Ricerca Sistema Elettrico	Sigla di identificazione	Rev.	Distrib.	Pag.	di
	NNFISS - LP3 - 054	0	L	68	117

- The second one investigates the influence of the bayonet tube channel flow area AY . The initial flow area is modeled equal to the SG lead channel configuration: $AY (=AX)$. $1.5AY$, $2AY$, $2.5AY$ and $3AY$ are analyzed. The main modifications applied to the input deck are described in Ref. [30].
- The last one deals with the combination of the previous, $AX-AY$. The analyses are described in Ref. [30].

Fig. 31 reports the flow area of the up flow outer channel (x axis) and the lead mass flow rate (y axis). The simulations are those at 900 s. Both max k and min k calculations are included. The green dotted curve represents the SGBT lead mass flow rate.

- At constant down-flow channel flow area AY , the lead mass flow rate does not reach 4 kg/s whatever is the up flow outer channel flow area (i.e. $10 AX$), red - black labeled points.
- On the other hands, at constant outer channel flow area $2AX$, the lead mass flow rate does not reach 5 kg/s whatever is the down-flow channel flow area (i. e. $3 AY$), black – blue labeled points.
- It is therefore necessary to reduce the distributed pressure losses limiting the lead velocity and thus increasing both the flow areas (red – blue labeled points). In particular, $4AX-2.5AY$, and $6AX-2.5AY$ have been selected as potential geometries. They allows to reach 6.5 – 7.4 kg/s.
- Concentrated pressure losses have in general a minor impact on the simulations, particularly at low flow areas. At high flow areas (i. e. $6AX-2.5AY$), the concentrated pressure losses highlight a certain influence on the results.

The main results are summarized in *Tab. 23*. The table reports the mass flow rates achieved in the simulations and highlights the influence of the computational time comparing the results obtained at 900 s with those obtained after 1100 s. In general, the calculations are in agreement with an error less than 1 %. In conclusion, the potential geometries have been fixed according to *Tab. 24*

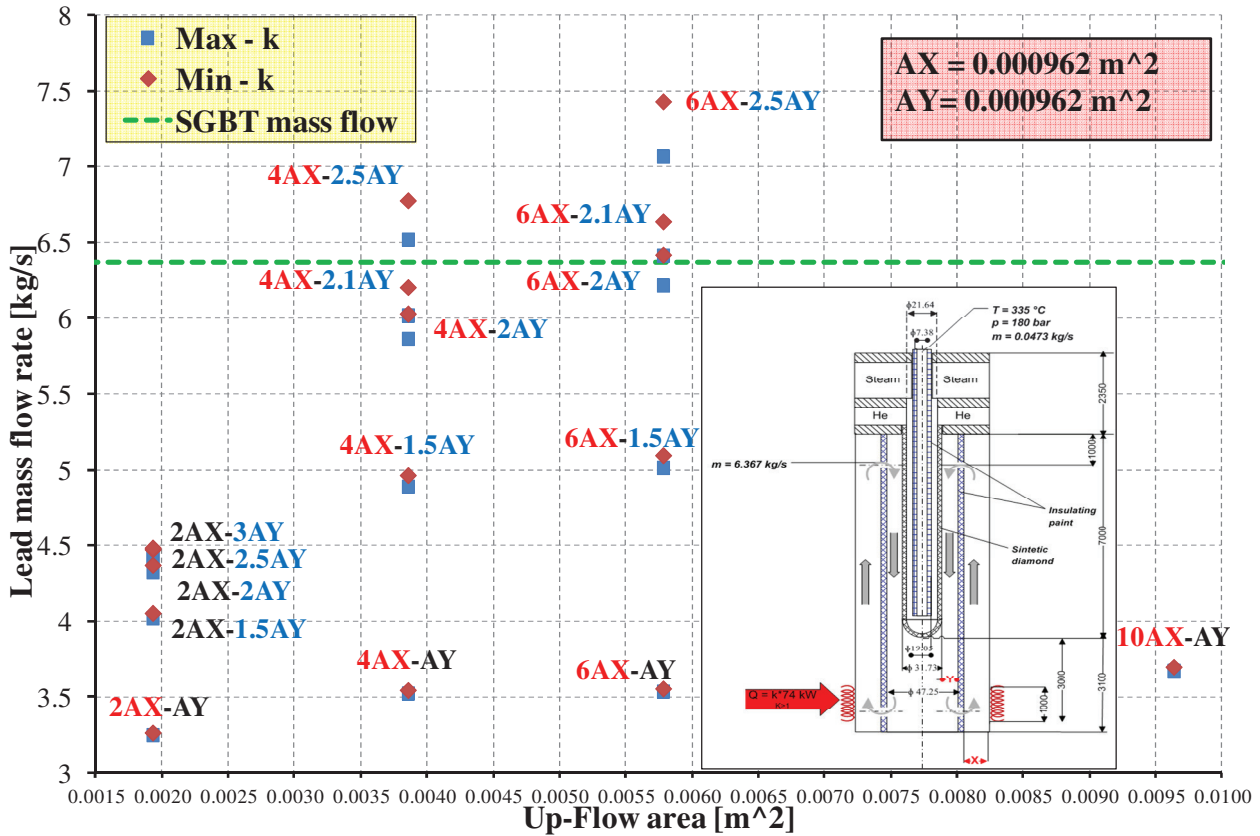


Fig. 31 – HERO Facility, calculations in support to the determination of the radial geometry.

Description	Max k		Min k	
	Mass flow 900 s [kg/s]	Mass flow 1100 s [kg/s]	Mass flow 900 s [kg/s]	Mass flow 1100 s [kg/s]
2Ax-Ay	3.25	3.25	3.26	3.26
4Ax-Ay	3.52	3.51	3.54	3.53
6Ax-Ay	3.53	3.52	3.55	3.54
10Ax-Ay	3.67	3.56	3.70	3.57
2Ax-1.5Ay	4.02	4.01	4.05	4.04
4Ax-1.5Ay	4.89	4.87	4.96	4.94
6Ax-1.5Ay	5.01	5.01	5.09	5.10
2Ax-2Ay	4.32	4.31	4.37	4.36
4Ax-2Ay	5.86	5.85	6.03	6.01
6Ax-2Ay	6.21	6.19	6.41	6.39
4Ax-2.1Ay	6.02	6.00	6.20	6.19
6Ax-2.1Ay	6.41	6.38	6.63	6.62
2Ax-2.5Ay	4.42	4.41	4.47	4.46
4Ax-2.5Ay	6.52	6.50	6.77	6.76
6Ax-2.5Ay	7.07	7.06	7.43	7.41
2Ax-3Ay	4.43	4.42	4.48	4.47

Tab. 23 – HERO Facility, calculations in support to the determination of the radial geometry, summary of the results.

Label	Parameter	Unit	Quantity
4AX-2.5AY	4AX up-flow area	m ²	0.003852
	2.5AY down-flow area	m ²	0.002407
	X	m	0.013437
	Y	m	0.016041
6AX-2.5AY	6 AX up-flow area	m ²	0.005778
	2.5 AY down-flow area	m ²	0.002407
	X	m	0.018997
	Y	m	0.014058

Tab. 24 – HERO Facility, definition of the potential radial geometries.

4.2.3 Assessment of the HERO Reference Configuration

4.2.3.1 Definition of the computational time

The preliminary calculations last 900 s and at 1100 s. They revealed minor deviations in the prediction of the lead mass flow rate. In order to fix a computational time that is representative of steady state conditions, further investigations are conducted extending the computational time up to 6000 s.

The time dependent trend of the mass flow of the investigated configurations is depicted in *Fig. 32* and *Fig. 33*. The initial transient reaches its peak at 500 s then it starts to match the steady state. The effective behavior is expected to be smoothed out oscillations.

The time dependent trend of the lead temperatures in pipe 140 is reported in *Fig. 34* and *Fig. 35*. Steady state conditions appear over 2500-3000 s. Should be mentioned that the initial lead temperature assumed in the calculations is 335°C and this impacts on the transient duration. During the transient phase, the temperature tends to increase of about 40 °C. Therefore, in order to capture the steady state temperatures as much as possible and to do not increase too much the duration of the calculations, 2500 s has been selected as computational time of all the calculations reported in the following sections. In order to favor the read-ability of the figures, they do not include the trend of min-k simulations: it is similar to max-k.

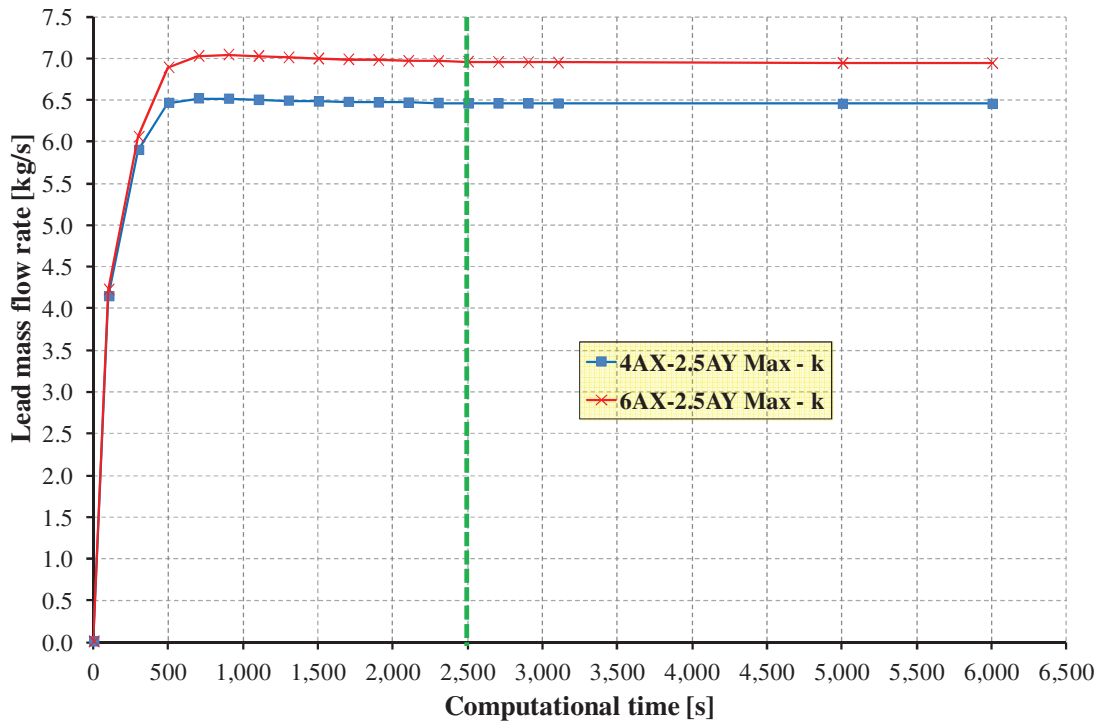


Fig. 32 – HERO Facility calculations in support to the determination of the computational time, mass flow rate.

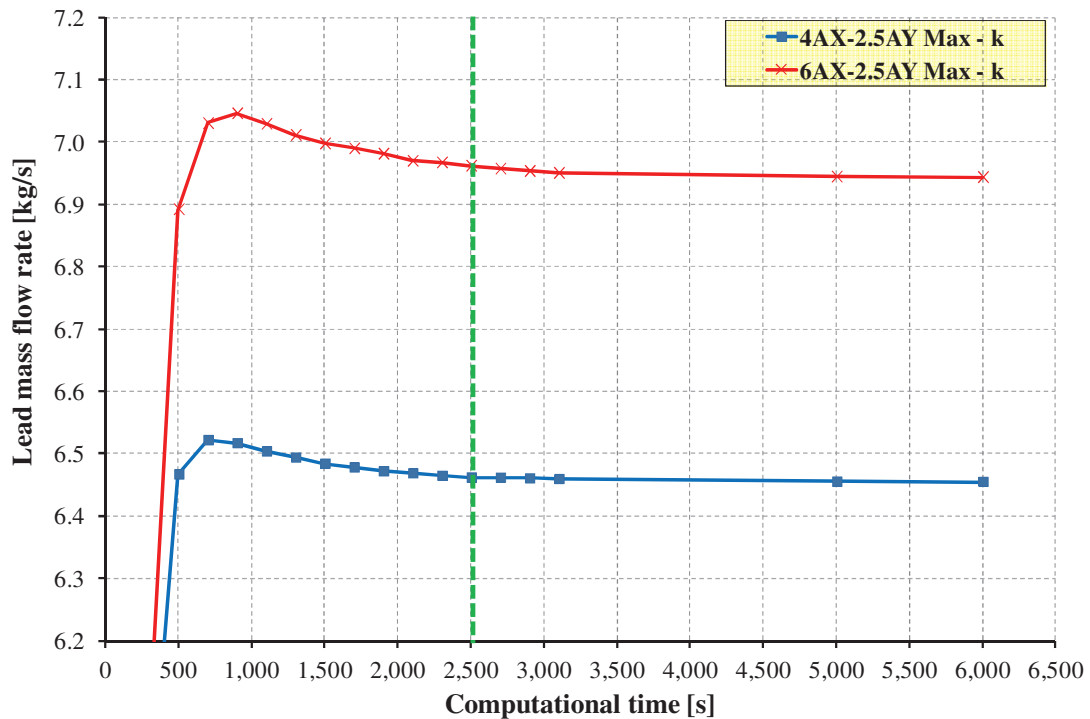


Fig. 33 – HERO Facility calculations in support to the determination of the computational time, mass flow rate zoom.

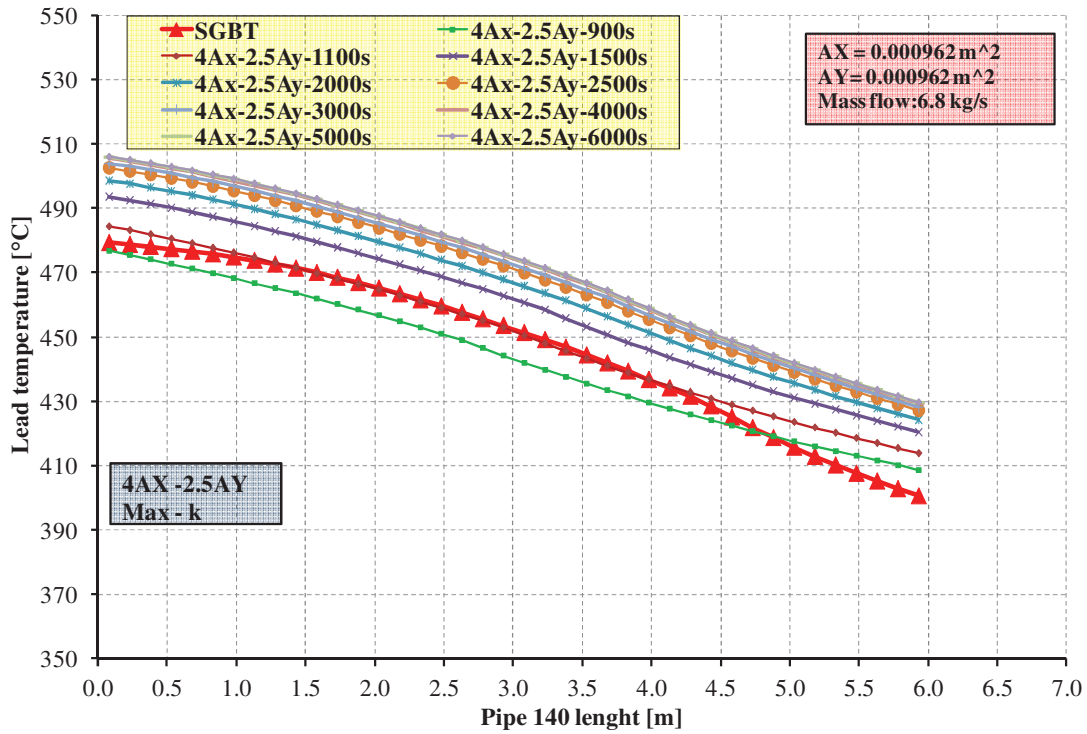


Fig. 34 – HERO Facility calculations in support to the determination of the computational time, lead temperature in pipe 140.

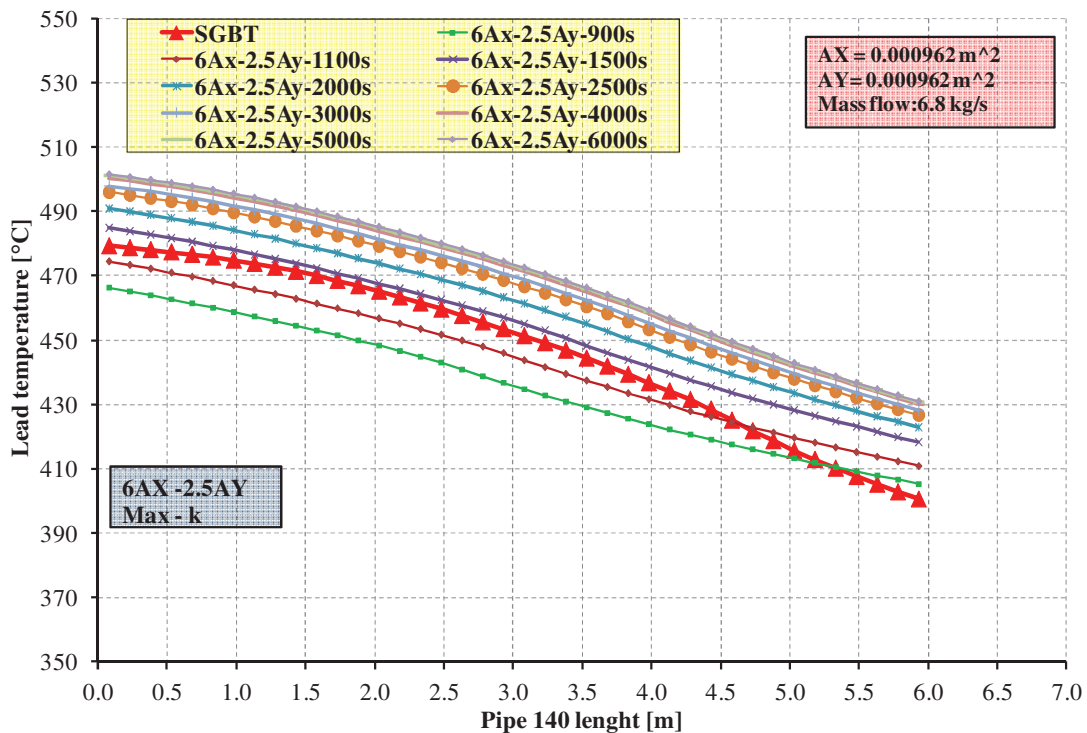


Fig. 35 – HERO Facility calculations in support to the determination of the computational time, lead temperature in pipe 140.

4.2.3.2 Assessment of the fissure geometry and determination of the mass flow curves

Eight fissure at the bottom and eight at the top are considered in this calculation. Each fissure is assumed 0.005m x 0.100 m. The fissures are located as depicted in Fig. 28. Their maximum flow area is 0.004 m².

The regulation curves of the selected configurations are depicted in Fig. 36 and Fig. 37. The main results are summarized in Tab. 25.

The configuration 4AX-2.5AY allows to achieve a flow rate in the range 6.9-7.0 kg/s (Fig. 36) at maximum flow area. The lead level largely affects the lead mass flow rate up to 50mm. Beyond this value, the lead level has a minor influence on the mass flow rate. The lead levels 25 mm (min -k) and 35 mm (max-k) correspond to the desired mass flow rate. Their total flow areas are 0.0010 m² and 0.0014 m² respectively, Tab. 25.

The configuration 6AX-2.5AY allows to achieve a flow rate in the range 7.7-7.8 kg/s at maximum flow area, Fig. 37. The lead level largely affects the lead mass flow rate up to 50 mm. Beyond this value, the lead level has a minor influence on the mass flow rate. The lead levels 17.5 mm (min -k) and 25 mm (max-k) correspond to the desired mass flow rate. Their total flow areas are 0.0007 m² and 0.0010 m² respectively, Tab. 25.

In the operating conditions (6.367 kg/s), the lead level seems to play high influence on the lead mass flow. In order to avoid mass flow changes related to level fluctuations (i.e. temperature transients), the fissures total flow area could be distributed into two or more axial elevations.

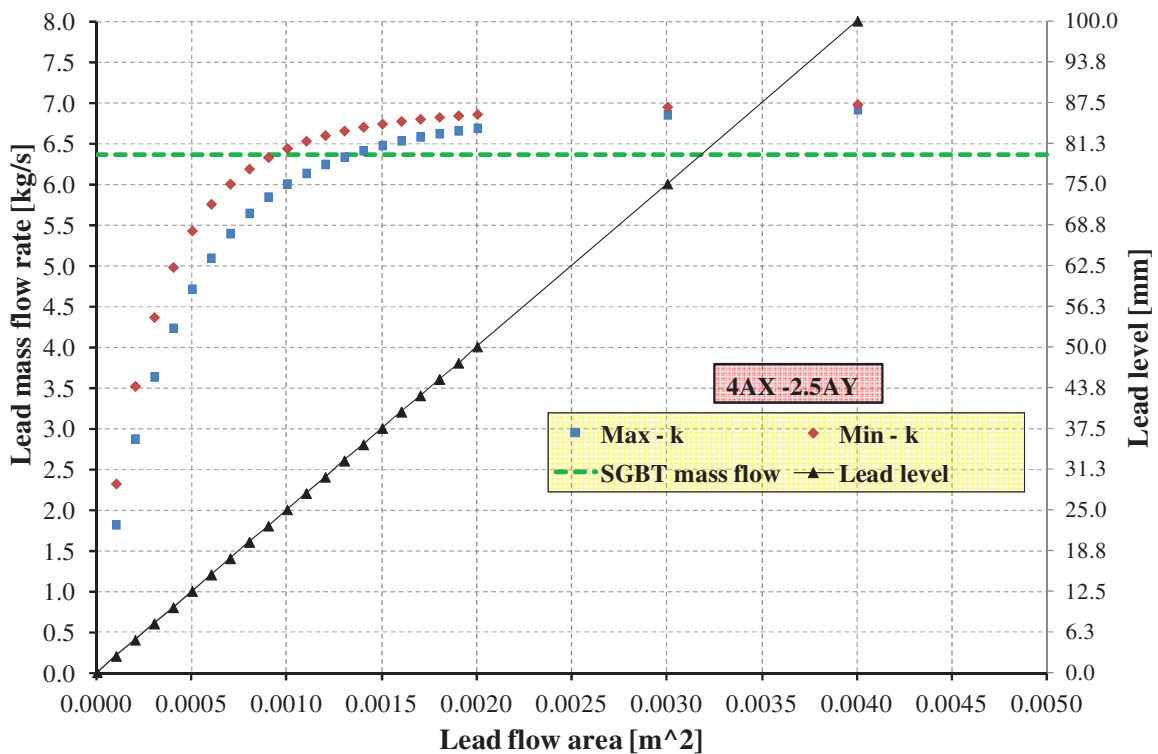


Fig. 36 – HERO Facility, 4AX-2.5AY, mass flow rate as function of lead level at the fissures inlet.

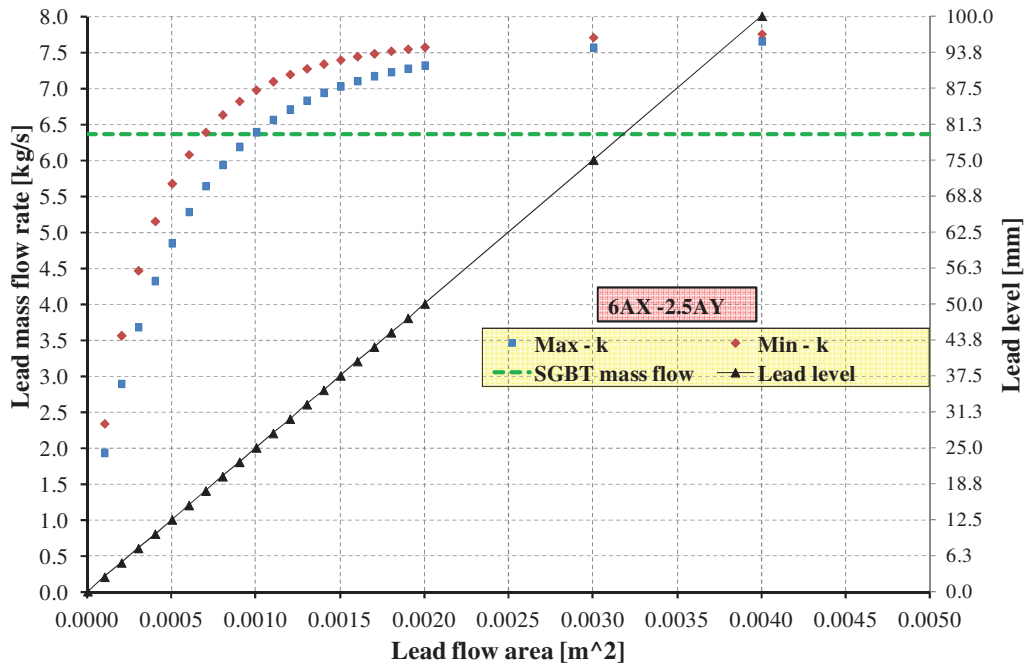


Fig. 37 – HERO Facility, 6AX-2.5AY, mass flow rate as function of lead level at the fissures inlet.

Level [mm]	Total flow area [m ²]	6AX-2.5AY		4AX-2.5AY	
		Max – k mass flow [kg/s]	Min – k mass flow [kg/s]	Max – k mass flow [kg/s]	Min – k mass flow [kg/s]
100.0	0.004	7.6530	7.7536	6.9140	6.9758
87.5	0.0035	7.6190	7.7343	6.8894	6.9635
75.0	0.0030	7.5633	7.7041	6.8518	6.9444
62.5	0.0025	7.4732	7.6507	6.7915	6.9127
50.0	0.0020	7.3172	7.5700	6.6850	6.8552
47.5	0.0019	7.2736	7.5428	6.6537	6.8382
45.0	0.0018	7.2240	7.5136	6.6183	6.8187
42.5	0.0017	7.1671	7.4795	6.5792	6.7960
40.0	0.0016	7.1003	7.4394	6.5326	6.7692
37.5	0.0015	7.0240	7.3919	6.4732	6.7371
35.0	0.0014	6.9363	7.3363	6.4099	6.6987
32.5	0.0013	6.8287	7.2703	6.3336	6.6515
30.0	0.0012	6.7056	7.1909	6.2426	6.5957
27.5	0.0011	6.5606	7.0923	6.1330	6.5268
25.0	0.0010	6.3885	6.9734	6.0003	6.4367
22.5	0.0009	6.1839	6.8175	5.8400	6.3269
20.0	0.0008	5.9345	6.6286	5.6394	6.1848
17.5	0.0007	5.6385	6.3870	5.3945	5.9996
15.0	0.0006	5.2800	6.0760	5.0885	5.7522
12.5	0.0005	4.8462	5.6735	4.7079	5.4244
10.0	0.0004	4.3207	5.1485	4.2305	4.9759
7.5	0.0003	3.6768	4.4625	3.6309	4.3625
5.0	0.0002	2.8901	3.5598	2.8700	3.5160
2.5	0.0001	1.9333	2.3339	1.8173	2.3188
0.0	0.0000	0.0000	0.0000	0.0000	0.0000

Tab. 25 – HERO Facility, assessment of the potential configurations, mass flow rates as function of fissures flow area (and lead level).

4.2.4 Comparison Between Selected Lead Levels and SGBT

The simulations that correspond to the desired lead mass flow rate are assessed in this section (bold red evidenced in *Tab. 25*). *Tab. 26* and *Tab. 27* compare the performances of the configurations with those of SGBT respectively for max-k and min-k assumptions. Negligible differences are evidenced between 4AX-2.5AY-00XX and 6AX-2.5AY-00YY. The index 00XX refers to the total flow area at the top fissures (i.e. 0014 means a total flow area of 0.0014 m²).

The hydraulic diameter of Pipe 140 does not differ too much with those of SGBT lead channel. Nevertheless, due to the increased flow area, the lead velocity in Pipe 140 is largely reduced (from 0.64 m/s to 0.26 m/s). Therefore, the Reynolds number results reduced of about 1/3. Consequently, the Nusselt number and the average heat transfer coefficient at Pipe 140 outer wall decreases down to 3000 W/m²K (instead of 10000 W/m²K). This causes increased temperature drop between the average fluid conditions and the Pipe 140 outer wall. From one hand, the average lead temperature increases (about 497 °C at tube inlet) and, from the other hand, the pipe 140 outer wall temperature decreases, *Fig. 39*, *Fig. 40*, *Fig. 42* and *Fig. 43*. Anyway, the superheated steam outlet temperature remains over 446 °C (reduced of about 7-10 °C) and the void fraction is predicted close to 1 within the first 3 meters (as in the SGBT) even if the trend is slightly different, *Fig. 38* and *Fig. 41*. Detailed investigations are ongoing at CR BRASIMONE by means of CFX to assess with great detail the lead side temperatures.

To reproduce in a more accurate manner the lead size conditions, a possible alternative is to introduce gas enhanced circulation. This allows to keep unchanged the SGBT channel geometry. In this last case, natural circulation will stabilize around 3.7 kg/s and could be the operating conditions to support the V&V of CFD – TH-sy coupled simulations. This operational mode is currently under investigation at CR BRASIMONE by means of RELAP-5.

Parameter	Unit	SGBT	HERO max-k 4AX-2.5AY-0014A	HERO max-k 6AX-2.5AY-0010A
Reynolds number, pipe 140	--	1.282E+05	4.477E+04	4.477E+04
Average HTC, pipe 140	W/m ² K	10000	3008	3001
Lead channel hydraulic diameter	m	0.039	0.032	0.032
Lead channel heated diameter	m	0.039	0.096	0.096
Lead channel flow area	m ²	0.00096	0.00241	0.00241
Lead mass flow rate	Kg/s	6.367	6.437	6.388
Lead inlet temperature	°C	479.40	499.00	497.40
Lead outlet temperature	°C	400.40	422.80	420.20
Feedwater inlet temperature	°C	334.40	334.40	334.40
Feedwater tube temperature drop	°C	1.30	1.20	1.20
Immersed tube steam temperature	°C	458.10	451.20	449.10
Superheated steam outlet temperature	°C	456.90	449.00	447.10
Void fraction	--	1.00	1.00	1.00
Pressure drop in the SGBT	bar	2.88	2.70	2.65
Lead velocity	m/s	0.64	0.26	0.26

Tab. 26 – HERO Facility, max-k, comparison between selected configurations and SGBT.

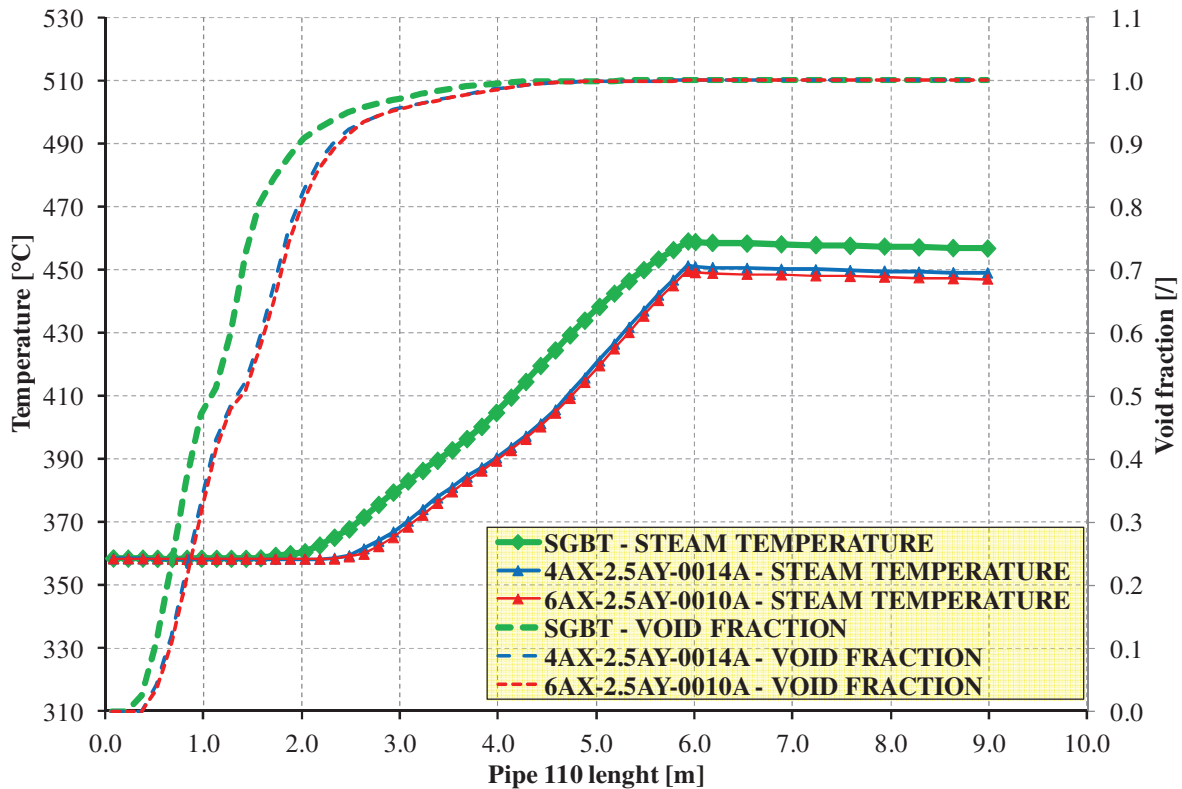


Fig. 38 – HERO Facility, max-k, 4AX-2.5AY-0014A and 6AX-2.5AY-0010A versus SGBT, steam-water side.

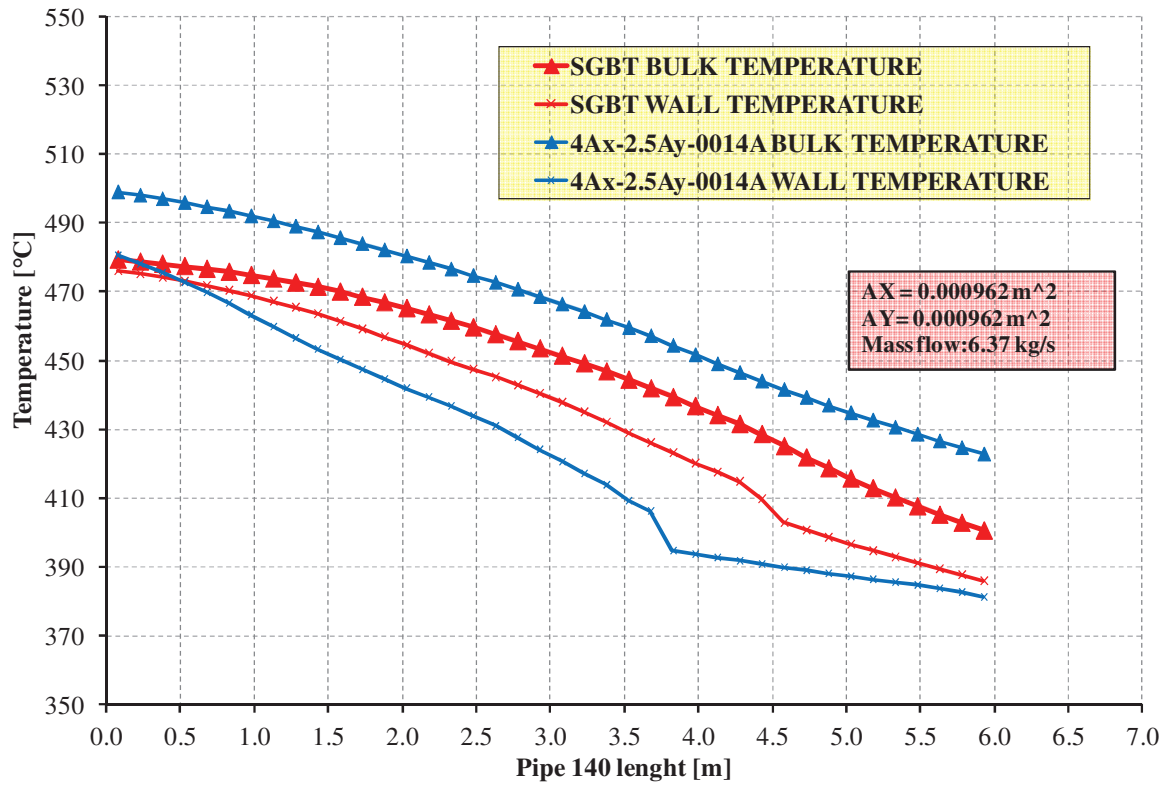


Fig. 39 – HERO Facility, max-k, 4AX-2.5AY-0014A versus SGBT, lead side.

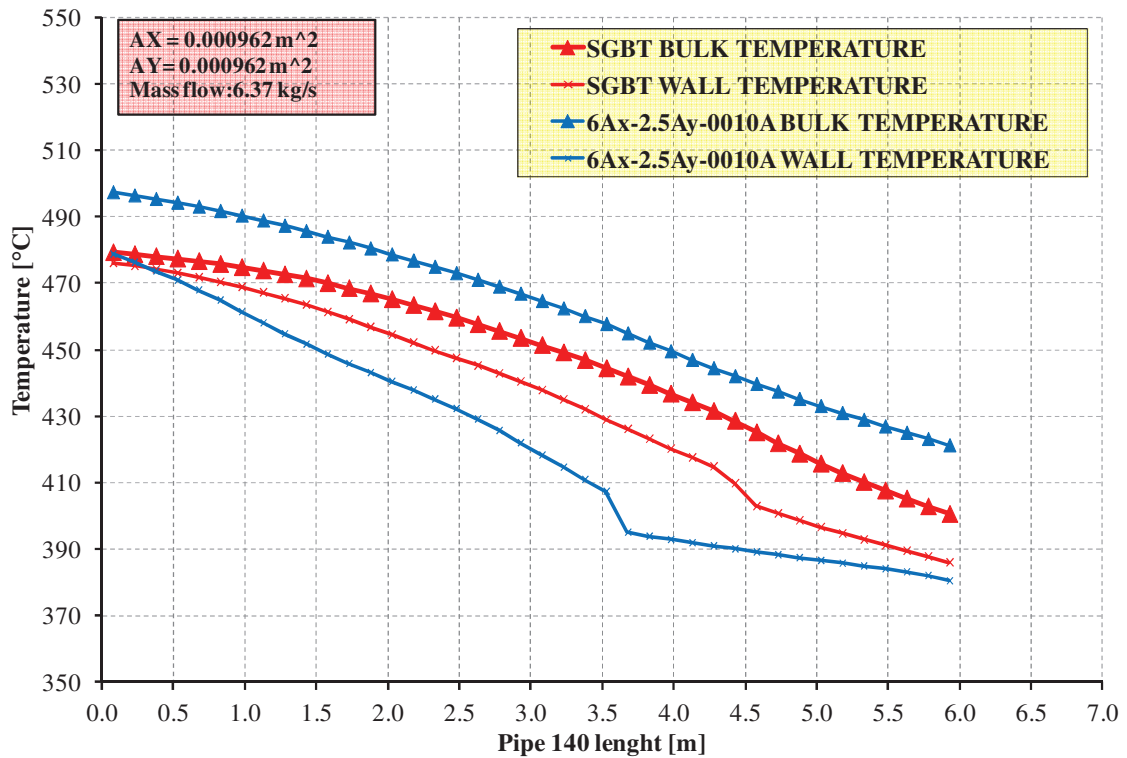


Fig. 40 – HERO Facility, max-k, 6AX-2.5AY-0010A versus SGBT, lead side.

Parameter	Unit	SGBT	HERO max-k 4AX-2.5AY-0010A	HERO max-k 6AX-2.5AY-0007A
Reynolds number, pipe 140	--	1.282E+05	4.477E+04	4.477E+04
Average HTC, pipe 140	W/m ² K	10000	3015	3000
Lead channel hydraulic diameter	m	0.039	0.032	0.032
Lead channel heated diameter	m	0.039	0.096	0.096
Lead channel flow area	m ²	0.00096	0.00241	0.00241
Lead mass flow rate	Kg/s	6.367	6.387	6.437
Lead inlet temperature	°C	479.40	498.79	497.38
Lead outlet temperature	°C	400.40	422.90	421.25
Feedwater inlet temperature	°C	334.40	334.40	334.40
Feedwater tube temperature drop	°C	1.30	1.10	1.10
Immersed tube steam temperature	°C	458.10	451.28	449.28
Superheated steam outlet temperature	°C	456.90	449.02	446.97
Void fraction	--	1.00	1.00	1.00
Pressure drop in the SGBT	bar	2.88	2.70	2.67
Lead velocity	m/s	0.64	0.26	0.26

Tab. 27 – HERO Facility, min-k, comparison between selected configurations and SGBT.

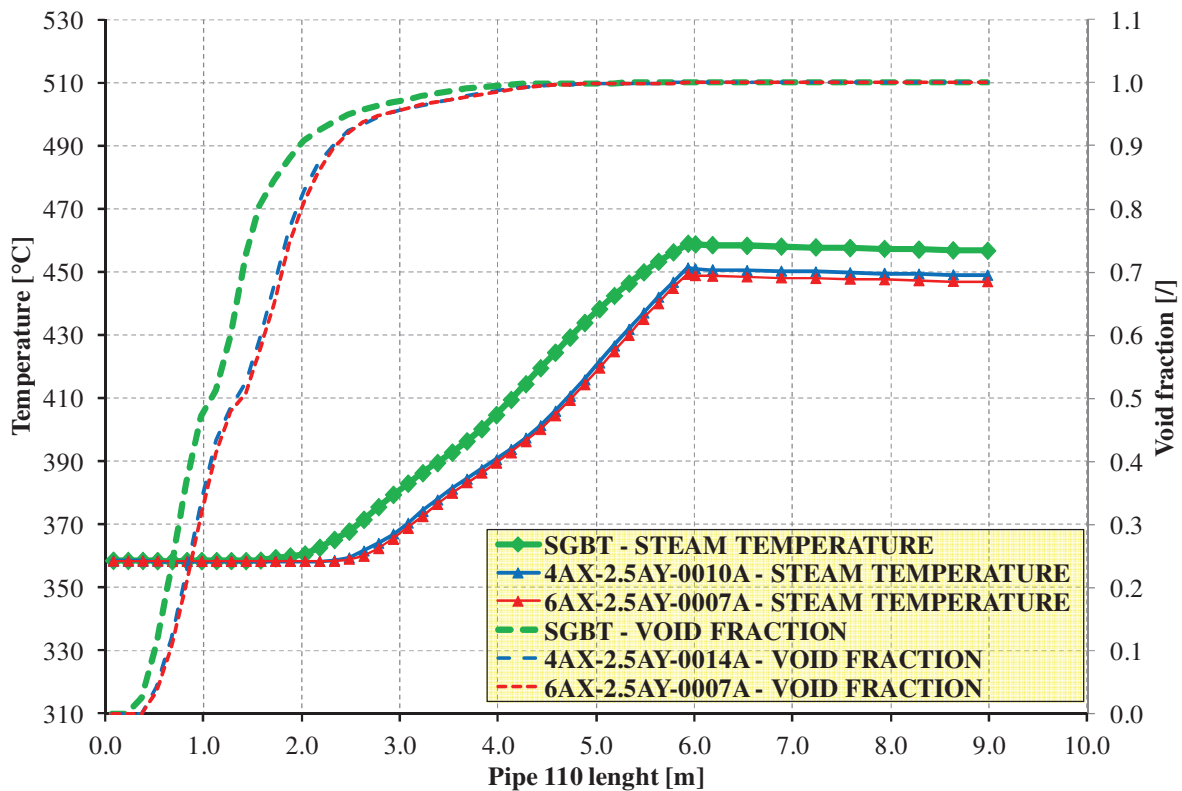


Fig. 41 – HERO Facility, min-k, 4AX-2.5AY-0010A and 6AX-2.5AY-0007A versus SGBT, steam-water side.

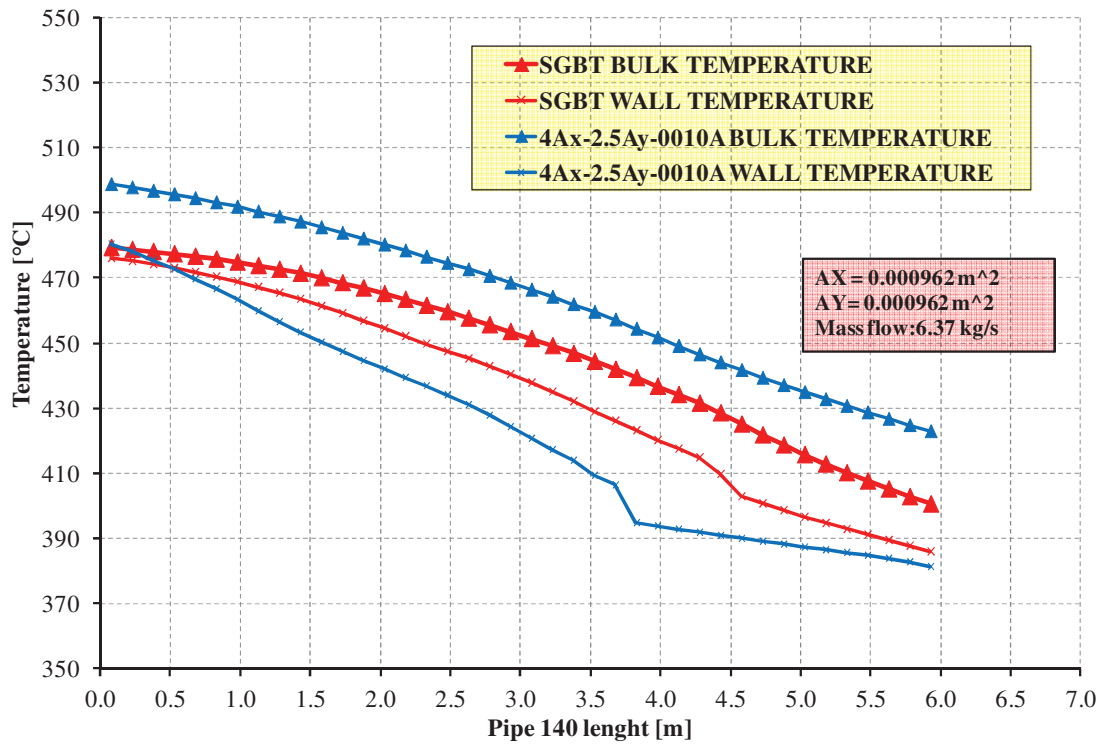


Fig. 42 – HERO Facility, min-k, 4AX-2.5AY-0010A versus SGBT, lead side.

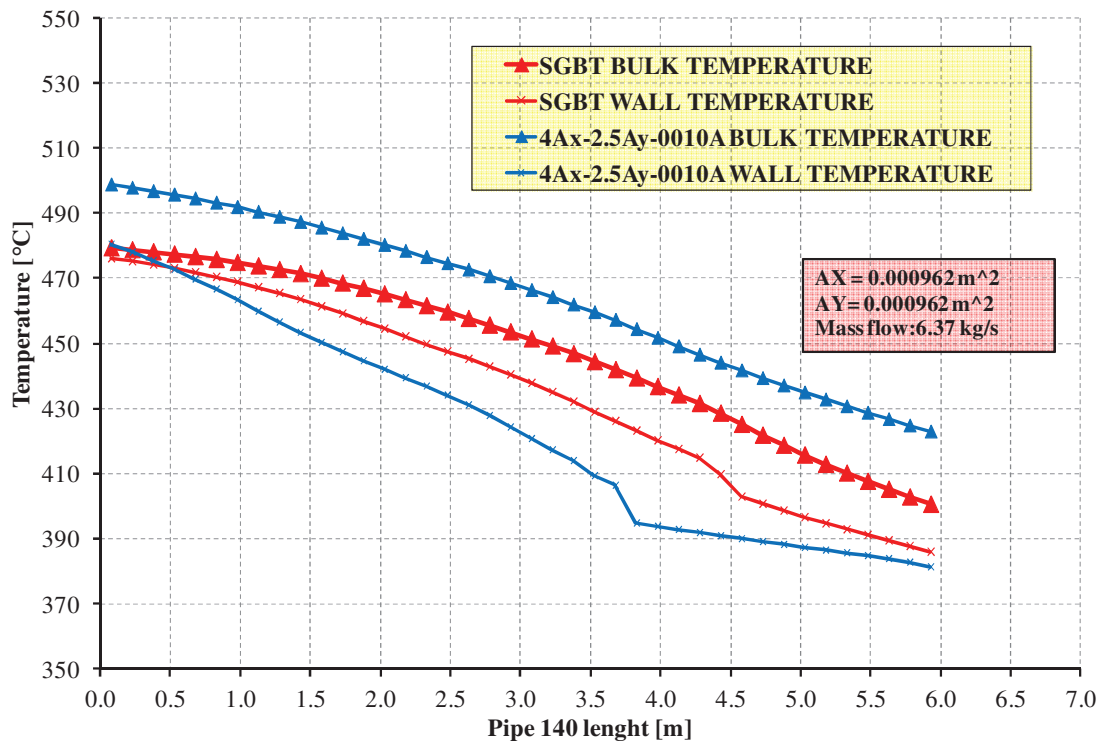


Fig. 43 – HERO Facility, min-k, 6AX-2.5AY-0007A versus SGBT, lead side.

4.3 Calculations in Support to the TH Design of HERO by FLUENT

4.3.1 Preliminary 2D Axial-Symmetric Simulations

In order to support the design of the HERO facility, three preliminary 2D axial-symmetric simulations were performed using the commercial CFD code ANSYS FLUENT v13.0 Ref. [31] and they are labeled A, B, and C. The simulations were performed assuming the area of the lead channel flow and the length of the facility as parameters, while the active length of the bayonet tube was assumed equal to 6 m (same length of the ALFRED SG tube) for all the simulations. The mass flow rate in the lead channel is monitored in all the simulations: the goal was to obtain in steady state condition a mass flow rate larger than 6.37 kg/s, possibly close to 7.0-7.5 kg/s. The adopted geometrical domain is showed in Fig. 44.

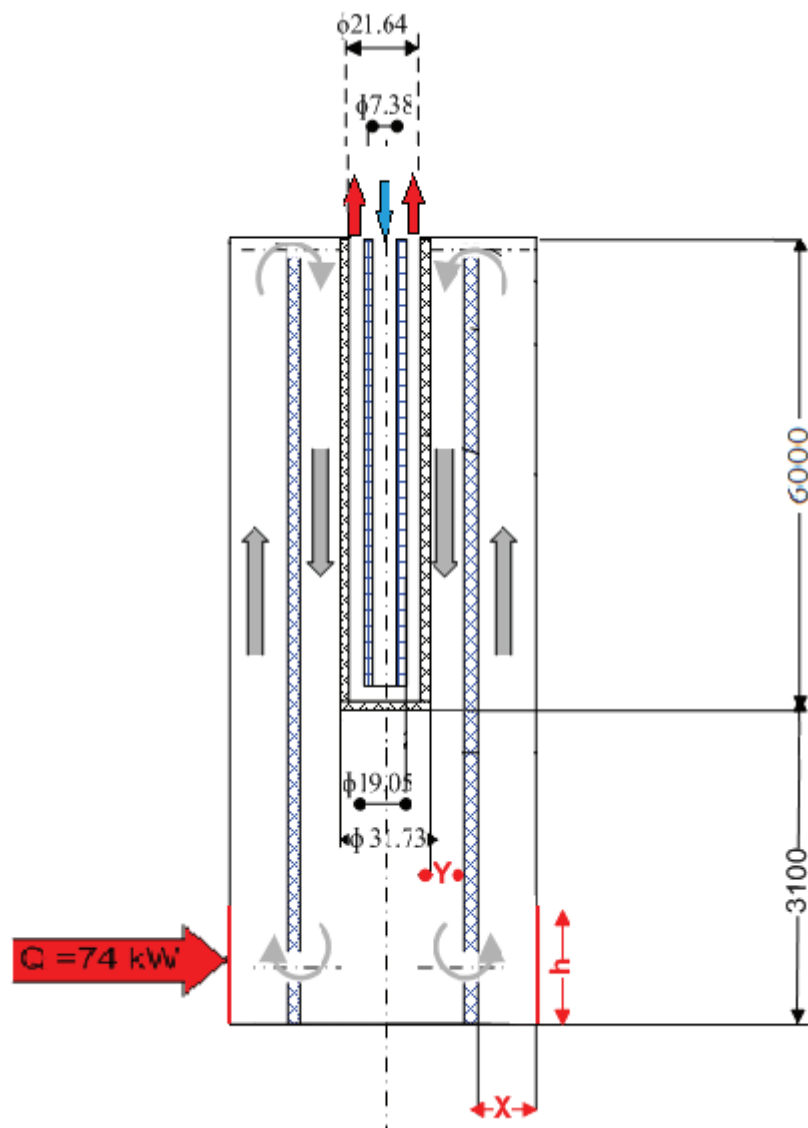


Fig. 44– HERO Facility, FLUENT simulations, 2D geometrical domain.

The first configuration (A) is according to Fig. 44. It has a lead channel flow area and a total length set equal, respectively, to the equivalent lead channel flow area and to 6000 + 3100mm.

In order to investigate the influence of the distance between the cold and hot sinks, the second configuration (*B*) is characterized by a lead channel flow area equal to the equivalent lead channel flow area of a single tube of the ALFRED steam generator and by a total length 2 m longer than case A (6000 + 5100 mm),.

In the third simulation (*C*) the pipe has the same length of case A while the lead channel flow area is 2.5 times greater than the equivalent lead channel flow area of the SG configuration.

Simulation	Lead flow area	Tube length
A	0.000962 m ²	9.1 m
B	0.000962 m ²	11.1 m
C	0.002407 m ²	9.1 m

Tab. 28 – HERO Facility, summary of the simulations.

Due to the lack of CFD tools in simulating two phase systems, only the primary lead circuit was modeled, while the effect of the secondary water circuit was taken into account imposing, by means of an User Defined Function (UDF), the temperature profile evaluated by RELAP5 simulations (according to Ref. [21]) on the SGBT outer surface (see Fig. 45)

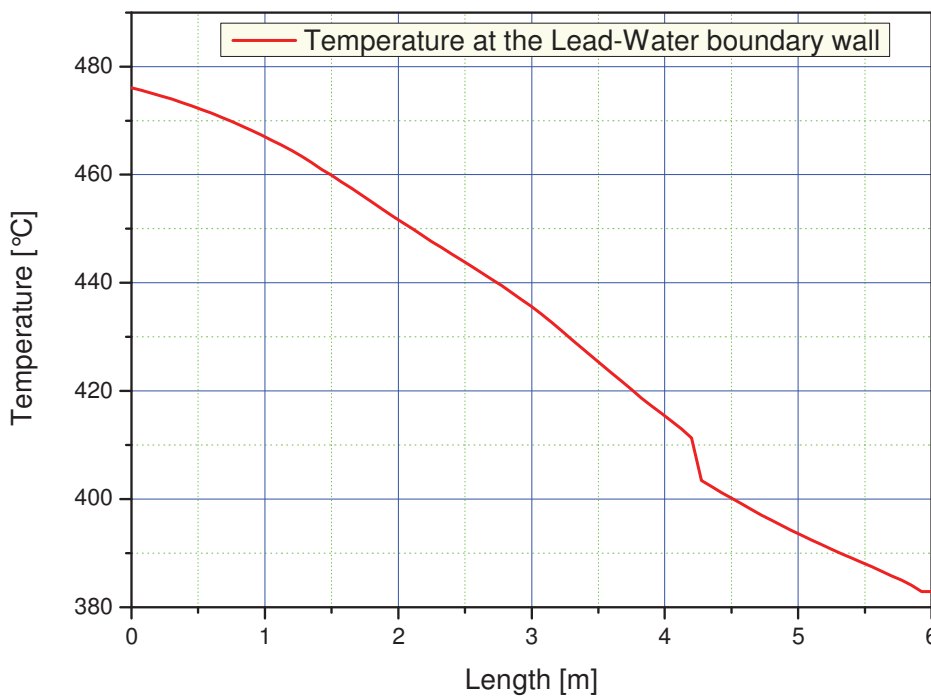


Fig. 45 – HERO Facility, FLUENT simulations, temperature profile imposed at the wall separating the primary and the secondary circuit (from RELAP5 simulation).

The heaters were considered as cylindrical, placed at the bottom of the facility on the external surface with an height of one meter and a total thermal power of about 74 kW, according to the power removed by a single SGBT of ALFRED. The wall between the lead down-flow and up-flow annular regions is considered adiabatic. The thermodynamic and thermo-physical properties of the lead, such as density, molecular viscosity, thermal conductivity and specific heat were chosen according to Ref. [32].

The geometrical domain was discretized adopting hexahedral mesh with special refinements near to the wall boundaries of the domain (see Fig. 46 and Fig. 47) to obtain values for y^+ near the wall in the order of 1. The turbulence model was the $k-\varepsilon$ RNG with enhanced wall treatment model.

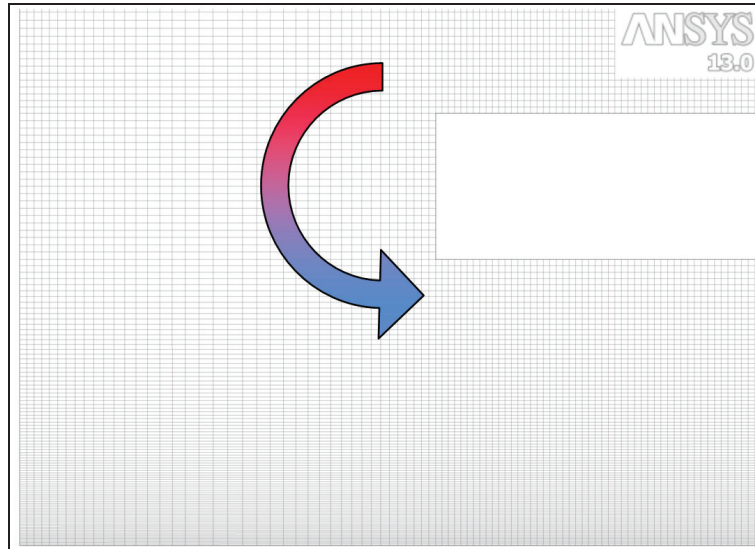


Fig. 46 – HERO Facility, FLUENT simulations, detail of the mesh at the entrance of the cooling annular channel.

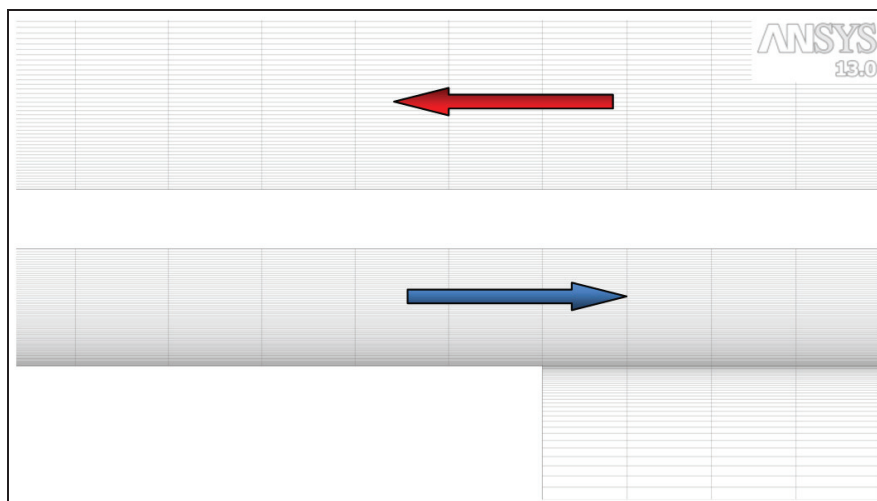


Fig. 47 – HERO Facility, FLUENT simulations, detail of the mesh at the exit of the cooling annular channel.

The simulations were performed in steady state conditions. The steady state was checked monitoring both the mass flow rate and the temperature trends at the inlet of the SGBT annular section (see *Errore. L'origine riferimento non è stata trovata.* and *Errore. L'origine riferimento non è stata trovata.*).

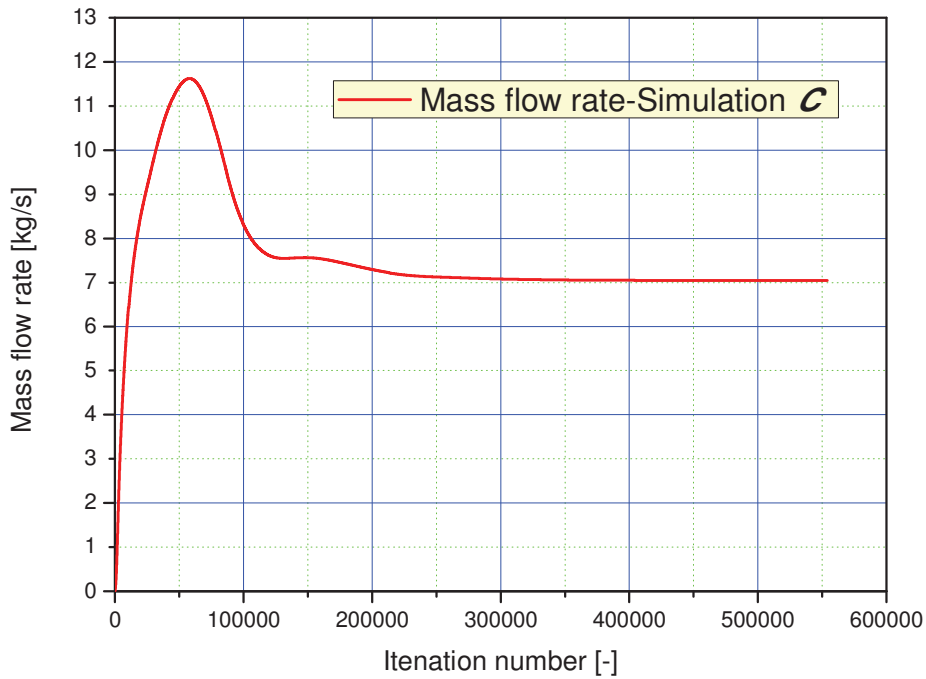


Fig. 48 – HERO Facility, FLUENT simulation C, mass flow rate at the inlet of the cooling channel.

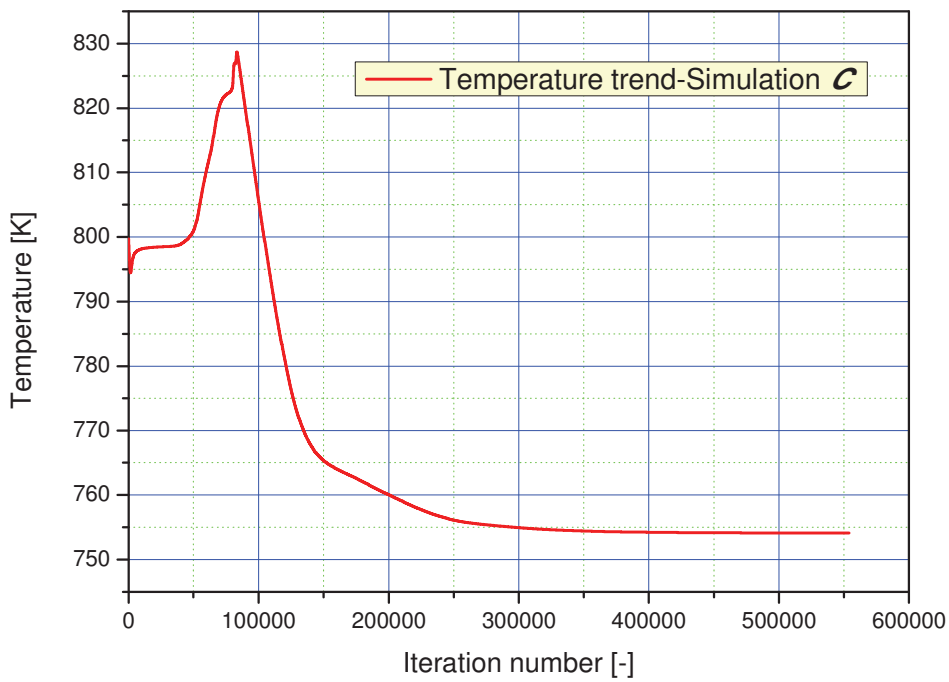


Fig. 49 – HERO Facility, FLUENT simulation C, temperature at the inlet of the cooling channel.

Tab. 29 summarizes the mass flow rates achieved through the SGBT annular channel in the three simulations.

Simulation	Mass flow rate
A	~ 4 kg/s
B	~ 4.23 kg/s
C	~ 7.04 kg/s

Tab. 29 – HERO Facility, FLUENT simulations, mass flow rate results.

For Simulation C, lead enters in the SGBT channel with an average temperature of about 481 °C and it leaves the channel with an average temperature of about 408 °C.

From the 2D simulations can be concluded that the desired mass flow rate obtained in natural circulation condition can not be reached maintaining the equivalent SGBT lead channel flow area. In addition, an increase in the distance between the hot source and cold sink gives negligible increase in the flow rate versus a significant increases in the sizes of the structure.

The increase of the lead channel flow area, hence, turns out to be the more efficient solution to achieve the desired value of mass flow rate. The selected potential radial geometries are thus the 4AX-2.5AY and 6AX-2.5AY (see Fig. 28 and Tab. 24).

4.3.2 Preliminary 3D Simulations

Three-dimensional calculations are performed on the geometrical domain related to the 4AX-2.5AY configuration. Further investigations on the 6AX-2.5AY configuration are ongoing.

The heating rods geometry are not simulated (as for the 2D-axis symmetric simulations), while their effects were simulated applying a total thermal power of about 74 kW on the external surface at the bottom of the facility, with an active height of one meter (see Fig. 50).

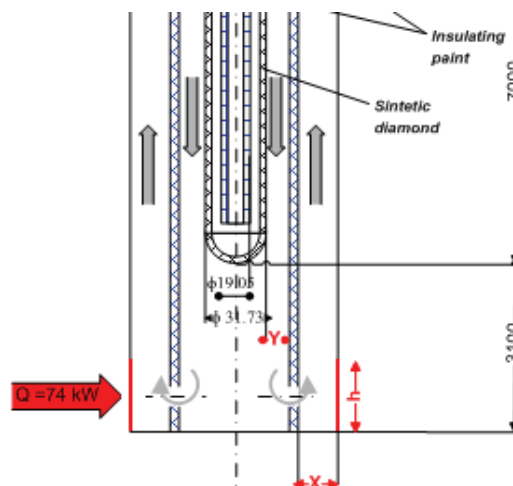


Fig. 50 – HERO Facility, FLUENT calculations, heater schematization for the 3D analyses.

In order to reduce the computational efforts, only 1/16 of the HERO facility was analyzed, taking advantage of the symmetry conditions (see Fig. 51 and Fig. 52)

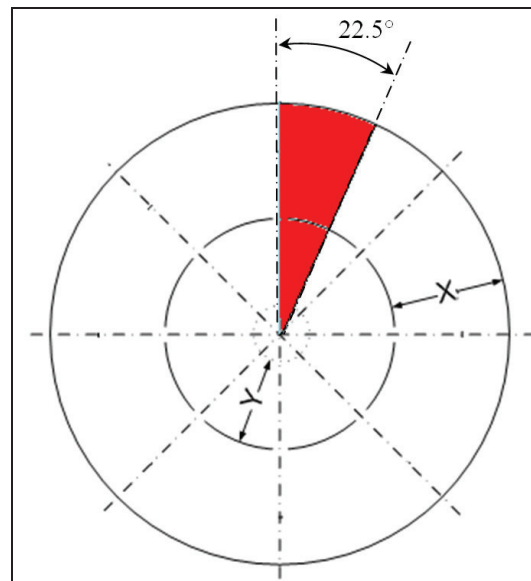


Fig. 51 – HERO Facility, FLUENT calculations, simplified geometry schematization

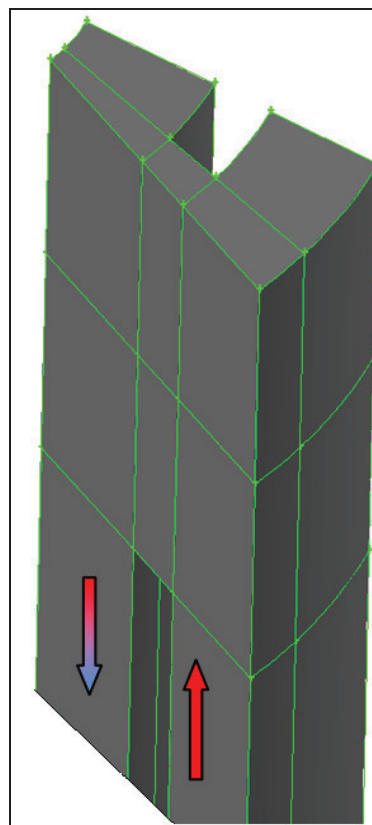
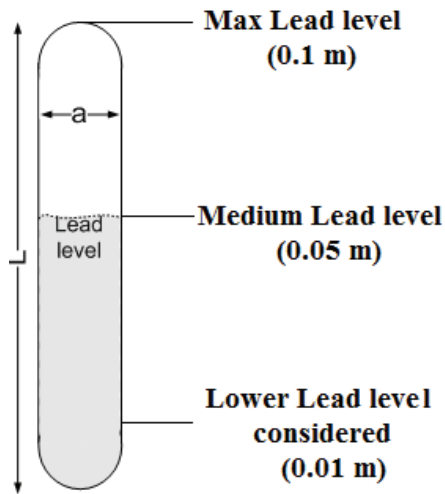


Fig. 52 – HERO Facility, FLUENT calculations, detail of the 3D geometry at the entrance of the cooling annular channel.

The fissures (16 identical fissures were considered, 8 located at the top and 8 at the bottom) were simulated by rectangular shape with a flow area of 0.001 m^2 each ones (10 mm wide and 100 mm height). In order to be conservative, the lead mass flow rate should be regulated in such a way. This is realized by means of lead level regulation at the top fissures: for this reason, three simulations were performed varying the lead level (see Fig. 53 and Tab. 30).



Simulation	Lead Level
4AX-2.5AY-01	0.1 m
4AX-2.5AY-005	0.05 m
4AX-2.5AY-001	0.001 m

Fig. 53 – Lead level regulation.

Tab. 30 – Test matrix of 3D simulations.

Only the primary lead circuit was simulated, while the effect of the secondary water circuit was taken into account imposing the temperature profile evaluated from improved RELAP5 calculations that agrees with 2.5 AY geometry (RELAP5 simulation II, section 4.2), on the wall separating the two circuit (see Fig. 54).

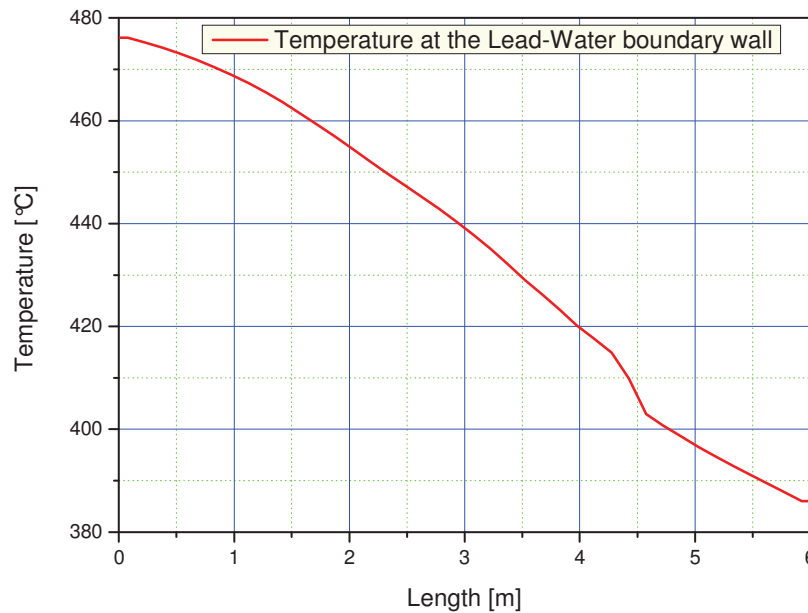
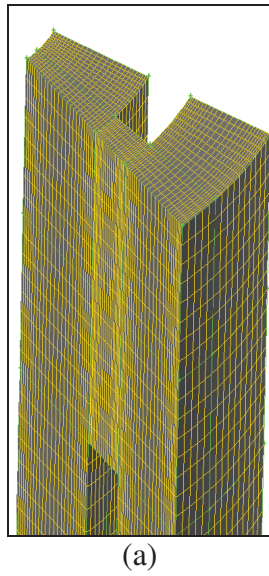
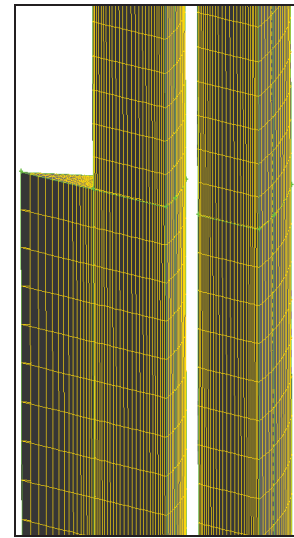


Fig. 54 – HERO Facility, FLUENT calculations, temperature profile imposed at the wall separating the primary and the secondary circuit (RELAP5 simulation II).

The geometrical domain was discretized using hexahedral mesh with the exception of the region below the bottom of the inner tube where a tetrahedral mesh was generated (see **Errore. L'origine riferimento non è stata trovata.** and Fig. 56). The total amount of cells was about 530000 for all the simulations. The turbulence model adopted is according to the 5 equations Reynolds Stress Model (RSM) with standard wall functions. The two equations turbulence models (in particular the $k-\epsilon$ and RNG) were investigated: they resulted inadequate to simulate this case because of convergence problems.



(a)



(b)

Fig. 55 – HERO Facility, FLUENT calculations, details of the mesh at the entrance (a) and at the exit (b) of the cooling annular region.

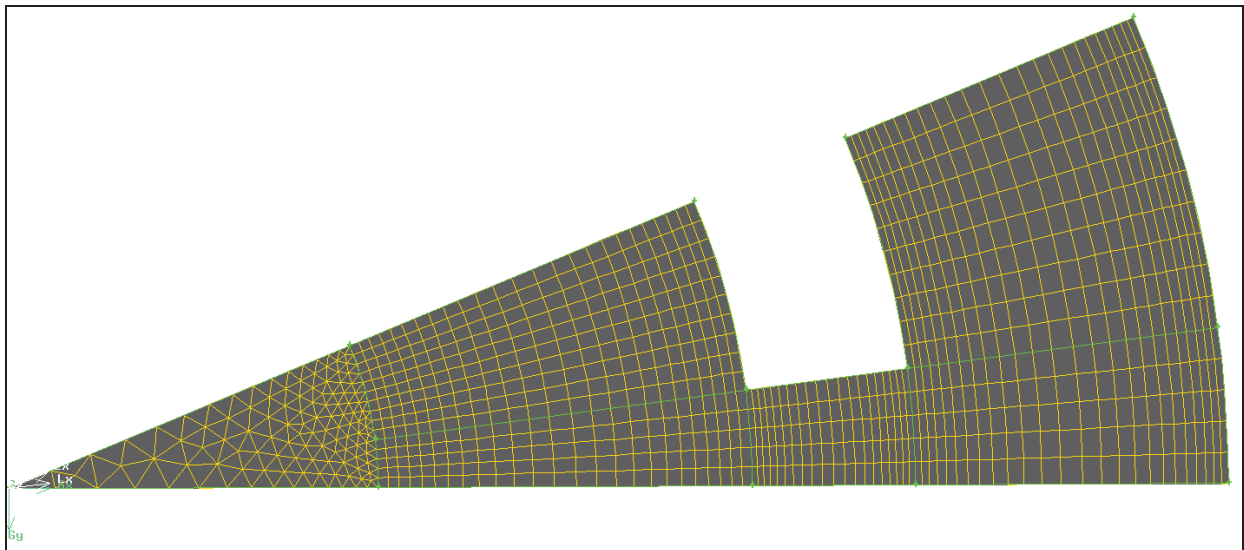


Fig. 56 – HERO Facility, FLUENT calculations, details of the mesh: top view.

The steady state conditions were assumed to be reached monitoring both the mass flow rate and the temperature time trends at the inlet of the cooling annular section; temperature was also monitored at the exit of the cooling annular channel. In Fig. 57 calculated mass flow rate time trend is depicted.

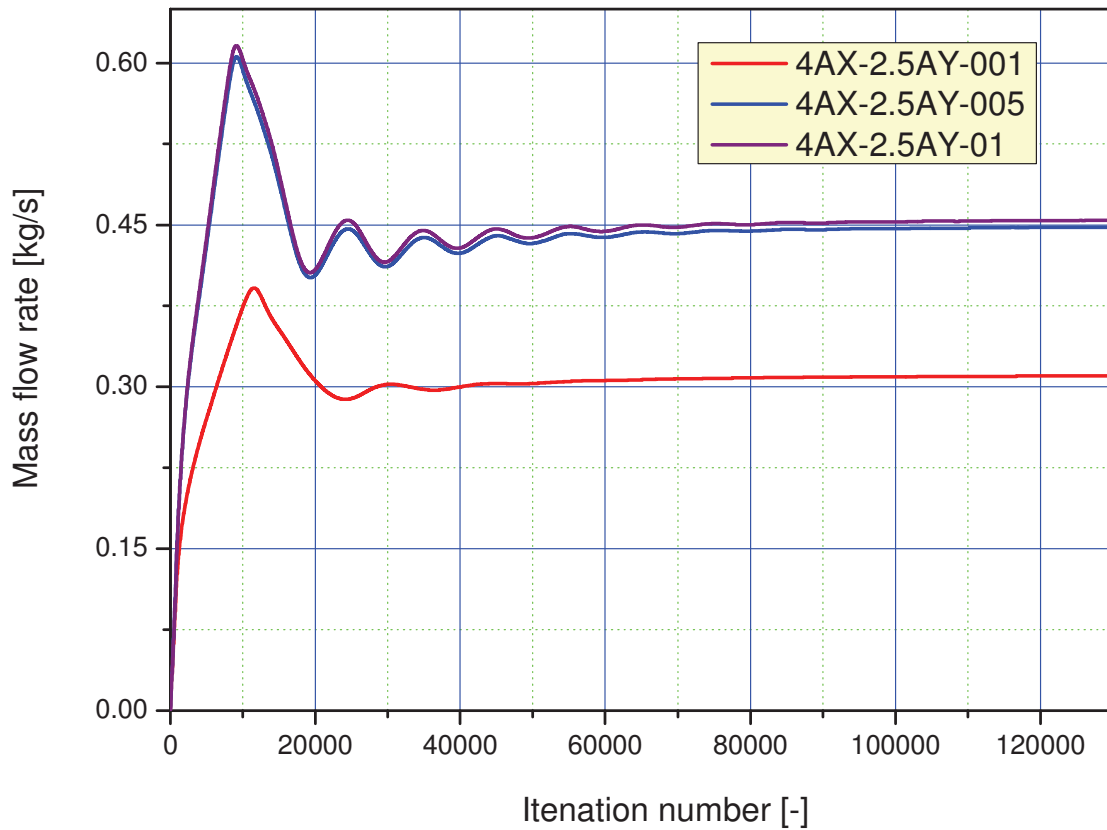


Fig. 57 – HERO Facility, FLUENT calculations, mass flow rate at the inlet of the cooling channel, (1/16).

In steady state conditions, increasing the lead level from 0.01 to 0.05 m the flow rate increases from a value of about 4.96 kg/s to a value of about 7.17 kg/s, while the flow rate for the maximum lead level is about 7.3 kg/s. It is clear that the regulation of the flow rate takes almost place in the first 0.05 m of the fissures and hence their height can be reduced.

Another open issue, concerning the adjustment of mass the flow rate by the variation of the lead free surface level, deals with the uncertainty due to the variations of the effective surface level caused by the changing in volume of the lead as a function of its average temperature.

In Fig. 58, the average lead temperature at the entrance of the cooling channel is showed.

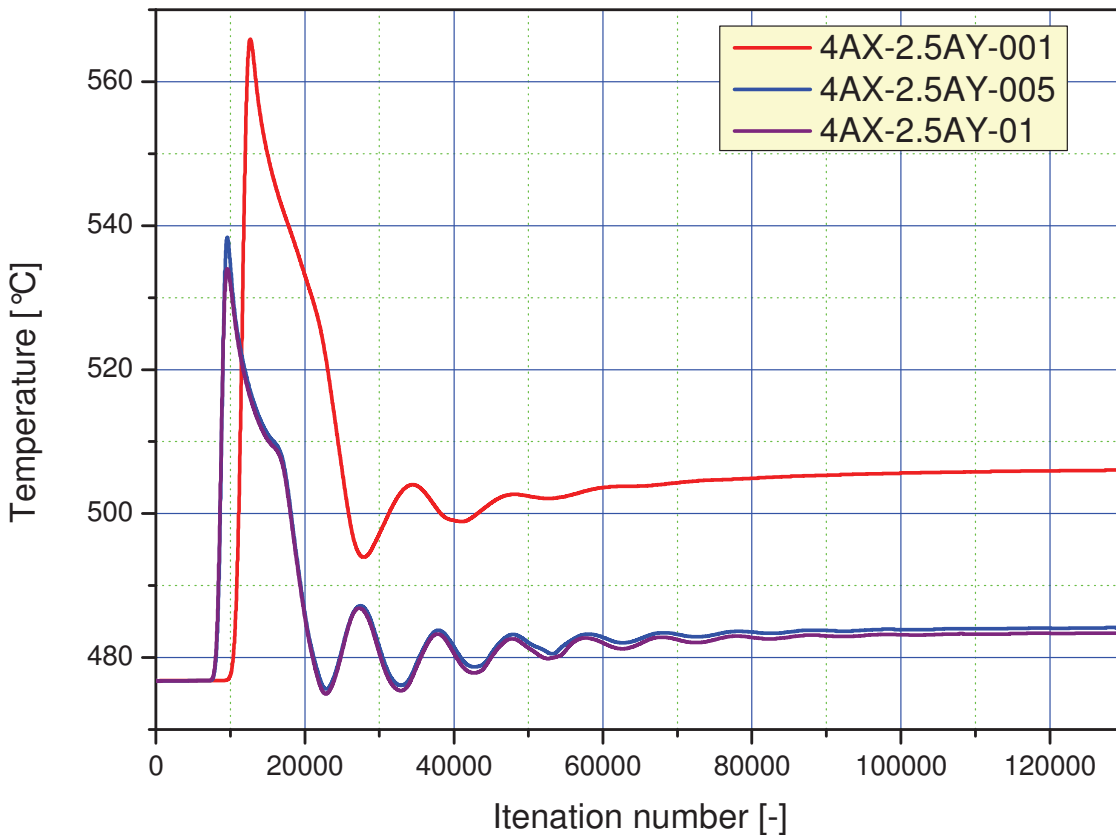


Fig. 58 – HERO Facility, FLUENT calculations, average lead temperature at the inlet of the cooling channel

In steady state conditions, an increase of the mass flow rate from 0.3 to 0.45 kg/s causes a decrease of the temperature at the inlet of the cooling channel from a value of about 506 °C (simulation 4AX-2.5AY-001) to 484 °C (simulations 4AX-2.5AY-005 and 4AX-2.5AY-01).

Fig. 59 shows the change during the iterations of the lead temperature difference between the inlet and the outlet section of the cooling annular region. In steady state conditions, for simulation 4AX-2.5AY-001 the ΔT is about 101.5 °C while for simulations 4AX-2.5AY-005 and 4AX-2.5AY-01 the ΔT is about 70°C.

Fig. 60, shows the temperature contours plot for the simulation 4AX-2.5AY-005, on horizontal planes at the entrance region of the cooling channel, on the fissures and immediately after the entrance. The lead flowing upward in the annular region of the lead pool has a constant average temperature of about 484 °C, while entering in the cooling annular region the temperature is no more uniform, starting to decrease due to the action of the secondary water circuit.

Fig. 61, shows, for simulation 4AX-2.5AY-005, the lead temperature on vertical plane passing through the symmetry plane of the fissures and on the three horizontal planes previously mentioned.

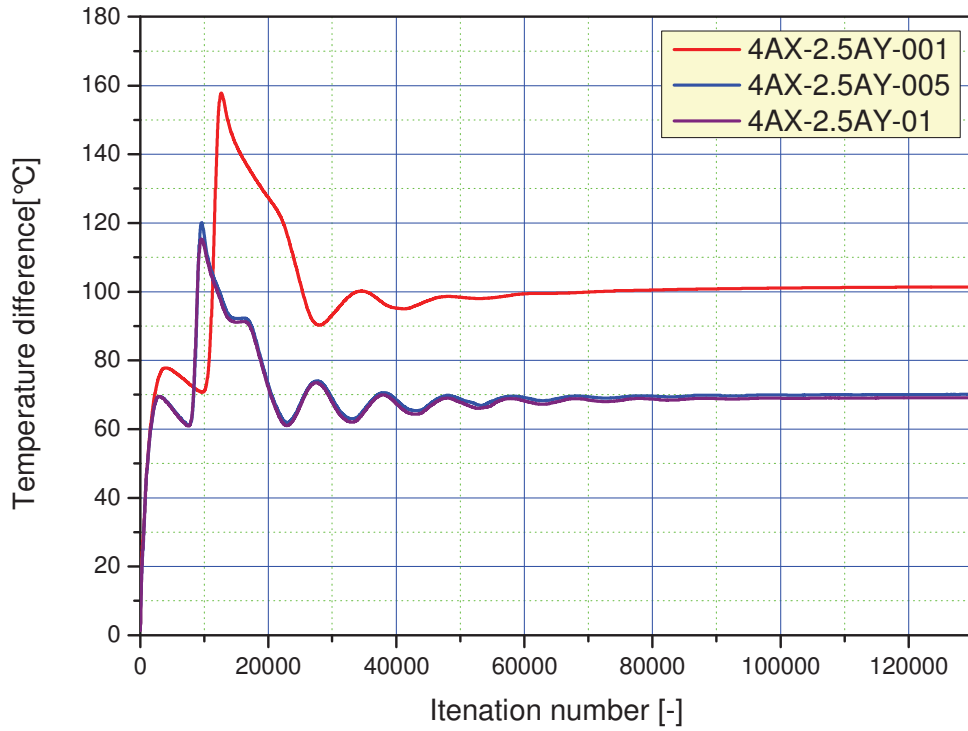


Fig. 59 – HERO Facility, FLUENT calculations, temperature difference between the inlet and the outlet of the cooling annular channel.

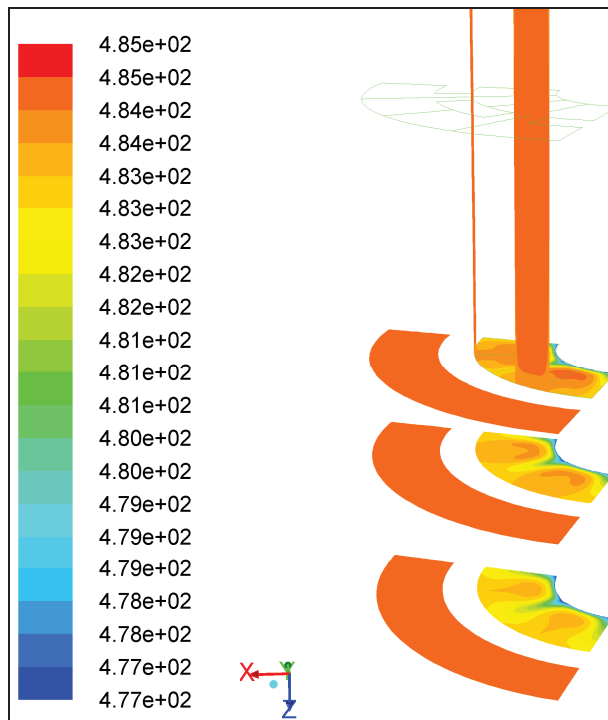


Fig. 60 – HERO Facility, FLUENT calculations, contours of temperature on the fissures and on three different z levels at the entrance of the cooling channel (simulation 4AX-2.5AY-005).

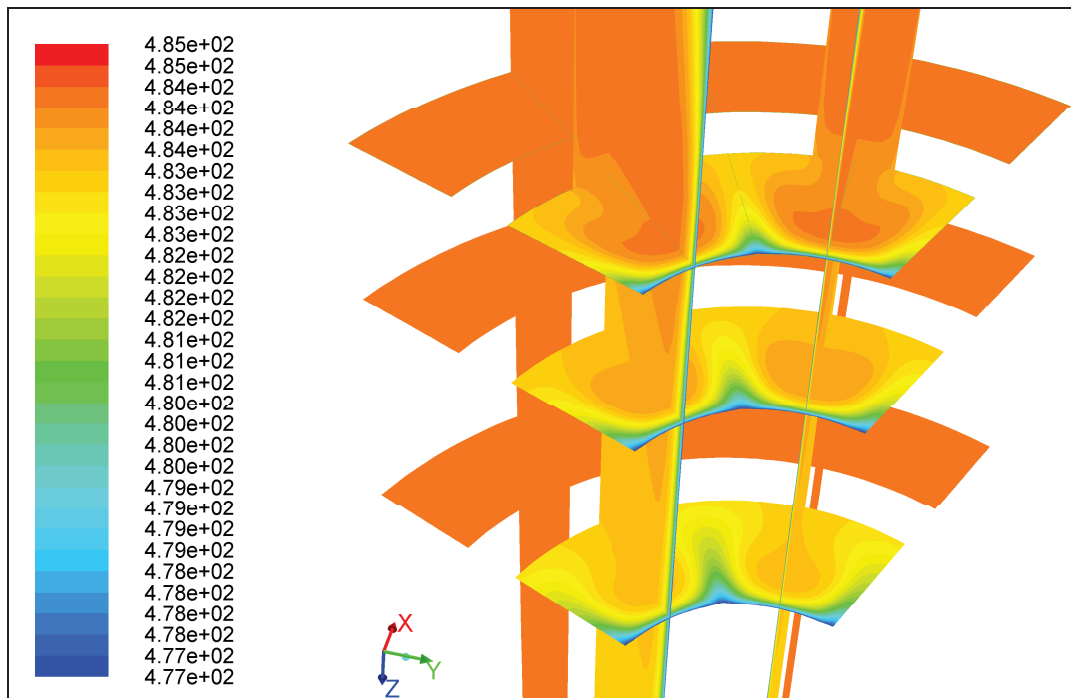


Fig. 61 – HERO Facility, FLUENT calculations, contours of temperature on three horizontal planes and on vertical planes trough the fissures symmetry planes at the entrance of the cooling channel (simulation 4AX-2.5AY-001).

Concerning the velocity field, the mean velocity at the exit of the annular cooling region is shown in Fig. 62. The mean value at the steady state condition is about 0.19 m/s for simulation 4AX-2.5AY-001, while for simulations 4AX-2.5AY-005 and 4AX-2.5AY-01 it is about 0.28 m/s.

Finally, in Fig. 63, the contour plot of the velocity field at the exit of the cooling annular region is reported for the simulation 4AX-2.5AY-005. It can be observed the plume exiting from the channel and a recirculation zone immediately under the bottom of the tube of the secondary water circuit (as evidenced in Fig. 64).

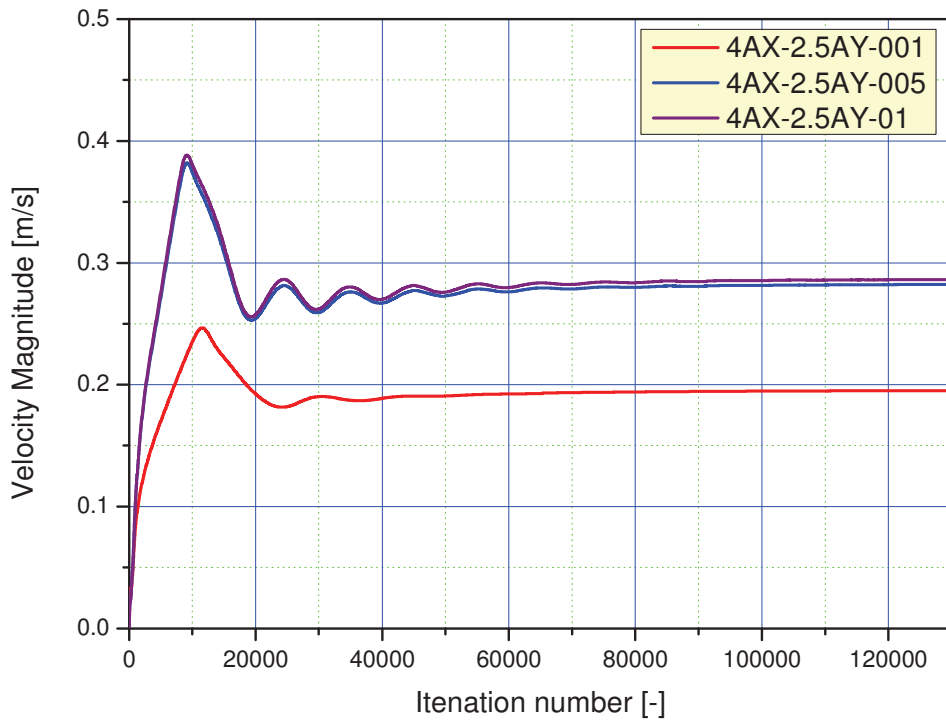


Fig. 62 – HERO Facility, FLUENT calculations, mean velocity magnitude at the exit of the cooling annular channel.

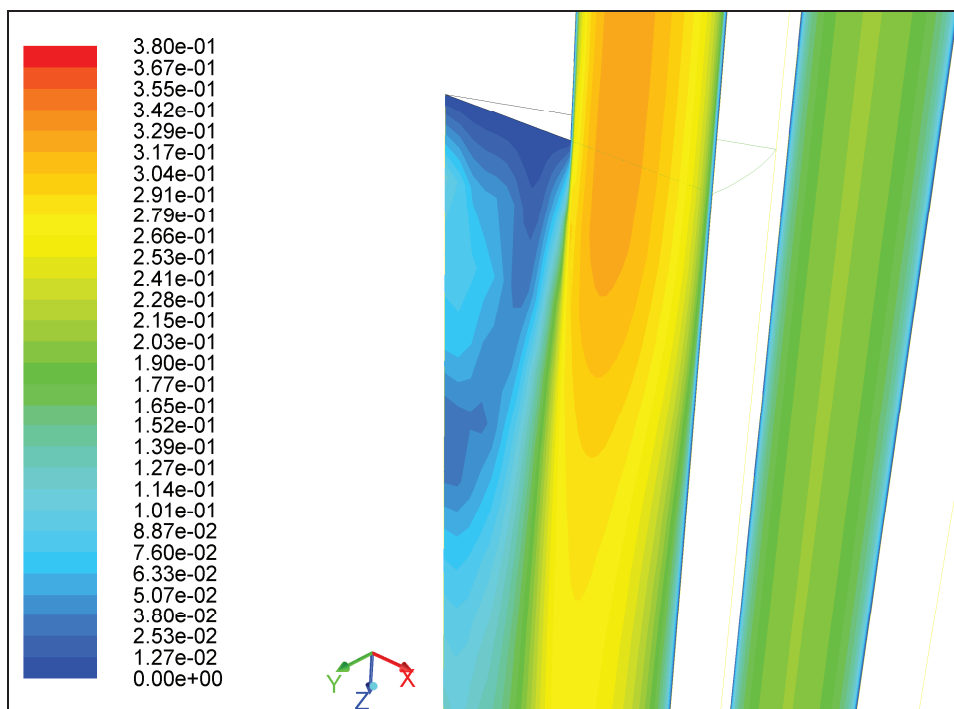


Fig. 63 – HERO Facility, FLUENT calculations, contour of velocity at the exit of the cooling annular channel (simulation 4AX-2.5AY-005).

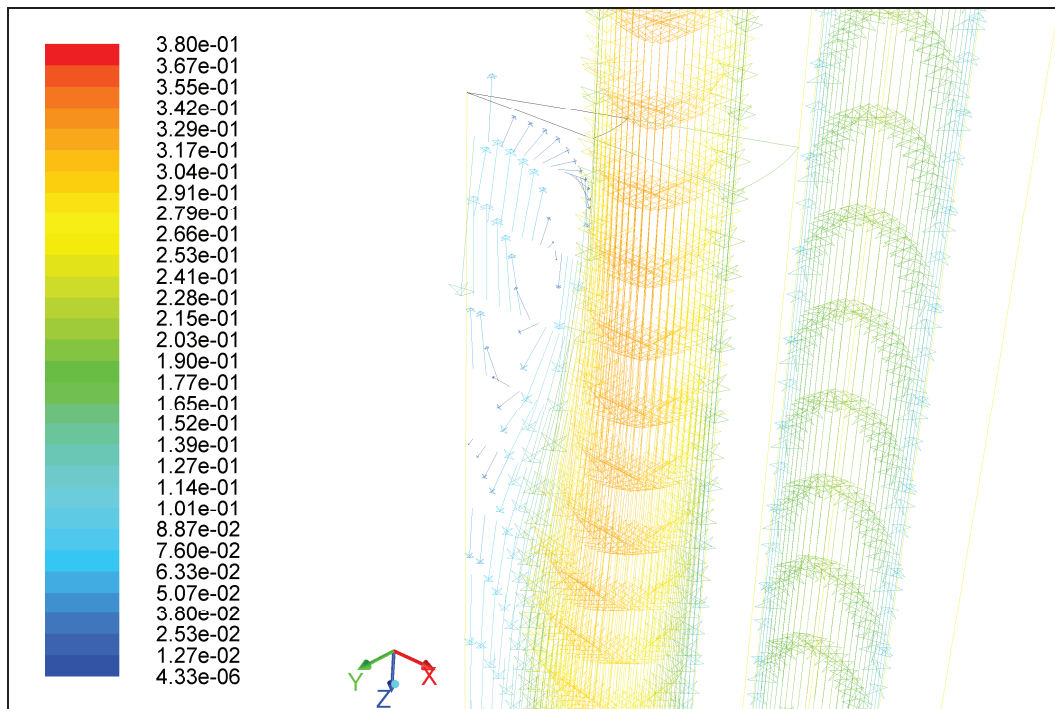



Fig. 64 – HERO Facility, FLUENT calculations, velocity magnitude vector at the exit of the cooling annular channel (simulation 4AX-2.5AY-005).



 Ricerca Sistema Elettrico	Sigla di identificazione	Rev.	Distrib.	Pag.	di
	NNFISS - LP3 - 054	0	L	95	117

5 Preliminary Piping and Instrumentation Diagram of HERO

5.1 Preliminary PID of the Heating Power System

The scheme of the PID for the HERO facility is reported in Fig.65. As can be noted, HERO consists of a main vessel (named S100) designed to operate up to 550°C and 15 bar, and properly conceived to host the test section. The test section, hanged on and bolted to the main flange of S100, consists of a 1:1 scale of the prototypical bayonet tube. An inner shell is installed (hanged to and welded on the test section flange) allowing to hydraulically separate the outer upward and inner downward lead flow. In the lower part of the main vessel, eight heating rods, with a total thermal power of 74 kW are installed. They allow to promote the natural circulation of the lead into the annular regions, providing the needed thermal power to properly simulate the thermal coupling between the lead and the bayonet tube.

To the main vessel is connected, by a suitable piping, to the Fill&Drain system. It consists basically of the storage vessel S200, designed to operate up to 400°C and 15 bar. The structural material chosen for that vessel is AISI304, being the thermal creep negligible. During the filling of S100, the S200 is pressurized by the cover gas circuit. On the contrary, the draining is performed by gravity. The isolation valve are actuated by electromagnetic actuator, and along the connecting piping between S100 and S200 a poral filter is installed allowing to capture the slugs engendered during the first fill of S200 or during the running of the experiment. A chemistry control system is foreseen on the Fill&Drain vessel, although oxygen sensors into the melt are not installed. The oxygen content both into the S100 and S200 cover gas is continuously examined, allowing to monitor a pollution of the system during the Fill&Drain procedure as well as during the operation of the facility.

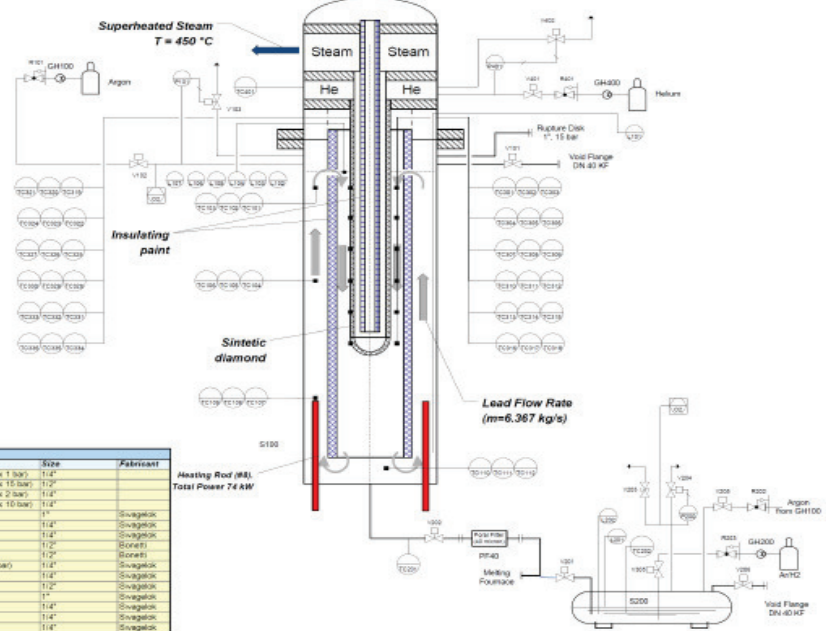
The pressure of the helium volume into the bayonet assembly is continuously monitored. The control system allows to regulate the helium pressure, achieving different operating condition into the gap filled by diamond powder. Concerning the instrumentations into the lead pool, they mainly consist of 18 TCs (TC301-TC318) placed on six different plane at different distance from the free level. They allow to monitor the bulk temperature of the lead flowing downward. On each plane three TCs are foreseen and placed at 120°. Further 18 TCs (TC319-TC336) are foreseen to monitor the bayonet outer wall temperature. Such TCs are placed on the same plane and with the same orientation of the ones above mentioned. These TCs will allow to assess the heat transfer coefficient on the lead side. To monitor the lead temperature along the upward stream, 9 TCs will be installed in the middle of the annulus, placed on the three different plane at 120° (TC101-TC109). The lead temperature on the outlet section of the inner shell will be monitored by the TCs TC100 to TC112. These set of TCs will allow to have a measurement of the lead flow rate solving the energy balance related to the lead flow.

Concerning the free level regulation into the pool, which drives the lead flow rate, 5 level sensors will be installed (L102-L107). They will be placed faced on the entrance holes sited on the upper part of the inner shell. Each sensor will be installed according to Fig. 37. A bubble tube (L101) will be installed to monitor the whole pressure and estimate the level variation into the pool during the Fill&Drain procedure.

HERO

Heavy liquid metal – pressurized water cooled tube facility

Feed Water
 $T = 335\text{ }^{\circ}\text{C}$
 $p = 180\text{ bar}$
 $m = 0.0473\text{ kg/s}$




Auxiliary components	
Description	Material
GH100 Gas Heater (500°C)	AI61 318L - Spiral Tube (15 mt)
GH200 Gas Heater (500°C)	AI61 318L - Spiral Tube (15 mt)
GH400 Gas Heater (500°C)	AI61 318L - Spiral Tube (15 mt)
S100 Main Vessel (15bar, 550°C)	AI61318L3
S200 Fill&Drain Vessel (15bar, 400°C)	AI61 304
FP40 Parallel Filter (40 micron)	

Instrumentation	
Description	Service Type
L301 Level Check (Bubble Tube)	
L302 Level Check (Lever)	
L303 Level Check (Lever=20mm)	
L304 Level Check (Lever=40 mm)	
L305 Level Check (Lever=60 mm)	
L306 Level Check (Lever=80 mm)	
L307 Level Check (Lever=36 mm)	
L301 Level Check (Riser)	
L302 Level Check (Lever)	
OS Oxygen Analyzer	
PT100 Pressure Transducer (1.5 bar)	
PT200 Pressure Transducer (3.20 bar)	
PT400 Pressure Transducer (0-15 bar)	
TC101 Thermocouple Lead 01 Type K, O.D. 3 mm	
TC102 Thermocouple Lead 1201 Type K, O.D. 3 mm	
TC103 Thermocouple Lead 2401 Type K, O.D. 3 mm	
TC104 Thermocouple Lead 01 Type K, O.D. 3 mm	
TC105 Thermocouple Lead 1201 Type K, O.D. 3 mm	
TC106 Thermocouple Lead 2401 Type K, O.D. 3 mm	
TC107 Thermocouple Lead 01 Type K, O.D. 3 mm	
TC108 Thermocouple Lead 1201 Type K, O.D. 3 mm	
TC109 Thermocouple Lead 2401 Type K, O.D. 3 mm	
TC110 Thermocouple Lead 01 Type K, O.D. 3 mm	
TC111 Thermocouple Lead 1201 Type K, O.D. 3 mm	
TC112 Thermocouple Lead 01 Type K, O.D. 3 mm	
TC201 Thermocouple Fill&Drain Type K, O.D. 3 mm	
TC302 Thermocouple Lead 1201 Type K, O.D. 3 mm	
TC301 Thermocouple Lead 2401 Type K, O.D. 3 mm	
TC302 Thermocouple Lead 1201 Type K, O.D. 3 mm	
TC303 Thermocouple Lead 01 Type K, O.D. 3 mm	
TC304 Thermocouple Lead 2401 Type K, O.D. 3 mm	
TC305 Thermocouple Lead 1201 Type K, O.D. 3 mm	
TC306 Thermocouple Lead 2401 Type K, O.D. 3 mm	
TC307 Thermocouple Lead 01 Type K, O.D. 3 mm	
TC308 Thermocouple Lead 1201 Type K, O.D. 3 mm	
TC309 Thermocouple Lead 2401 Type K, O.D. 3 mm	
TC310 Thermocouple Lead 01 Type K, O.D. 3 mm	
TC311 Thermocouple Lead 1201 Type K, O.D. 3 mm	
TC312 Thermocouple Lead 2401 Type K, O.D. 3 mm	
TC313 Thermocouple Lead 01 Type K, O.D. 3 mm	
TC314 Thermocouple Lead 1201 Type K, O.D. 3 mm	
TC315 Thermocouple Lead 2401 Type K, O.D. 3 mm	
TC316 Thermocouple Lead 01 Type K, O.D. 3 mm	
TC317 Thermocouple Lead 1201 Type K, O.D. 3 mm	
TC318 Thermocouple Lead 2401 Type K, O.D. 3 mm	
TC319 Thermocouple Trawl 01 Type K, O.D. 8 mm	
TC320 Thermocouple Trawl 1201 Type K, O.D. 8 mm	
TC321 Thermocouple Trawl 2401 Type K, O.D. 8 mm	
TC322 Thermocouple Trawl 01 Type K, O.D. 8 mm	
TC323 Thermocouple Trawl 1201 Type K, O.D. 8 mm	
TC324 Thermocouple Trawl 2401 Type K, O.D. 8 mm	
TC325 Thermocouple Trawl 01 Type K, O.D. 8 mm	
TC326 Thermocouple Trawl 1201 Type K, O.D. 8 mm	
TC327 Thermocouple Trawl 2401 Type K, O.D. 8 mm	
TC328 Thermocouple Trawl 01 Type K, O.D. 8 mm	
TC329 Thermocouple Trawl 1201 Type K, O.D. 8 mm	
TC330 Thermocouple Trawl 2401 Type K, O.D. 8 mm	
TC331 Thermocouple Trawl 01 Type K, O.D. 8 mm	
TC332 Thermocouple Trawl 1201 Type K, O.D. 8 mm	
TC333 Thermocouple Trawl 2401 Type K, O.D. 8 mm	
TC334 Thermocouple Trawl 01 Type K, O.D. 8 mm	
TC335 Thermocouple Trawl 1201 Type K, O.D. 8 mm	
TC336 Thermocouple Trawl 2401 Type K, O.D. 8 mm	
TC401 Thermocouple Helium Type K, O.D. 3 mm	

Valves	Description	Size	Material
R101 3" Reducer (Pmax 1 bar)	1 1/2"		
R202 3" Reducer (Pmax 15 bar)	1 1/2"		
R203 3" Reducer (Pmax 2 bar)	1 1/2"		
R201 3" Reducer (Pmax 10 bar)	1 1/2"		
V101 Isolation Valve	1"		Swagelok
V102 Isolation Valve	1 1/4"		Swagelok
V103 Discharge Valve	1 1/4"		Swagelok
V201 Isolation Valve	1 1/2"		Bonetti
V202 Isolation Valve	1 1/2"		Bonetti
V203 Safety Valve (15 bar)	1 1/2"		Swagelok
V204 Discharge Valve	1 1/2"		Swagelok
V205 Isolation Valve	1 1/2"		Swagelok
V206 Isolation Valve	1"		Swagelok
V305 Isolation Valve	1 1/4"		Swagelok
V401 Isolation Valve	1 1/4"		Swagelok
V402 Discharge Valve	1 1/4"		Swagelok

Fig. 65 – PID scheme of the heating power system of HERO.

 Ricerca Sistema Elettrico	Sigla di identificazione	Rev.	Distrib.	Pag.	di
	NNFISS - LP3 - 054	0	L	97	117

5.2 Preliminary PID of the Pressurized Cooling Water System

The scheme of the PID for the pressurized cooling water system is that reported in *Fig. 66*. As can be seen, the mass flow rate will be automatically controlled by the DAS acting on a regulation valve located after the pump or acting on an inverter that allows the variation in the frequency of the power supplied to the pump electric motor. A flow rate sensor must be placed along the water line, just before the inlet into the SGBT test section. The signal coming from this transducer will be used to regulate the water mass flow rate. Temperature sensors must be placed at the inlet and outlet sections of both the SGBT and to the aerotherm HX. The pressure difference must be monitored between the inlet and the outlet section of the SGBT, in addition to the absolute values of the pressure in both the sections. Finally, the temperature and the pressure of the expansion vessel must be checked.

Particular care should be spend for the test start-up phase. In this phase, the water must be heated and pressurized and its cooling should be avoided. For this reason, a by-pass line of the water cooling system was foreseen. The heating system can be supplied directly by electrical heaters inserted on the bottom side of the expansion vessel.

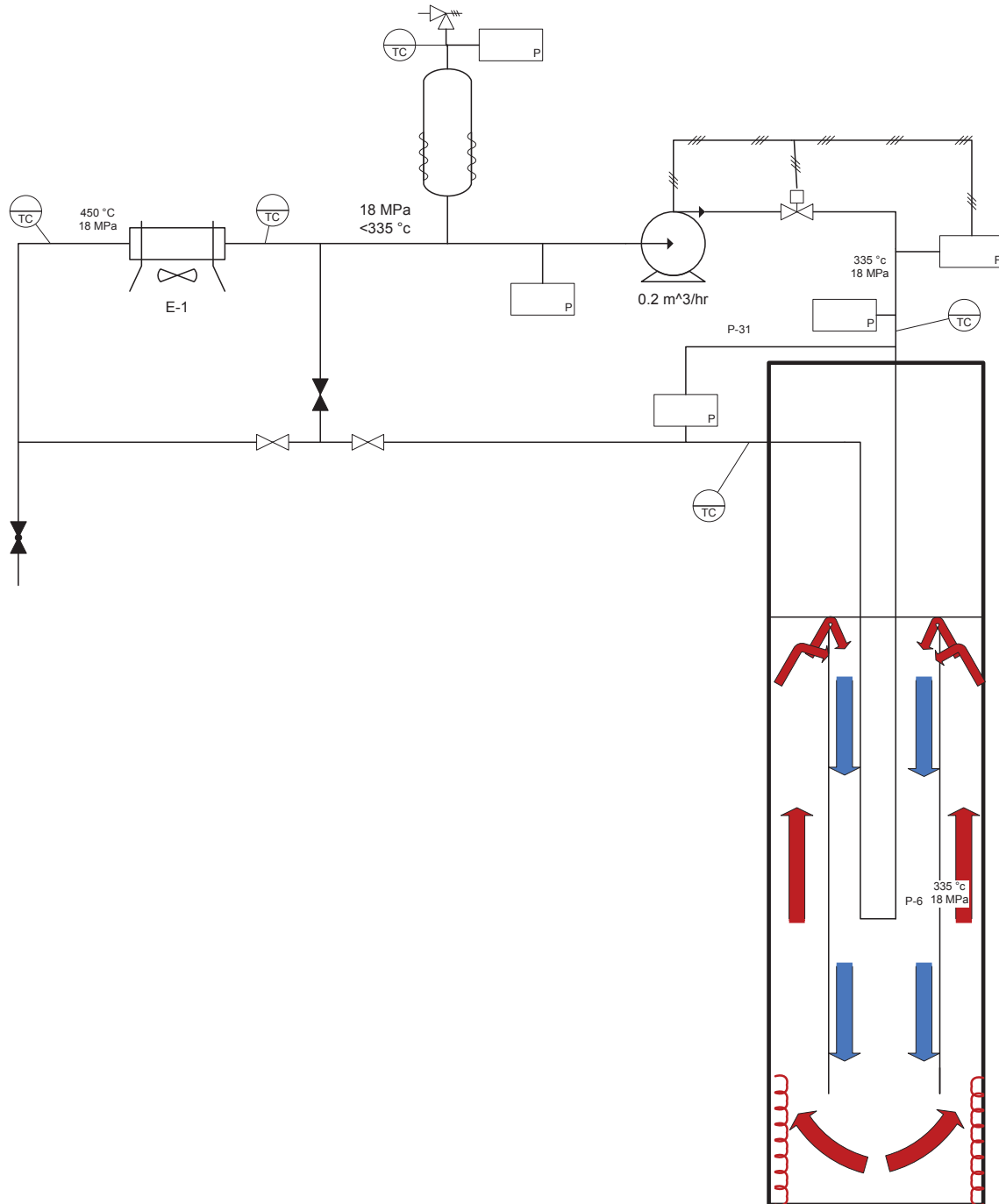


Fig. 66 – PID scheme of the pressurized cooling water system of HERO.

6 Status of the TxP Facility

The main objective of the Tubes for Powders (TxP) Facility is connected to the evaluation of the thermal performance of high conductivity powders for the application to the ALFRED SG. In particular it is aimed to:

- Determine the thermal conductivity of the powders into a representative annular gap.
- Determine the influence of the powder compaction grade on the conductivity.
- Investigate the influence of the filling gas (Helium) pressure.
- Investigate the impact of selected thermal cycles.

6.1 Description of TxP

The TxP facility consists of three concentric tubes whose conceptual scheme is reported in *Fig. 67*. The tube labeled as IT (Inner Tube) contains an Heating Rod (HR) that generates 25 kW (maximum). The gap between the IT and the powder tube (PT) is designed to test several powders specimens, it is about 6 mm in width. The free volume between the HR and the IT (High conductivity Powder zone, HP) is filled with high conductivity powders. The intent of this zone (15 mm in width), is to obtain fruitful data on very high conductivity materials if the gap temperature drop results negligible. In the outer tube, WT (Water Tube), a water flow removes the generated thermal power.

The design includes 48 + 1 thermocouples located in three azimuthal and four axial directions. Twelve are inserted at HR outer surface, 24 are located in IT (12 at the inner, 12 at the outer surfaces). The remaining 12 thermocouples are positioned at the inner surface of WT. One thermocouple is contained in the heating rod, at its center. The main data are given in *Tab. 31*.

The PID is reported in *Fig. 68*. Power control purpose requires the instrumentation of two sides. In the heating rod side, it is realized by means of a watt-meter and in the water loop by means of two thermocouples (at inlet-outlet) and a flow-meter. The power control is operated with a temperature set point connected to the measure of the HR temperature. The system is capable to shutdown the HR if a maximum temperature is reached in the HR. The power is checked with the value obtained from the waterside.

The water side does not require for pumps, the service water pressure is about 5 bars. In order to check the pressure drop, two manometers are required: the first one placed at the facility inlet and the second at the facility outlet. The water flow is adjusted by means of a control valve. Two safety components are inserted in the water line. The first is the safety valve located in the inlet-line (after the manometer). The second is located in the outlet-line line, it consists of a flux checker that reveal loss of water flux, it is connected to a safety relief valve.

The He line is connected to a pressurized tank (200 bar). The pressure reducer (with an incorporated safety valve) brings the He pressure to 4 bar. The gas enters the TxP continuously from the top of IT, and then it enters from the bottom into the gap region. When it reaches the closure of the gap region, it flows into one dedicated channel. The system operates in variable pressure (1-4 bar). Two valves fulfil this purpose: the first one closes when He flow is detected in the outlet open tank, the second closes when the selected pressure is measured by the pressure transducers.

Geometrical Parameters								
Tube label	Material	Unit	Inner radius		Outer radius		Thickness	length
HR	AISI304L	mm	r ₀	14.50	r ₁	16.00	1.50	1200 active
IT	AISI304L	mm	r ₂	31.34	r ₃	36.34	5.00	1500
PT	AISI304L	mm	r ₄	42.45	r ₅	44.45	2.00	1400
WT	AISI304L	mm	r ₆	51.13	r ₇	57.15	6.02	1400
Other Parameters								
Water Temp. inlet	14 °C	Reynolds					3523	
Water Temp. outlet	30 °C	Nusselt (by means of Dittus Boelter)					30	
Water average Temp.	22 °C	Helium pressure					4 bar	
Water mass flow	0.4 kg/s	Service water pressure					6 bar	
Water average velocity	0.2 m/s	HR Power					25 kW	

Tab. 31 – TxP main data.

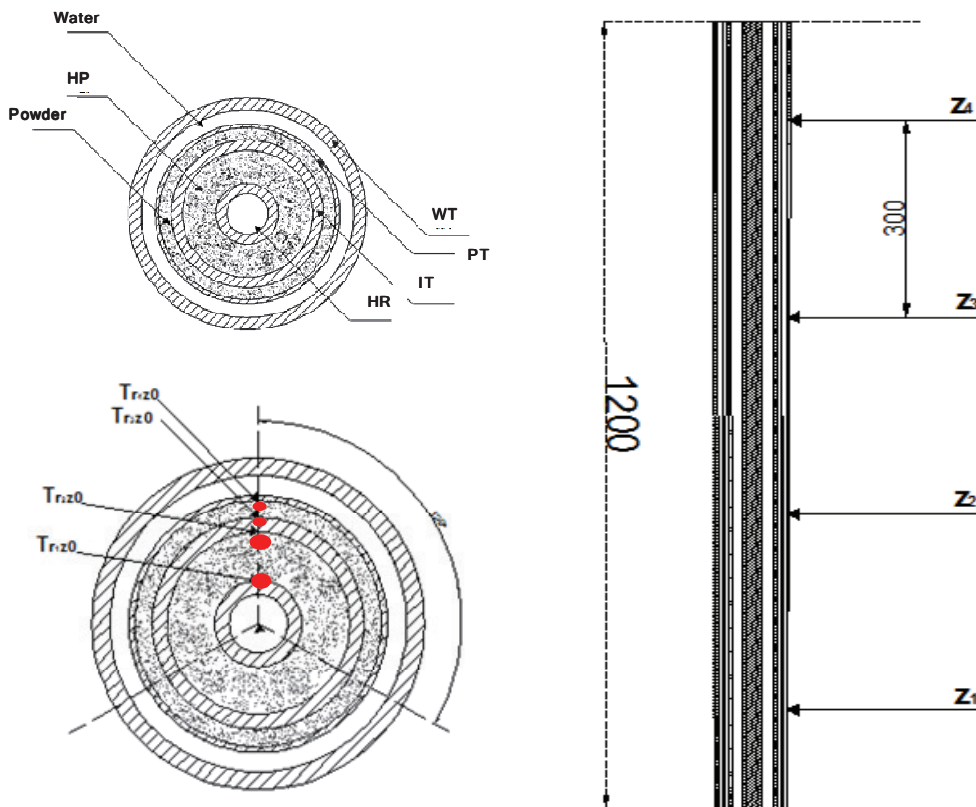
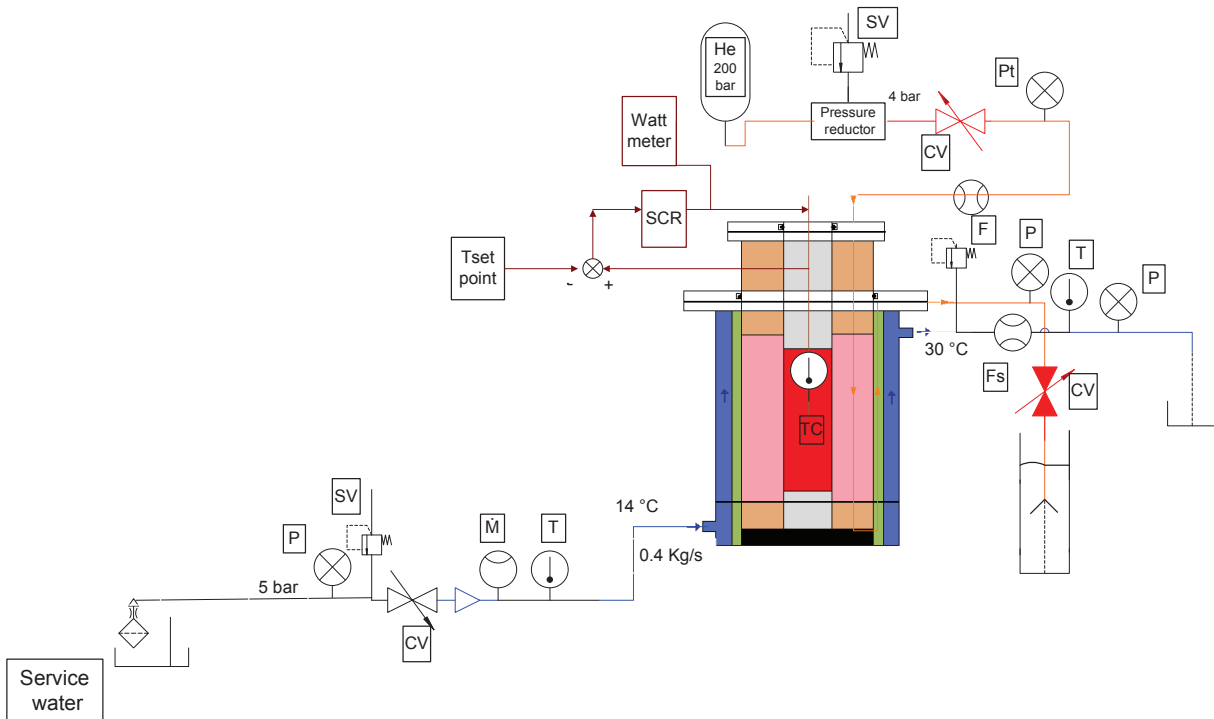


Fig. 67 – TxP conceptual scheme.



INSTRUMENTATION			
P	Manometer	Fs	Flux checker
T	Thermo-resistance	M	Flow meter
TC	Thermocouple	CV	Control valve
F	Flux meter	SV	Safety valve

Fig. 68 – TxP design: PID.

6.2 Status of TxP

The facility has been supplied by LIMAINOX. The components were subjected to the refinements given in Tab. 32 at the mechanical unit of Brasimone. TxP has been successfully pre-assembled. The final assembling is scheduled before December 2012.

ID	Description	Work done	Notes
1	Bottom flange	Planarity check OR side	--
		Processing of Hug Φ 85	Check of the connection 1 - 2
2	Inlet flange	Processing of chamber Φ 89	Check of the connection 2 - 15
3	Thermal stress absorber	--	--
4	Small pipe rodlet	--	--
5	Upper flange	Processing of Hug Φ 102	Check of the connection 5 - 18
		Processing of chamber Φ 89	Check of the connection 5 - 19
6	Al large flange	Transversal hole execution Φ 5	--
7	Upper flange of 6	Planarity check of smooth surface	--
8	Threaded pipe	Processing of the Thread	--
		processing of the connection 7 - 8	--
9	Threaded flange	--	--
10	Al small flange	Transversal hole execution Φ 5	--
11	Upper flange of 10	--	--
12	Spacer	Processing of Φ 68	Check of the connection 12 - 1
13	Lower flange of 10	--	--
14	Inlet H ₂ O pipe	Processing of the welded grid	Check connection 15 - 14
15	Intermediate pipe	--	--
16	Annular refractory	Fabrication	Check of the connection 16-17
17	Heating rod housing	Fabrication	Check connection 12 - 28
18	Outlet H ₂ O pipe	--	--
19	Intermediate pipe	--	--
20	Intermediate pipe	--	--
21	Intermediate pipe	--	--
22	Intermediate pipe	--	--
23	Small pipe rodlet	--	--
24	Small pipe rodlet	--	--
25	Small pipe rodlet	--	--
26	Small pipe rodlet	--	--
27	Basement	--	--
28	Heating rod	--	--

Tab. 32 – TxP, schedule of the processing activities performed at the mechanical unit of Brasimone.

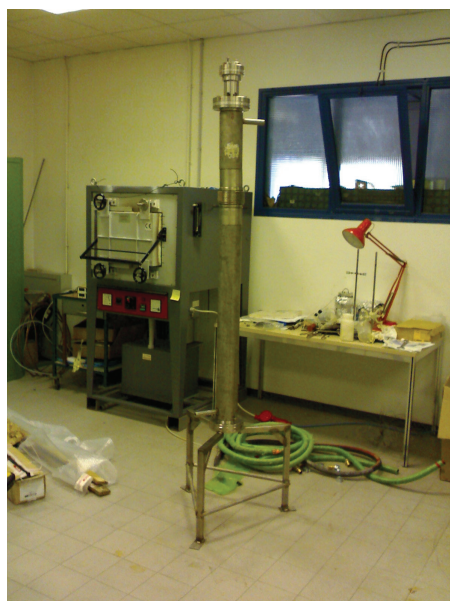



Fig. 69 – TxP pre-assembly.

 Ricerca Sistema Elettrico	Sigla di identificazione	Rev.	Distrib.	Pag.	di
	NNFISS - LP3 - 054	0	L	103	117

6.3 Activities in Support to the Planning of the TxP Experimental Campaigns

Based on the candidate powders selected in Ref. [13], preliminary experiments were performed at ENEA CR Brasimone to study the compaction behavior of candidate powders when subjected to constant thermal loads and support the planning of the experimental campaigns in the TxP Facility.

The investigated powders are:

- Copper (electrolytic) type LT-12
- Copper type W-60-M
- Brass type OT-63
- Stainless steel type AISI-316
- Sintetic diamond
- Silicon Carbide
- Aluminum Nitride

6.3.1 Description of the Experiments

The experiments consist of (*Fig. 70*):

1. Loading the furnace with powders samples
2. Heating the furnace at 200 °C (Test 1) in Ar atmosphere
3. Keeping constant the temperature for 24 hrs
4. Repeating the procedure at 300°C (Test 2), 400°C (Test 3) and 500°C (Test 4)

The experiments require the following components (*Fig. 71*):

- Furnace
- Four stainless steel canisters to contain the powders
- Zirconium refractory plate (as basement of the canisters)
- One pressurized vessel of Ar with relative piping and valves (to vent Ar into the furnace)
 - a. Type Ar-1

The instrumentations consist of:

- A manometer and a pressure reducer
- One thermocouple to be located inside one canister (AISI – 316)
 - a. Thermocouple ELSI type K
- One system able to record the measured temperatures
 - a. Yokogawa 30 channels – with printer
- Equipments for metallographic examinations
 - a. Stereo-scope NIKON - SMZ (SMA 02)
 - b. Electronic-microscope FEI - Inspect S (SEM 02)

Sintetic diamond, SiC and Al-N were subjected to the fourth thermal load test only. In order to simplify the examinations, powders that experience visible compaction are not further tested. The powders were characterized by means of metallographic examinations before and after the tests.

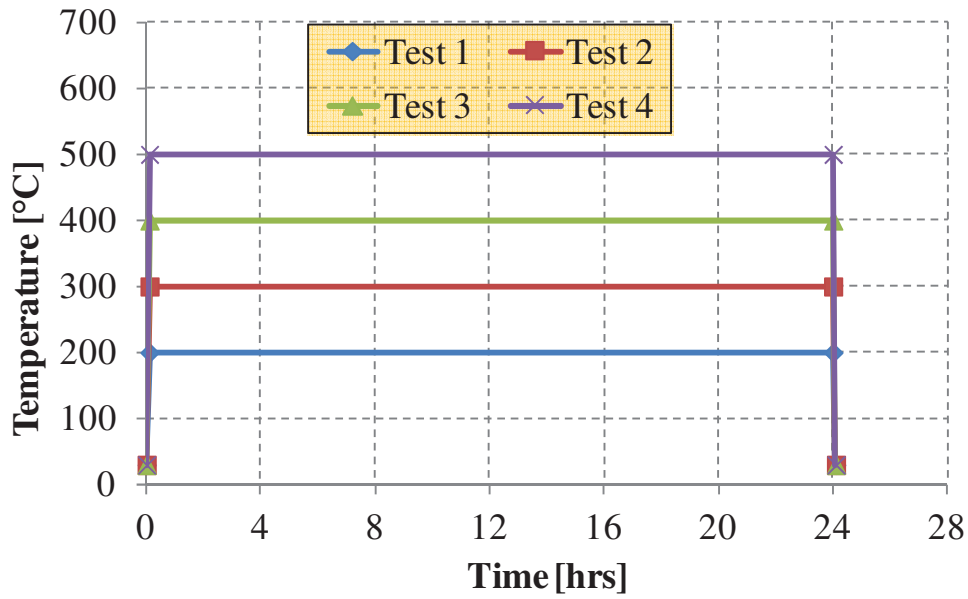


Fig. 70 – Thermal loads applied to test the candidate powders, scheme.

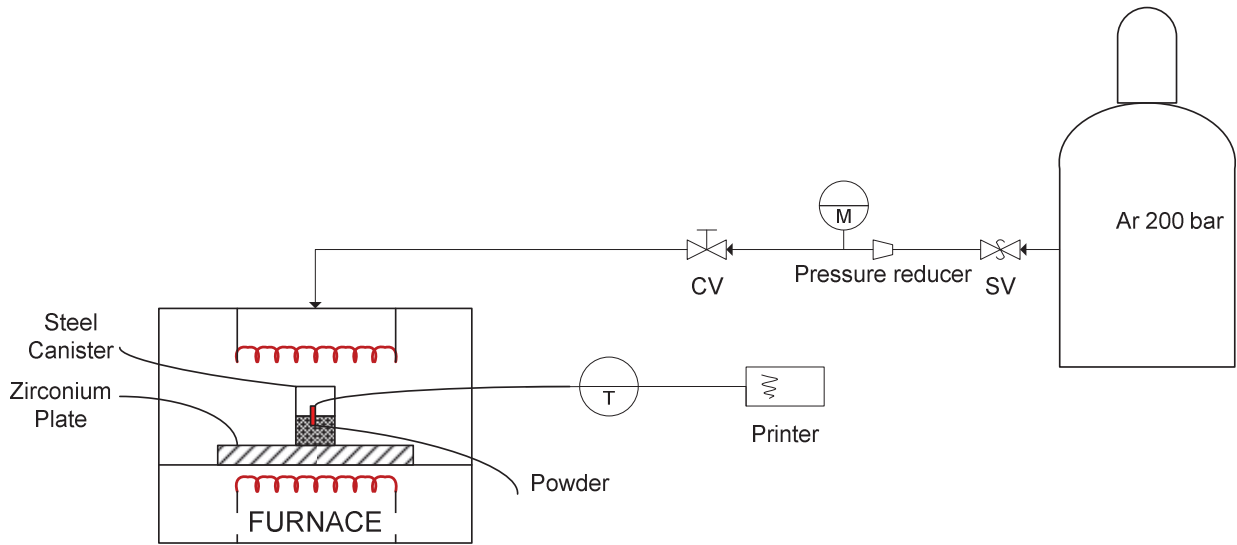


Fig. 71 – Scheme of the experimental facility.

6.3.2 Powders Pre-Characterization

Pre-characterization was conducted by means of Stereoscopy and SEM in order to make comparisons after the tests. The results are depicted from *Fig. 72* to *Fig. 78*.

Due to their fabrication process, Al-N (*Fig. 77*) and Si-C (*Fig. 78*) evidenced high compaction at ambient conditions and high dimension heterogeneity. In fact, they were obtained by sintering. These powders will be supplied again after an end of sintering treatment and re-tested based on fabricant recommendations. Additional details are given in Ref. [12].

Measurement

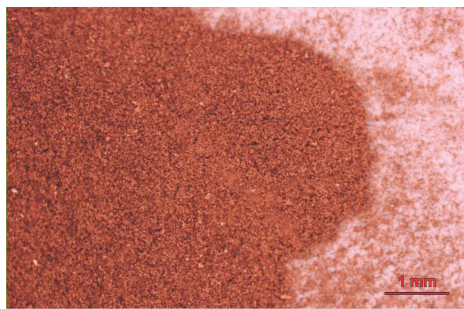
Tool:

Stereo-Scope

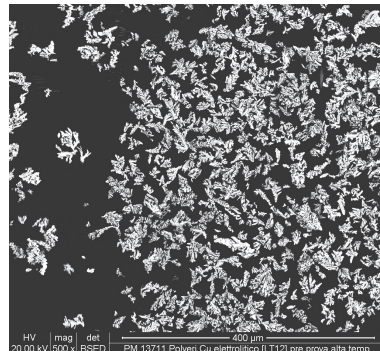
Powder

compaction:

None



PM 13711 Polvere rame elettrolitico LT 12 [verGINE]
Assenza di compattazione



Measurement

Tool:

Electronic-microscope

Powder

compaction:

None

Fig. 72 – Electrolytic copper powder LT-12 - 20°C.

Measurement

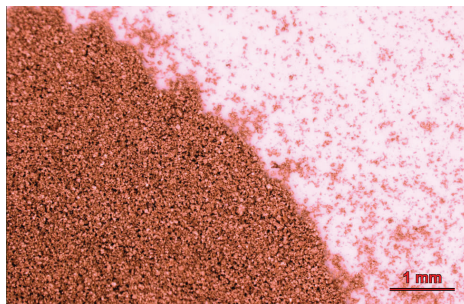
Tool:

Stereo-Scope

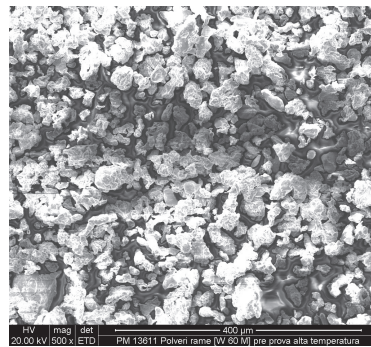
Powder

compaction:

None



PM 13611 Polvere rame W 60 M [verGINE]
Assenza di compattazione



Measurement

Tool:

Electronic-microscope

Powder

compaction:

None

Fig. 73 – Copper powder W-60-M - 20°C.

Measurement

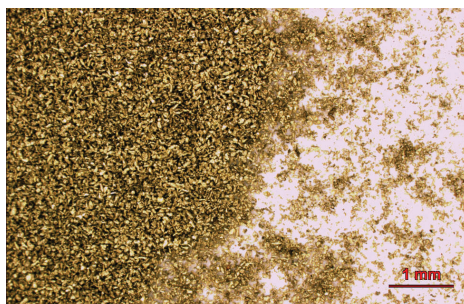
Tool:

Stereo-Scope

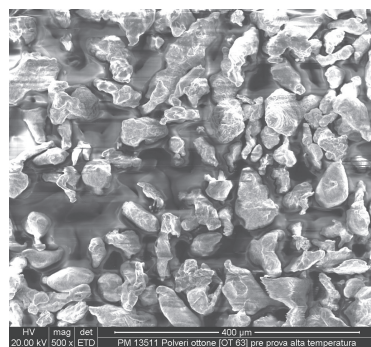
Powder

compaction:

None



PM 13511 Polvere ottone OT 63 [verGINE]
Assenza di compattazione



Measurement

Tool:

Electronic-microscope

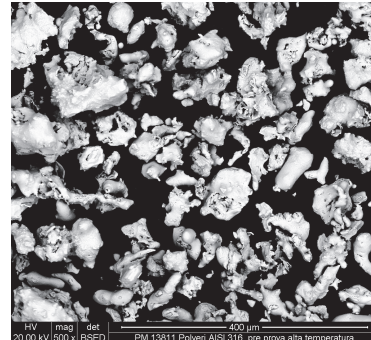
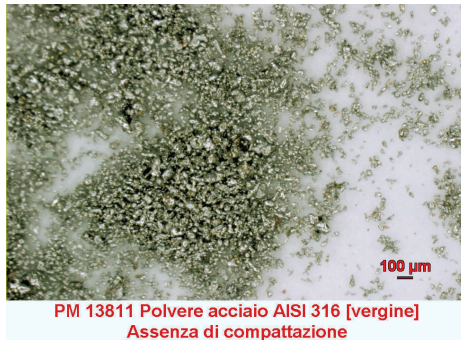
Powder

compaction:

None

Fig. 74 – Brass powder OT-63 - 20°C.

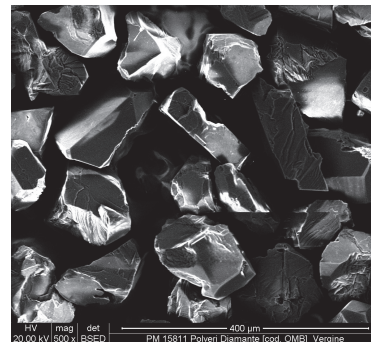
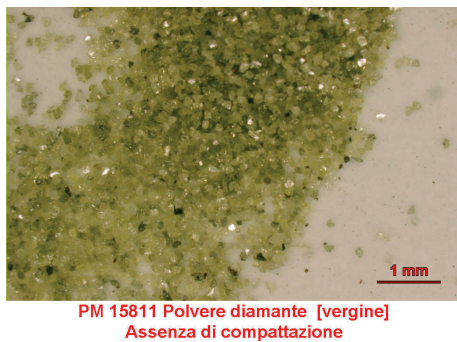
Measurement Tool:
Stereo-Scope
Powder compaction:
None



Measurement Tool:
Electronic-microscope
Powder compaction:
None

Fig. 75 – AISI-316 powder - 20°C.

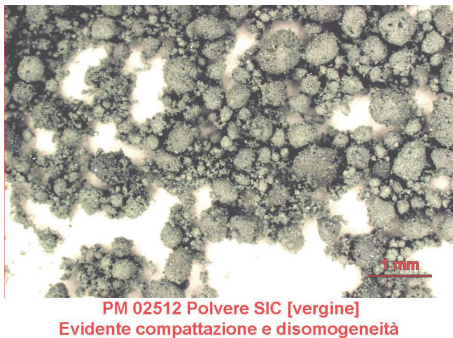
Measurement Tool:
Stereo-Scope
Powder compaction:
None



Measurement Tool:
Electronic-microscope
Powder compaction:
None

Fig. 76 – Synthetic diamond powder - 20°C.

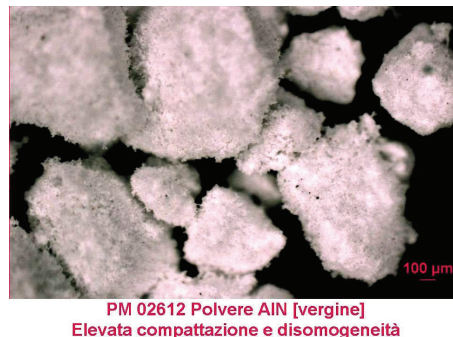
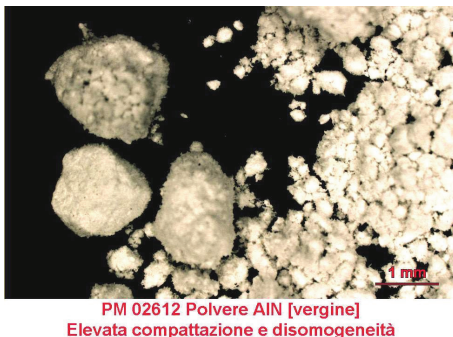
Measurement Tool:
Stereo-Scope
Powder compaction:
Total compaction



Measurement Tool:
Electronic-microscope
Powder compaction:
Total compaction

Fig. 77 – Si-C powder - 20°C.

Measurement Tool:
Stereo-Scope
Powder compaction:
Total compaction



Measurement Tool:
Electronic-microscope
Powder compaction:
Total compaction

Fig. 78 – Al-N powder - 20°C

6.3.3 Main Achievements from the Experiments

The main achievements from the experiments can be summarized as follows:

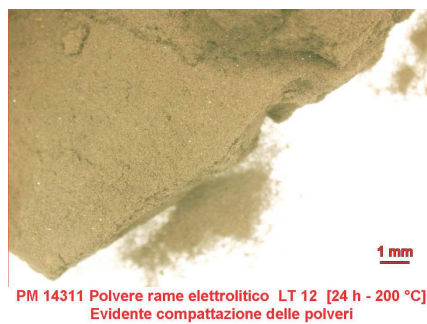
- Electrolytic copper powder LT-12 experienced compaction at 200 °C, the phenomenon was clearly visible during Visual Inspection (V-I), *Fig. 79*.
- Copper powder W-60-M experienced compaction at 200 °C, the phenomenon was clearly visible during Visual Inspection (V-I), *Fig. 80*.
- Brass powder OT-63 revealed a good performance up to 500 °C. In this last test, a new powder morphology was created and compaction was appreciable from Visual Inspection (V-I), *Fig. 81*.
- AISI-316-SS powder revealed very low compaction at 300 and 400 °C. The phenomenon was captured during Electronic-microscope examination. In the last test (500 °C), compaction remained low even if it was visible during stereo-scope examinations, *Fig. 82*
- Sintetic diamond powder survived the test at 500°C without compaction, *Fig. 83*.
- Al-N and Si-C remained similar to the initial state characterized by high compaction and dimension heterogeneity. This is due to their fabrication process (incomplete sintering).

The results are summarized in *Tab. 33*. For each material the table reports an indication about the color. It is compared with the initial one (assumed as reference). The compaction state is given. In case of compaction, the roughest tool that capture the phenomenon is mentioned (visual inspection, stereoscopy and SEM). The grain dimensions in term of max and min measured grain lengths are included. They are obtained by atom-contrast. Due to the limited number of measured grains, the range must be intended as a qualitative. Additional details are given in Ref. [12].

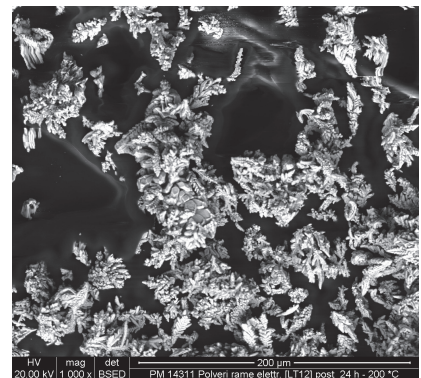
In conclusion, sintetic diamond is confirmed as most promising material for the application in ALFRED and should be tested in TxP. AISI-316 is suitable as pathfinder for calibration tests in TxP. Further investigations are necessary for Si-C, in particular it should be re-tested after end of sintering treatments. The experiment evidences the lack of instrumentations: porosity-meter and riddles for powders are essential to assess, respectively, powder conductivity and powder compaction.



Measurement Tool: Visual Inspection
Powder compaction: Total compaction

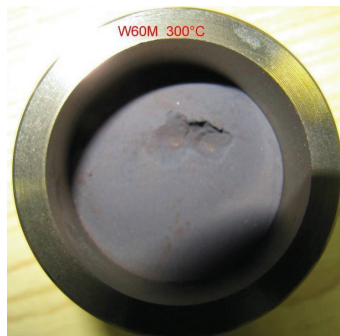


Measurement Tool: Stereo-Scope
Powder compaction: Total compaction

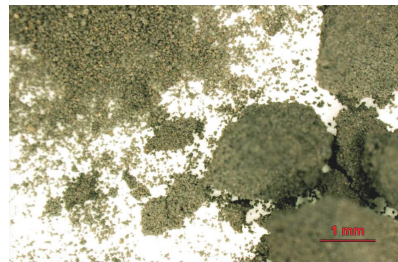


Measurement Tool: Electronic-microscope
Powder compaction: Total compaction

Fig. 79 – Electrolytic copper powder LT-12 - 200°C.

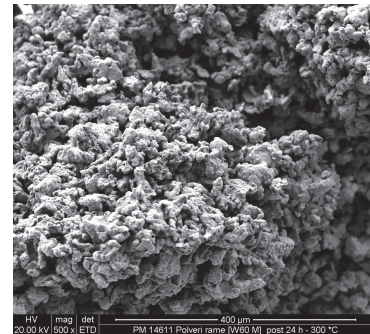


Measurement Tool: Visual Inspection
Powder compaction: Total compaction



PM 14611 Polvere rame W 60 M [24 h - 300 °C]
Compattazione evidente

Measurement Tool: Stereo-Scope
Powder compaction: Total compaction



Measurement Tool: Electronic-microscope
Powder compaction: Total compaction

Fig. 80 – Copper powder W-60-M - 300°C.

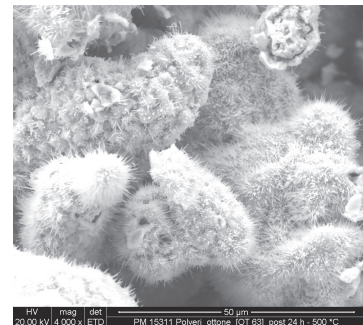


Measurement Tool: Visual Inspection
Powder compaction: Total compaction



PM 15311 Polvere ottone OT 63 [24 h - 500 °C]
Totale Compattazione

Measurement Tool: Stereo-Scope
Powder compaction: Total compaction



Measurement Tool: Electronic-microscope
Powder compaction: Total compaction

Fig. 81 – Brass powder OT-63 - 500°C.

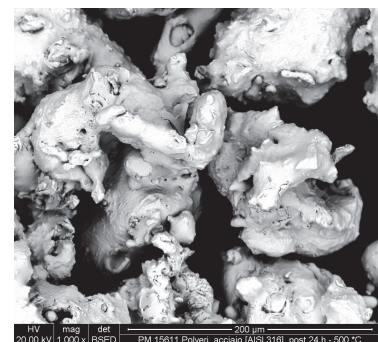


Measurement Tool: Visual Inspection
Powder compaction: None



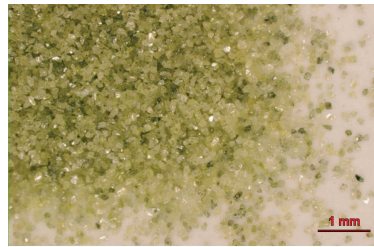
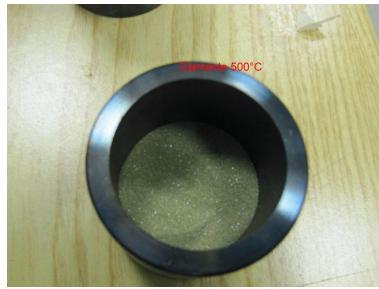
PM 15611 Polvere acciaio AISI 316 [24h - 500 °C]
Lieve compattazione

Measurement Tool: Stereo-Scope
Powder compaction: Low

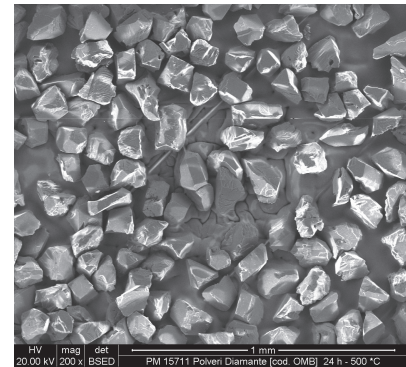


Measurement Tool: Electronic-microscope
Powder compaction: Low

Fig. 82 – AISI-316 powder - 500°C.



PM 15711 Polvere diamante [24h - 500 °C]
Assenza compattazione



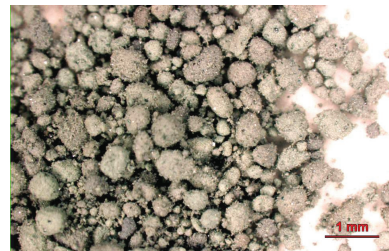
Measurement Tool: Visual Inspection
Powder compaction: None

Measurement Tool: Stereo-Scope
Powder compaction: None

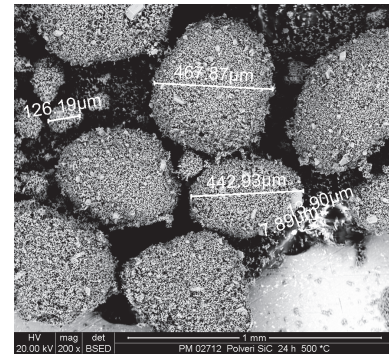
Measurement Tool: Electronic-microscope
Powder compaction: None

Fig. 83 – Sintetic diamond powder - 500°C.

Not Available



PM 02712 Polvere SiC [24 h - 500 °C]
Elevata compattazione



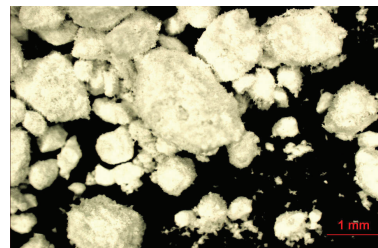
Measurement Tool: Visual Inspection
Powder compaction:

Measurement Tool: Stereo-Scope
Powder compaction: Total compaction

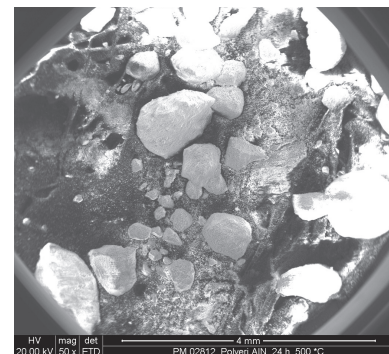
Measurement Tool: Electronic-microscope
Powder compaction: Total compaction

Fig. 84 – Si-C powder - 500°C.

Not Available



PM 02812 Polvere AlN [24 h - 500 °C]
Presenza di polveri fini e grossi agglomerati



Measurement Tool: Visual Inspection
Powder compaction:

Measurement Tool: Stereo-Scope
Powder compaction: Total compaction

Measurement Tool: Electronic-microscope
Powder compaction: Total compaction

Fig. 85 – Al-N powder - 500°C

Powder	Pre-test 20 °C		Test-1: 200 °C		Test-2: 300 °C		Test-3: 400 °C		Test-4: 500 °C	
Copper LT-12	Color	ref	Color	Darker than ref	Color	Darker than ref	Not Addressed (N/A)		N/A	
	Compaction	none	Compaction	Total V-I	Compaction	Total V-I				
	Max grain	43 µm	Max grain	N/A	Max grain	N/A				
	Min grain	6 µm	Min grain	N/A	Min grain	N/A				
Copper W-60-M	Color	ref	Color	Darker than ref	Color	Darker than ref	N/A		N/A	
	Compaction	none	Compaction	Very Low - SEM	Compaction	Total V-I				
	Max grain	77 µm	Max grain	153 µm	Max grain	N/A				
	Min grain	16 µm	Min grain	44 µm	Min grain	N/A				
Brass OT-63	Color	ref	Color	Darker than ref	Color	Darker than ref	Color	Darker than ref	Color	Darker than ref
	Compaction	none	Compaction	Very Low - SEM	Compaction	Very Low - SEM	Compaction	Very Low - SEM	Compaction	Total V-I
	Max grain	120 µm	Max grain	74 µm	Max grain	97 µm	Max grain	90 µm	Max grain	N/A
	Min grain	17 µm	Min grain	58 µm	Min grain	58 µm	Min grain	49 µm	Min grain	N/A
SS – AISI-316	Color	ref	Color	as ref	Color	as ref	Color	Darker than ref	Color	Darker than ref
	Compaction	none	Compaction	Very Low - SEM	Compaction	Very Low - SEM	Compaction	Very Low - SEM	Compaction	Beginning - SEM
	Max grain	103 µm	Max grain	179 µm	Max grain	130 µm	Max grain	227 µm	Max grain	188 µm
	Min grain	6 µm	Min grain	74 µm	Min grain	80 µm	Min grain	167 µm	Min grain	127 µm
Sintetic diamond	Color	ref	N/A	N/A	N/A	N/A	N/A	N/A	Color	As ref
	Compaction	none							Compaction	None
	Max grain	124 µm							Max grain	137 µm
	Min grain	82 µm							Min grain	78 µm
SiC	Color	ref	N/A	N/A	N/A	N/A	N/A	N/A	Color	As ref
	Compaction	Total V-I							Compaction	Total V-I
	Max grain	400 µm							Max grain	468 µm
	Min grain	2 µm							Min grain	2 µm
Al-N	Color	ref	N/A	N/A	N/A	N/A	N/A	N/A	Color	As ref
	Compaction	Total V-I							Compaction	Total V-I
	Max grain	1400 µm							Max grain	1490 µm
	Min grain	3 µm							Min grain	3 µm

Tab. 33 – Summary of the experiments.

7 Conclusions

The Lead-cooled European Advanced DEMonstration Reactor (LEADER) project belongs to the 7th Framework Program. The main objective of LEADER deals with the design of a 300 MWth low cost and fully representative scaled down European LFR Technology Demonstrator Reactor (ETDR) named ALFRED (Advanced Lead Fast Reactor European Demonstrator). In this framework, a new configuration of Steam Generator (SG) has been proposed: the super-heated steam double wall once through bayonet tube type. This conceptual design was studied since 60' for Sodium Reactor application. An example of facility that operates with this concept is CIRCE (at ENEA Brasimone) even if it is limited to the heat exchange function.

The present activity aims to investigate the TH performance of the single bayonet tube. Its main objective is to test a single 1:1 bayonet tube (eventual improved in design) into an experimental facility representative of its TH in reactor behavior: the Heavy liquid mEtal – pRessurized water cOoled tube Facility (HERO Facility). The activity starts on 2011 and spans over three years. During 2012, the following sub-objectives have been reached and documented in this report that is the result of a collaboration between UNIPI-UNIROMA1 and ENEA:

- Assessment of the SG single tube conceptual design with focus on the main design aspects that impact on its performance by means of TH system codes (RELAP-5).
- Definition of the main geometrical data of the heating power system of the Heavy liquid mEtal – pRessurized water cOoled tube Facility (HERO Facility) by means of TH system codes and CFD calculations.
- Setup of a preliminary PID of the heating power system and of the pressurized water loop of HERO.
- Experimental activities in support to the planning of the experimental campaigns in the TxP facility and status of construction of TxP.

Assessment of the SGBT by RELAP-5

Should be pointed out that RELAP5 code has been designed for Light Water Reactor (LWR) and it is suitable for these types of SG. Therefore, it is not completely accurate in simulating the bayonet tube configuration and the accuracy of the results should be verified experimentally. The reference input deck is set up according to the design proposed by ANSALDO except the gap between the steam-water and the molten lead side. Sintetic diamond powder is modeled as filling material. In order to account for the lack of knowledge of the powder conductivity, two different reference simulations are presented, they are labeled case 1 and case 2. They provide a lower bound of the operational behavior. The analysis brings to the conclusions reported in the following:

- The maximum steam temperature is predicted in the range 438-456 °C depending on the diamond conductivity (Case 2 and Case 1 respectively). The ANSALDO simulation agrees with Case 1.
- In all the simulations the lead temperature drop is in the order of 80 °C.
- Superheated steam is always predicted, a void fraction close to 1.0 is reached within the first 3 meters of the annular riser (Case 1, Case 2 and ANSALDO).
- In the reference simulations, the total pressure drop in the bayonet tube is predicted in the range of 2.6 bar – 2.8 bar. These values are close to the ANSALDO results even if they are slightly lower.

- In the reference simulations, the feedwater tube heat flux at the inner side shows three discontinuities. The first one is at the steam outlet, the second one is about 4 meters far from the outlet, close to the end of the active region and, the last one, is in the active region between 5-7 m. This is connected with the occurrence of condensation at the outer surface.
 - Two large zones in which condensation takes place at low and high void fractions are predicted in the active length. They are separated by a zone in which relatively high temperature liquid film is predicted at tube surface that induces the code to assume single-phase liquid convection at supercritical pressure heat transfer mode.
 - Wall drying and single-phase vapor convection takes place in the higher part of the active length.
 - Condensation starts again at the tube outlet, 2.5 m far from the active length. The liquid fraction is very low and the code predicts $v_l = 1.1E-06$ (comparable to the cutting error).

Several sensitivity analyses were carried out. They allow the development of an improved input deck. The improved input deck differs with the reference one in the initialization: hot start-up is assumed instead of cold start-up. The analysis of this simulation points out the reduction of the condensation zones. In particular, it disappears at tube outlet. A possible explanation for the disappearance of this phenomenon at tube outlet could be related to code numeric.

In conclusion, the reference and the improved simulations are consistent with the ANSALDO calculations. Condensation phenomenon takes place in the bayonet tube close to the first tube outer surface. It seems to be limited to the first part of the active length even if its extension is affected by uncertainties.

TH conceptual design of the HERO Facility

The main aim of the facility is to study a 1:1 bayonet tube under conditions that represent, as much as possible, its operation in the ALFRED SG. The facility is expected to be a suitable tool to support the validation process of TH-Sy and CFD codes coupled simulations. The facility consists of two concentric pipes. The bayonet tube is located in the upper part of the inner tube. The lower part of the facility is 3.1 m in length and houses 8 heating rods (1 m in length). They are located between the inner tube and the outermost tube annular region. They supply 74 kW that allows natural circulation of lead. The coolant heats up in the first meter of the facility and moves-up in the annular region between the outer most tube and the inner tube. At its top, it enters 8 fissures and moves down inside the inner tube (it wets the bayonet tube for 6m). At the bottom part of the inner tubes it enters 8 fissures (that are identical to the top fissures) and reaches again the heating rod zone.

The RELAP5 and CFD Fluent calculations carried out in support to the TH conceptual design of the Heavy liquid metal – pressurized water cooled tube (HERO) are presented in this document. The performed analysis bring to the following conclusions:


- The equivalent SGBT lead channel flow area cannot be reproduced. It must be increased of a factor 2.5 in order to obtain the effective lead mass flow (6.367 kg/s).
- The flow area of the up-flow annular region must be 6 times the equivalent lead channel flow area because of two reasons: the first is to obtain the effective mass flow, the second is related to feasibility (it houses the heating rods whose diameter is about 8 mm).
- Therefore, the preliminary configuration selected is 2.5Ay-6Ax (where $A_x = A_y =$ SGBT lead channel equivalent flow area).

- Each fissure is 5 mm in width and 100 mm in height. This allows facility control by variation of the lead level. The range of control is 0 - [7.0 7.7] kg/s depending of the effective concentrated pressure losses.
- The behavior of the SGBT as modeled with RELAP is not completely reproduced because of reduced Reynolds number and increased heated diameter. From one hand, the average lead temperature increases (about 497 °C at tube inlet instead of 480 °C) and, from the other hand, the outer wall bayonet tube temperature decreases. Anyway, void fraction close to 1 is predicted in the first 3 m of the annular riser (as in the simulation of the single tube) and the steam outlet temperature is 449 °C. CFD calculations predict a lead average temperature similar to the SGBT configuration. Further investigations are ongoing to explain these discrepancies between the two simulations.
- The three-dimensional CFD simulations evidenced the difficulty in a precise control of the natural circulation mass flow rate in the HERO facility by regulating the level of the upper LBE free surface. In fact, the regulation of the mass flow rate can take place in a very low variation of the elevation of free surface LBE level (some centimeters). In order to avoid mass flow rate changes during the initial transient phase, related to level fluctuations (i.e. average temperature variation), the fissures total flow area should be distributed into two or more axial elevations. Should be pointed out that CFD models the fissure 10mm width x100mm height (two times in width than the selected value).
- A possible alternative to reproduce accurately the lead size conditions is to adopt gas enhanced circulation. This allows to keep unchanged the SGBT channel geometry. In this last case, natural circulation will stabilize around 3.7 kg/s and could be the operating conditions to support the V&V of CFD – TH-sy coupling. This operational mode is currently under investigation at Brasimone by means of RELAP-5.

TxP Facility

The main objective of the Tubes for Powders (TxP) Facility is connected to the evaluation of the thermal performance of high conductivity powders for the application to the ALFRED SG. The facility has been supplied by LIMAINOX. The components were subjected to the refinements at the mechanical unit of Brasimone. TxP has been successfully pre-assembled. The final assembling is scheduled before December 2012. Based on the selection process of candidate powders performed in 2011, preliminary experiments are experienced at ENEA CR Brasimone to study their compaction when subjected to constant thermal loads and support the planning of the experimental campaigns in the TxP Facility. The main achievements from the experiments can be summarized as follows:

- Electrolytic copper powder LT-12 experienced compaction at 200 °C, the phenomenon was clearly visible during visual inspection.
- Copper powder W-60-M experienced compaction at 200 °C, the phenomenon was clearly visible during visual inspection.
- Brass powder OT-63 revealed a good performance up to 500 °C. In this last test, a new powder morphology is observed and compaction was appreciable from visual inspection.
- AISI-316-SS powder revealed very low compaction at 300 and 400 °C. The phenomenon was captured during electronic-microscope examination. In the last test (500 °C), compaction remained low even if it was visible during stereo-scope examinations.
- Sintetic diamond powder survived the test at 500°C without compaction.
- Al-N and Si-C remained similar to the initial state characterized by high compaction and dimension heterogeneity. This is due to their fabrication process (incomplete sintering).

 Ricerca Sistema Elettrico	Sigla di identificazione	Rev.	Distrib.	Pag.	di
	NNFISS - LP3 - 054	0	L	114	117


In conclusion, sintetic diamond is confirmed as most promising material for the application in ALFRED and should be tested in TxP. AISI-316 is suitable as pathfinder for calibration tests in TxP. Further investigations are necessary for Si-C, in particular it should be re-tested after end of sintering treatments.

The experiment evidences the lack of instrumentations: porosity-meter and riddles for powders are essential to assess, respectively, powder conductivity and powder compaction.

REFERENCES

- [1] www.gen-4.org, *GEN-IV technology website*.
- [2] *DOE NERAC, GIF, A Technology Roadmap for Generation IV Nuclear Energy Systems*, GIF-002-00, December 2002.
- [3] *D. Rozzia, M. Tarantino N. Forgiione, State of Development of LFR and ADS Technologies and R&D Needs*, HELIMNET Project WP-5 DEL 5.1, February 2012.
- [4] *C. F. Smith, L. Cinotti, H. Sekimoto, Lead-cooled Fast Reactor (LFR) ongoing R&D and key issues*, GIF Symposium – Paris (France) – 9-10 September, 2009.
- [5] *OECD/NEA, Handbook on Lead-bismuth Eutectic Alloy and Lead Properties, Materials Compatibility, Thermal-hydraulics and Technologies*, ISBN 978-92-64-99002-9, 2007.
- [6] *IAEA, Comparative assessment of thermo-physical and thermo-hydraulic characteristics of lead, lead-bismuth and sodium coolants for fast reactors*, IAEA-TECDOC-1289, Vienna, 2002.
- [7] www.leader-fp7.eu. *LEADER Project website*.
- [8] *J. Carlsson, General Synthesis Report of ELSY*, FI6W-036439, DEL/10/04, 23 March 2010.
- [9] **Leader 2nd Project Coordination Committee meeting**, Genova, May 12th 2011.
- [10] *D. Rozzia, A. Toti, M. Tarantino, Double-wall Bayonet Tube Steam Generator for LFR Application. Preliminary Characterization*, NNFISS – LP3 – 032, September 2011.
- [11] *A. Toti, Preliminary Characterization of a Double-Wall Bayonet Tube Steam Generator for LFR Application*, Master thesis on nuclear engineering, University of Roma Sapienza, 28-10-2011.
- [12] *D. Rozzia, M. Agostini, A. Ventura, G Venturi, M. Tarantino, Experimental Assessment of Powders Compaction When Subjected to Thermal Loads*, DR_/PhD/01(12)-IIR-Rev0a, Brasimone, February 2012.
- [13] *D. Rozzia, A. Toti, M. Tarantino Experimental Investigation on Powders Thermal Performance to Support the Design of Innovative SG for LFR*, DR_/PhD/01(11)-IIR-Rev1a, Brasimone, May 2011.
- [14] *M. Moretti, D. Rozzia, M. Tarantino, Investigation on insulating materials and design solutions for superheated steam double wall bayonet tube bundle for Gen. IV applications*, 07-03-12-Insulating-BRR-01(12), Brasimone April 2012.

- [15] *A. Toti, D. Rozzia, M. Tarantino*. **Heat Transfer Enhancement techniques in forced convection when applied to superheated steam flow**. 24-05-11-HEE-BRR-02(11) Brasimone, June 2011.
- [16] *NUREG/CR-5535*, **RELAP5/MOD3.3 Code Manual, Volume 1: Code Structure, System Model, and Solution Methods**, Information Systems Laboratories Inc., March 2003.
- [17] *NUREG/CR-5535*, **RELAP5/MOD3.3 Code Manual, Volume II Appendix A: Input Requirements**, Information Systems Laboratories Inc., June 2004.
- [18] *O. E. Dwyer, H. C. Berry*, **Heat Transfer to Liquid Metals Flowing Turbulently and Longitudinally Through Closely Spaced Rod Bundle, Part I**, Nuclear Engineering and Design Vol. 23 pp. 273-294, 1972.
- [19] *M. Palmero, F. Fionelli*, **ALFRED – Steam Generator Design**, LEADER meeting, Power Point presentation, 11 May 2011, Genova.
- [20] *W. Pfrang, D. Struwe* **Assessment of Correlations for Heat Transfer to the Coolant for Heavy Liquid Metal Cooled Core Designs** Institut für Reaktorsicherheit Forschungszentrum Karlsruhe GmbH, Karlsruhe, 2007.
- [21] *M. Moretti, D. Rozzia, A. Del Nevo, M. Tarantino*, **Modeling of SG Bayonet Tube for GEN-IV Applications by Means of RELAP-5**, 24-04-SGBT-assessment-TR-03(12), Brasimone June 2012.
- [22] *Todreas, M. Kazimi*, **Nuclear Systems I, Thermal Hydraulic Fundamentals**. Massachusetts Institute of Technology, 1993.
- [23] *J. H. Lienhard IV, J. H. Lienhard V*, **A Heat Transfer Textbox third edition**, Published by Phlogstone Press, Cambridge Massachusetts, USA 2003.
- [24] *W. Ambrosini, N. Forgiione* **Single and Two-Phase Flow Thermal Hydraulics**. University of Pisa June 19 - 30, 2006.
- [25] *NUREG/CR-5535*, **RELAP5/MOD3.3 Code Manual, Volume IV: Models and Correlations**, Information Systems Laboratories Inc., December 2001.
- [26] *D. Rozzia, A. Toti et al.*, **Experimental evaluation of thermal performance of powders for GEN-IV applications**, Proc. of UIT Nat. Conf., June, 2011, Torino, Italy.
- [27] *D. Rozzia, A. Toti et al.*, **Basis for the Experimental Evaluation of Powders Conductivity in the TxP Facility for Generation IV Technology Application**, Proceeding of NENE-2011 Int. Conf. Bovec, Slovenia 12-15 September 2011.
- [28] *W. Pfrang, D. Struwe* **Assessment of Correlations for Heat Transfer to the Coolant for Heavy Liquid Metal Cooled Core Designs** Institut für Reaktorsicherheit Forschungszentrum Karlsruhe GmbH, Karlsruhe, 2007.
- [29] *I. E. Idelchik* **Handbook of Hydraulic Resistance third edition**. ISBN 1-56700-074-6, Begell House, 1996.

 Ricerca Sistema Elettrico	Sigla di identificazione	Rev.	Distrib.	Pag.	di
	NNFISS - LP3 - 054	0	L	117	117

- [30] *D. Rozzia, A. Del Nevo, M. Moretti, M. Tarantino. Preliminary Calculations in Support to the HERO Facility Heating Power System, DR_PhD /05(12)-IIR, Brasimone, July 2012.*
- [31] **Ansys Fluent 14 User's Guide Documentation**, Ansys Inc, 2011.
- [32] AA. VV. **Handbook on Lead-bismuth Eutectic Alloy and Lead Properties, Material Compatibility, Thermal-hydraulics and Technologies**, OECD/NEA, 2007.